

Los Alamos National Laboratory is operated by the University of California for the United States Department of Energy under contract W-7405-ENG-36

TITLE PRELIMINARY ESTIMATES OF WATER FLOW AND RADIONUCLIDE
TRANSPORT IN YUCCA MOUNTAIN

AUTHOR(S) Bryan J. Travis, ESS-5
Steve W. Hodson, ESS-5
H. Eric Nuttall, University of New Mexico
Thomas L. Cook, ESS-5
Robert S. Rundberg, INC-11

SUBMITTED TO NNWSI Milestone Report
Department of Energy
Nevada Operations Office

By acceptance of this article the publisher recognizes that the U.S. Government retains a nonexclusive, royalty-free license to publish or to have published the published form of this contribution, or to allow others to do so, for U.S. Government purposes.

The Los Alamos National Laboratory requests that the publisher identify this article as work performed under the auspices of the U.S. Government.

Los Alamos Los Alamos National Laboratory
Los Alamos, New Mexico

HYDROLOGY DOCUMENT NUMBER 241

Preliminary Estimates of Water Flow and Radionuclide
Transport in Yucca Mountain

B. J. Travis
S. W. Hodson
H. E. Nuttall
T. L. Cook
R. S. Rundberg

Los Alamos National Laboratory
Los Alamos, New Mexico 87545

I. Introduction

A potential site for a storage repository for high-level radioactive waste has been identified in Yucca Mountain at the Nevada Test Site (NTS) in southeastern Nevada. Figure 1 presents a cross section of the mountain. The potential site lies in the Topopah Spring Member, some 300 m below the surface, and about 200 m above the water table. A detailed account of the stratigraphy appears in a recent report.¹

In summary, Yucca Mountain at the repository location consists of several stratigraphic units. Surficial units are alluvium and densely to moderately welded, fractured Tiva Canyon tuff. Below this lies the upper clastic unit, which consists of bedded and nonwelded tuffs of the Yucca Mountain and Pah Canyon Paintbrush tuffs. This unit is highly porous and believed to be relatively (matrix) permeable. The next unit down is termed simply the densely welded unit and consists of a thin upper and a thin lower vitrophyre and a thick central zone of densely welded ashflow layers. The matrix permeability of this central zone of the Topopah Spring member is very low, but the rock is highly fractured. Below this lies the lower clastic unit which consists of nonwelded ashflow, ashfall, and reworked tuffs (the lowest part of the Topopah Spring tuff and the Calico Hills tuff). This unit is highly porous and relatively permeable. Below this unit are several nonwelded to moderately welded tuffs with some thinner layers of densely welded ashflow and bedded ashfall tuffs. These rocks appear to be moderately fractured. Much of this unit is below the water table.

A major concern of this siting project is the ability of the tuff to retard the movement of any radionuclides that might leak from waste canisters. The repository would be in unsaturated but fractured tuff. The

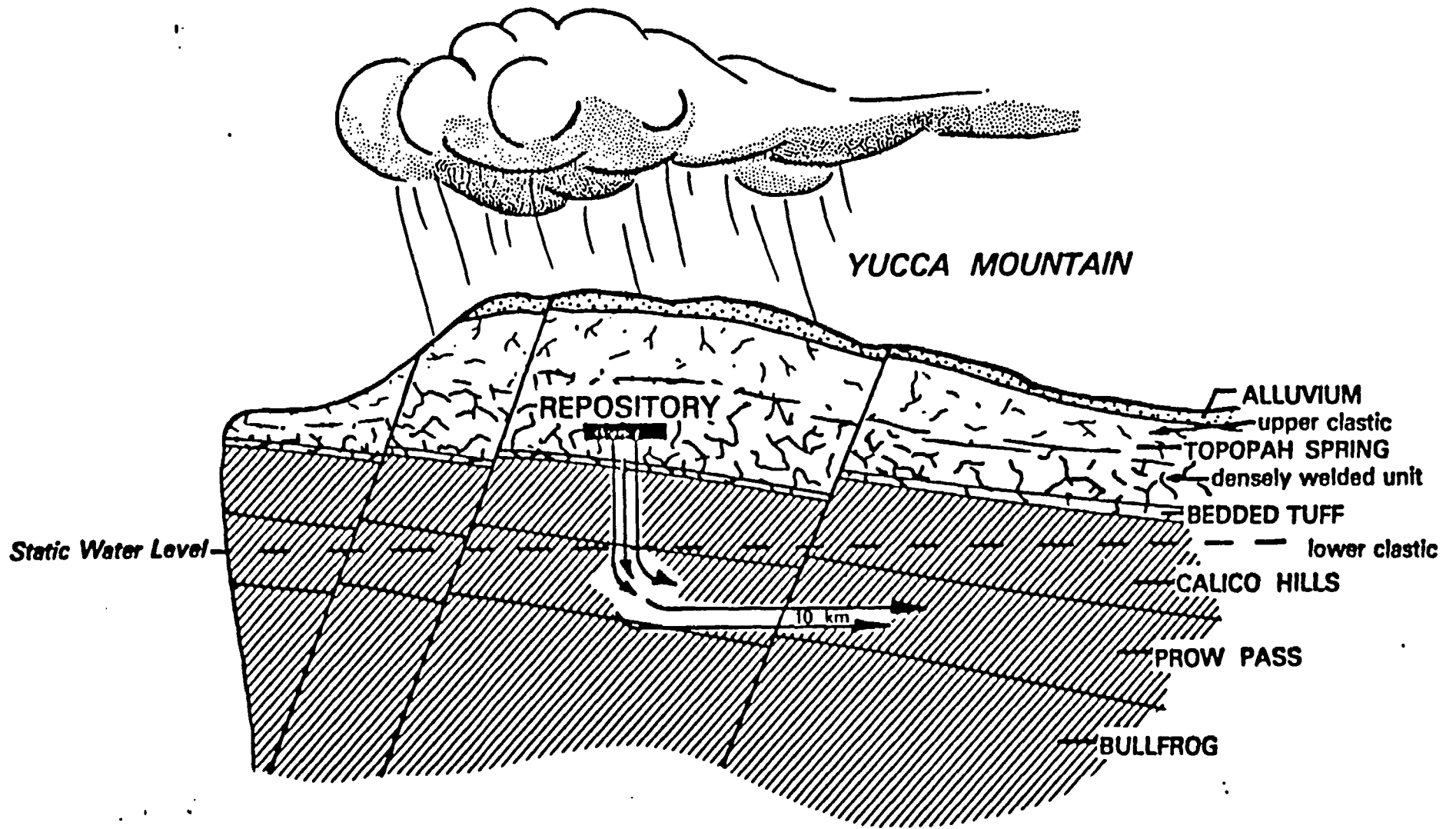


Fig. 1. CONCEPTUAL RADIONUCLIDE TRANSPORT PATH

fundamental question is: How long before any of the waste reaches the "accessible" environment (about 10 km from the repository)? Transport factors involved include fracture flow, porous matrix flow, diffusion, fracture spacing and aperture, and chemical sorption. A definitive answer may not be possible at present because of insufficient data. However, reasonable estimates probably can be made and the sensitivity of radionuclide migration times to the various transport processes can be examined.

The purpose of this report is to examine the effect of lithology and the presence of fractures on water flow and radionuclide transport in Yucca Mountain at the NTS. In particular, we present a preliminary sensitivity analysis of transport along a one-dimensional pathway that passes vertically downward through the densely welded unit (Topopah Spring Member and the bedded tuff) and the lower clastic unit (Calico Hills) and then horizontally in the saturated region through the Prow Pass, Bullfrog, or Tram tuffs.

II. Approach

Our approach to analyzing flow and transport in fractured tuff is both analytical and numerical. A great deal can be learned from fairly simple models and from dimensional analysis.

Dimensional analysis can be a useful tool by showing what combination of physical parameters are important. Nondimensionalizing a set of equations usually results in a few nondimensional parameters made up from physical properties, length, and time scales. Only a few solutions need be computed instead of the many required if each physical parameter were varied in turn.

More complicated problems require numerical solutions. Our numerical tools include the TRACR3D code,² which computes saturated and unsaturated two-phase flow in fractured porous media with transport of sorbing radionuclides; the WAFE³ code, which computes water, air, vapor, and energy movement in porous media; and analytic solutions for transport of sorptive species down single fractures with matrix diffusion for steady water flows.^{4,5,6}

III. Sensitivity Analysis

In the remainder of this report we analyze the sensitivity of water flow and species transport to several physical processes--fracture flow, matric potential, diffusion, and chemical adsorption. Three questions are considered in this report.

- (1) How far down can water flow through fractures in unsaturated tuff?
- (2) How well can the fractured and nonfractured tuff layers retard radionuclide transport?
- (3) What is the effect of repository heat load on hydrology?

Only partial answers to these questions are given here. Further studies and more data are needed to provide complete answers.

A. Flow in Fractures

In the absence of fractures, flow and transport will be diffusive. At the recharge rate in Yucca Mountain of a few millimeters per year (based both on heat flow⁷ and on percent of precipitation infiltrating^{8, 9, 10}), radionuclides would not reach the water table below a repository in Topopah Spring tuff via vertical porous flow for roughly 10,000-20,000 years after release (assuming current climatic conditions). Most of the nuclides, in fact, would take much longer than this to reach the water table because of retardation due to adsorption.

If fractures are present, these figures may be reduced significantly. Almost all the waste species of interest are water borne. Therefore, we need to consider first how much faster water can flow through fractured tuff than through unfractured tuff.

Describing water flow in fracture systems in unsaturated rock is a difficult task. Several general observations¹¹ can be made concerning fractures and fracture flow. Fracture length and aperture distributions frequently can be represented mathematically as log-normal distributions. Saturated flow in fractures obeys a cubic flow law for low flow rates. Fracture flow can be approximated by flow between parallel plates with an equivalent aperture.

When a saturated fracture drains, a thin film is left on the crack walls. Flow can continue through the thin film, but the flux will be diminished greatly. For a set of parallel fractures with log-normally distributed apertures, fracture drainage flux is very strongly dependent¹¹ on

wide saturated fractures. That is, the few widest saturated cracks strongly dominate flow because of the cubic flow law.

In Yucca Mountain, fractured and unfractured units alternate. In the highly fractured, densely welded unit which will contain the repository, it is not clear what the effect of fractures on flow and transport will be. Will the recharge water move vertically through unfractured layers and then enter fractures? To enter a fracture from the porous rock, water would have to overcome capillary tension; this requires saturations close to unity. If water did enter fractures, would it move as a film or as a slug? Film flow would be very much slower than slug flow. More experimental and field data are needed to answer these questions. In the analysis presented below, we have taken a conservative approach and assumed that water enters fractures in pulses (corresponding to episodic precipitation) and travels down fractures as slugs. Since the rock surrounding the fractures is partially saturated, water can be drawn from the slugs into the rock. The depth to which a water slug will penetrate under gravity flow can be quantified as a function of the important physical parameters.

The following scenario is used. A series of parallel vertical fractures of half-width W passes through competent rock of porosity ϵ and saturated permeability K_0 . The rock is partially saturated (S_0). The cracks lie at a distance $2L$ apart. We assume $W \ll L$. Water enters a fracture as a pulse. It is further assumed that water will move down the crack as a slug of height H (see Fig. 2). As it flows down, water is continually sucked into the rock by capillary action. The water slug moves down the crack at a velocity V_c given by

$$V_c = \rho_l g \frac{(2W)^2}{12 \mu} \quad (1)$$

where ρ_l is water density, g is the gravity constant, and μ is water viscosity. Here we are using the results of saturated crack flow experiments.¹² A water slug will move down the fracture under the action of gravity until its length H decreases (due to matric suction) to the point at which capillary action in the crack can support it. For example, a 100- μ wide crack can generate about 15 mb of tension (assuming the capillary tube

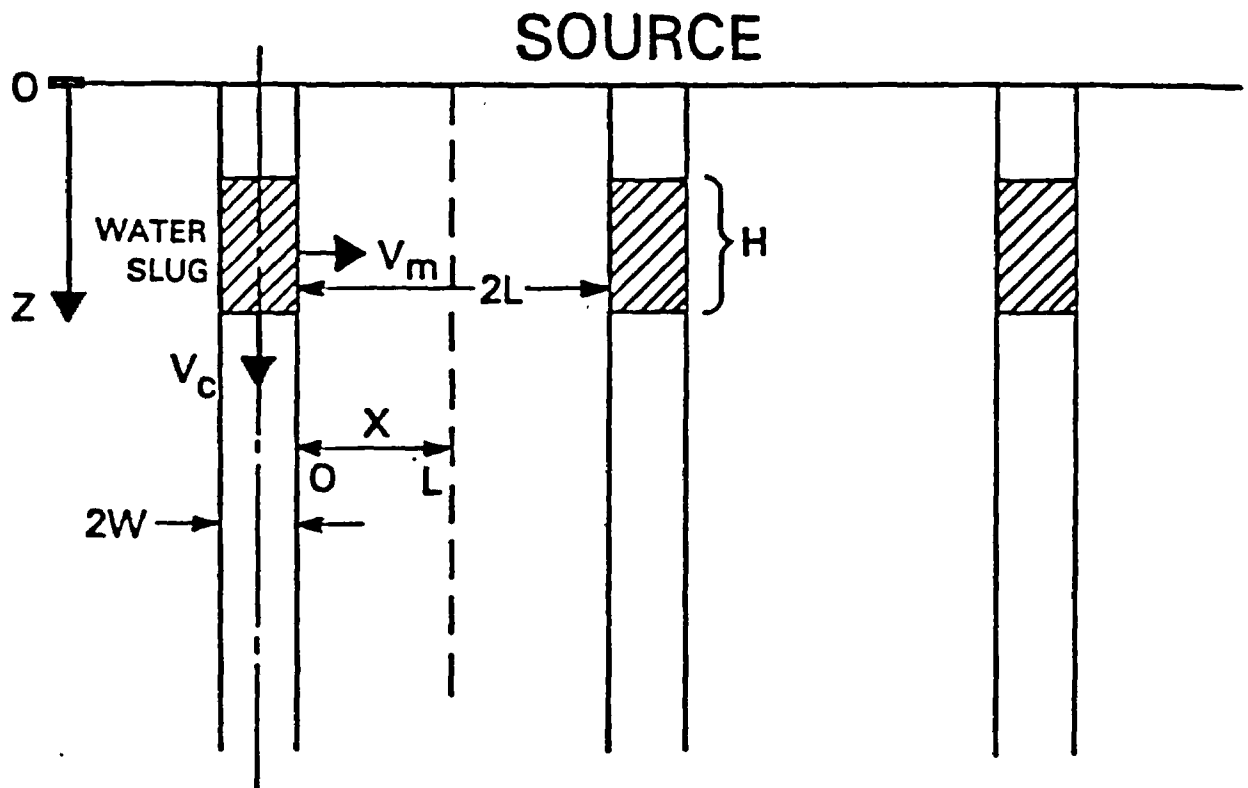


Fig. 2. Scenario used for fracture flow analysis.

equation is equal to $\frac{2\sigma_t}{W}$, where σ_t is surface tension). This means if H is 15 cm or less, the water slug will not be able to move.

In the rock matrix, we assume that water saturation $\sigma(x,z,t)$ is governed by the expression (which neglects gravity)

$$\frac{\partial \sigma}{\partial t} = \frac{-1}{\epsilon} \nabla \cdot \frac{k}{\mu} \nabla P_c = \nabla \cdot \left(\frac{b K_o P_o}{\epsilon \mu} \right) \sigma^c \nabla \sigma = \nabla \cdot (A \sigma^c \nabla \sigma) \quad , \quad (2)$$

where P_c is capillary pressure ($P_c = P_o \cdot \sigma^{-b}$) and permeability is $k = K_o \cdot \sigma^a$ and $c = a-b-1$. (Initial estimates of a and b for saturations above 60% for Topopah Spring tuff are $a = 13$, $b = 5$, and $c = 7$.) Auxiliary conditions needed for solving (2) are an initial condition

$$\sigma(x,z,t=0) = S_o \quad , \quad (3)$$

and boundary conditions

$$\sigma(0,z,t) = 1 \text{ if } t_1(z) < t < t_2(z) \text{ where } t_1(z) = z/v_c \quad ,$$

$$t_2(z) = t_1(z) + \frac{H(t_2)}{v_c} \quad , \quad (4)$$

$$\frac{\partial \sigma}{\partial x}(0,z,t) = 0 \text{ if } t < t_1(z) \text{ or } t > t_2(z) \quad ,$$

and

$$\frac{\partial \sigma}{\partial x}(L,x,t) = 0 \quad . \quad (5)$$

We are assuming water flows down each of the parallel cracks at the same time (infinite horizontal source). In Eq. (4), water can flow into the rock from a crack at a specified depth only while the slug is moving past that depth. At greater depth, H is less than H_o , the original height, and so the time during which water can flow into the rock at that depth is less than at shallower depths.

The slug thickness H decays at a rate given by

$$\frac{dH}{dt} = -\frac{1}{W} \int_{V_c \cdot t - H}^{V_c \cdot t} V_m(o, z, t) dz \quad , \quad (6)$$

where

$$V_m(o, z, t) = -A \sigma^c \frac{\partial \sigma}{\partial x}(o, z, t) \quad (7)$$

is the horizontal water velocity at the edge of the crack.

1. Analytic Solution

Solution of Eqs. (1)-(7) will provide the rate of progress of a water slug down a vertical fracture and the change in matrix saturation. An approximate solution can be obtained by making a few reasonable assumptions. The coefficient A represents a diffusion of water into the rock. It has units of X^2/T . The time scale T can be chosen as H_0/V_c . Then the characteristic distance X is $\sqrt{AH_0/V_c}$. If the scale time T is small enough, $V_m(o, z, t)$ will be approximately constant while a water slug passes. Then Eq. (6) simplifies to

$$\frac{dH}{dt} = -\frac{H}{W} V_m \quad (8)$$

whose solution is

$$\frac{H}{H_0} = e^{-V_m t/W} \quad (9)$$

Consider fractures of width $2W = 10 \mu$, 100μ , and 200μ . Then $V_c = 0.008 \text{ cm/s}$, 0.8 cm/s , and 3.2 cm/s , respectively. Let $H_{01} = 2000 \text{ cm}$, $H_{02} = 200 \text{ cm}$, $H_{03} = 100 \text{ cm}$, and $L = 5 \text{ cm}$. For each crack size, this is equivalent to a 2-mm layer of water over the rock surface, all of which drains down the cracks. For Topopah Spring tuff, $K_0 = 100 \text{ nanodarcys}$ and P_0 (bubbling pressure on matrix potential curve) = 50 kPa , so that $A = 2.5 \cdot 10^{-6} \text{ cm}^2/\text{s}$. The diffusion length $X = 0.79 \text{ cm}$, 0.025 cm , and

0.0088 cm, respectively, and so $V_m = 3.89 \cdot 10^{-7}$ cm/s, $1.23 \cdot 10^{-5}$ cm/s, and $3.5 \cdot 10^{-5}$ cm/s, respectively (assuming a saturation of 60%), and

$$\frac{H_1}{H_{01}} = e^{-7.78 \cdot 10^{-4} t} ,$$

$$\frac{H_2}{H_{02}} = e^{-2.46 \cdot 10^{-3} t} ,$$

$$\frac{H_3}{H_{03}} = e^{-3.5 \cdot 10^{-3} t} , \text{ respectively.}$$

For $2w = 10 \mu$, $H_{T1} = 150$ cm,
 $2w = 100 \mu$, $H_{T2} = 15$ cm,
 $2w = 200 \mu$, $H_{T3} = 7.5$ cm,

where H_T is the plug thickness which can be supported in the crack by capillary tension.

The time then for H to shrink to H_T in each case is $t = 3329$ s, 1053 s, and 740 s, respectively. The depth reached in each case is given by $V_c t$ and is 0.27 m, 8.4 m, and 23.7 m, respectively. It would appear that cracks whose aperture is about 100 μ or so would allow transport over short distances. But for a water slug to reach from the repository to the water table through a fracture, the fracture width would have to be much larger than 200 μ or the matrix would have to be almost saturated.

2. Numerical Solution

The estimates made above were based on the assumption of constant $V_m(o, z, t)$. A simple numerical calculation using the TRACR3D code allows us to remove that assumption, and to compute crack flow for a range of parametric values (A, W, saturation).

For each value of matrix water saturation and coefficient A, a one-dimensional TRACR3D calculation was made, solving the system

$$\frac{\partial \sigma}{\partial t} = \frac{A}{c+1} \frac{\partial^2 \sigma^c + 1}{\partial x^2} , \quad 0 < x < L, \quad 0 < t < T_{\max} \quad (10)$$

with boundary conditions

$$\sigma(0,t) = 1 \text{ and } \frac{\partial \sigma}{\partial x}(L,t) = 0 \quad (11)$$

and initial condition

$$\sigma(x,0) = \sigma_0 \quad (12)$$

The end time T_{\max} was chosen to equal H_0/V_c . At each time step in these one-dimensional calculations, the water flow $V_m = -Ac^c \frac{\partial \sigma}{\partial x}$ at $x = 0$ is saved to be used in numerical evaluation of the integral in Eq. (6). A few of these computations were repeated, including the movement of air as well as of water. Results were essentially unchanged. This does not mean, however, that entrapped air would not be important in a long-term cumulative process.

Results of Eq. (6) using the numerical solution of Eqs. (10)-(12) are summarized in Figs. 3-6, which are plots of depth reached by water slugs as a function of A , crack width W , and matrix water saturation. Penetration to hundreds of meters requires either very wide cracks and/or high matrix saturations and/or small A values (low permeability or weak matrix suction or much greater slug thickness H_0). It is also apparent that the analytic solution [Eq. (9)] underestimates the depths reached.

3. Additional Considerations

Travel times for the water slugs ranged from a few minutes to about eight hours. A point to remember is that the molecular identity of a water slug changes as it moves down a crack due to self diffusion of water molecules through the rock matrix. A water slug reaching considerable depths will not consist of the same molecules it contained initially.

We have considered only fractured lithology. There are two relatively unfractured layers, the upper clastic and the lower clastic (Calico Hills), which lie below the fractured Tiva and the fractured Topopah Spring layers, respectively. Water moving down fractures eventually will encounter these porous layers. These layers will act as buffers, controlling the rate at which water moves into fractures below. For example, water cannot flow into fractures in the Topopah Spring below the Pah layer any faster than the hydraulic conductivity of the Pah layer permits.

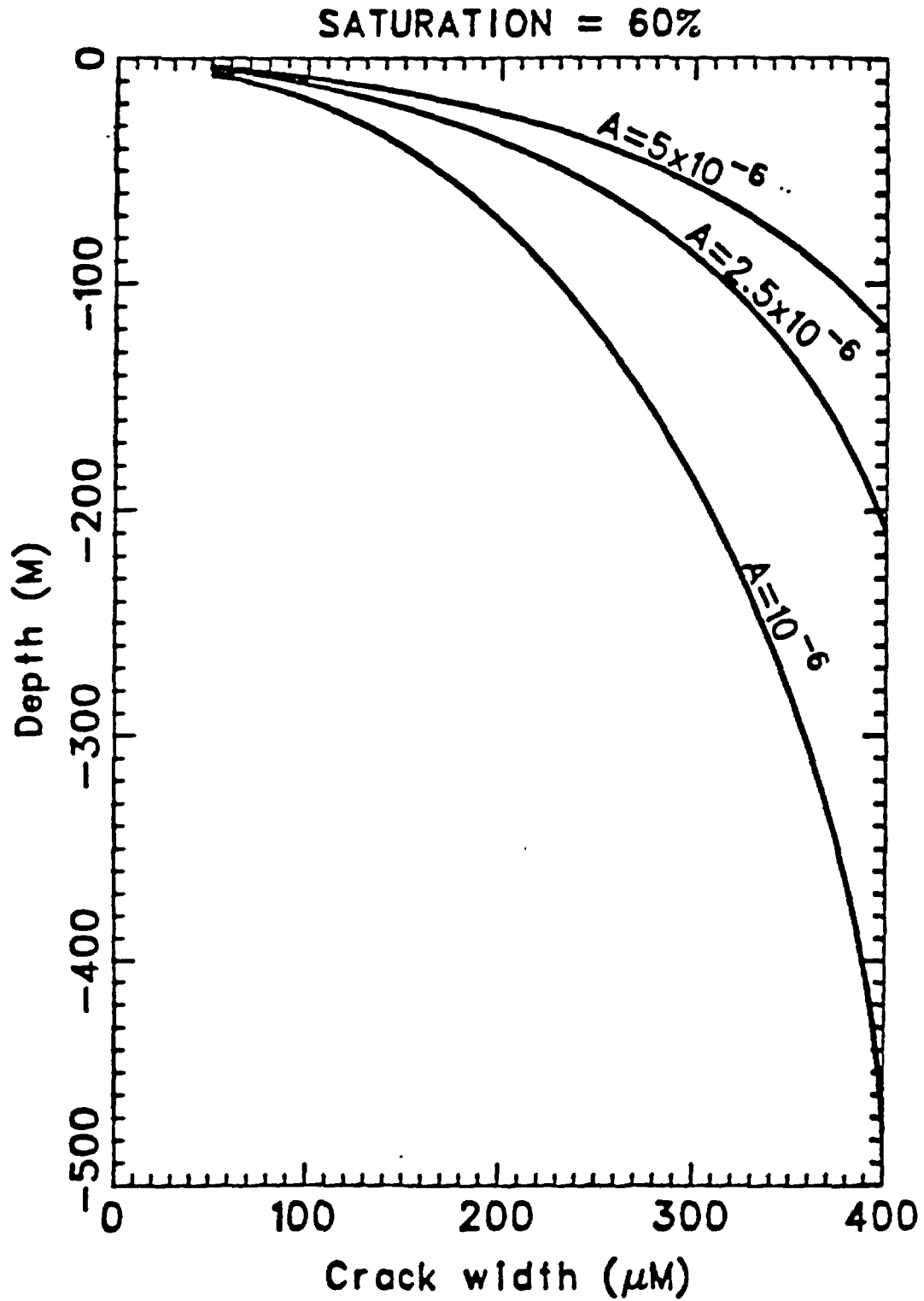


Fig. 3. Depth reached by water slug as a function of crack width and diffusion coefficient A for matrix saturation of 60%.

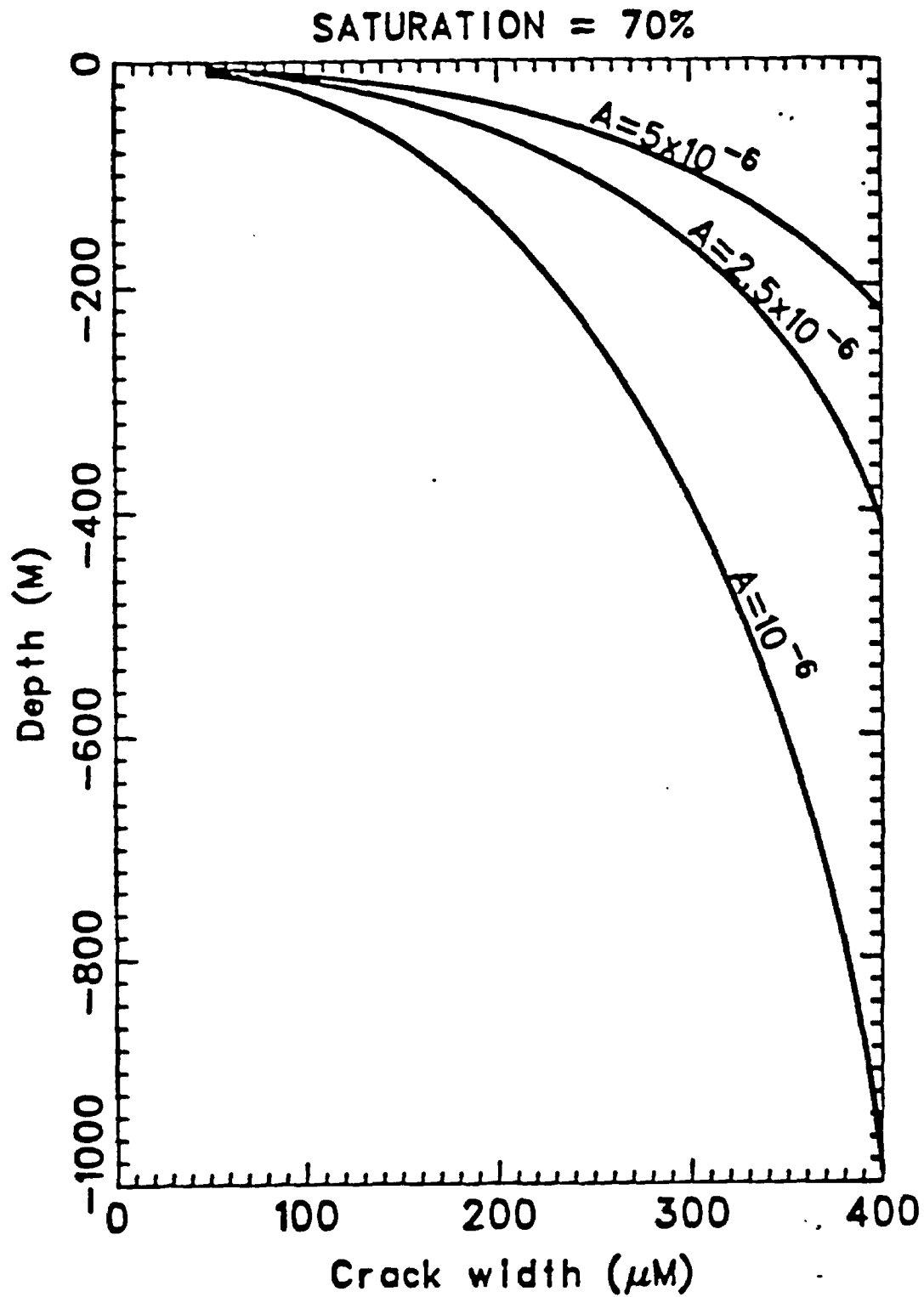


Fig. 4. Depth reached by water slug as a function of crack width and diffusion coefficient A for matrix saturation of 70%.

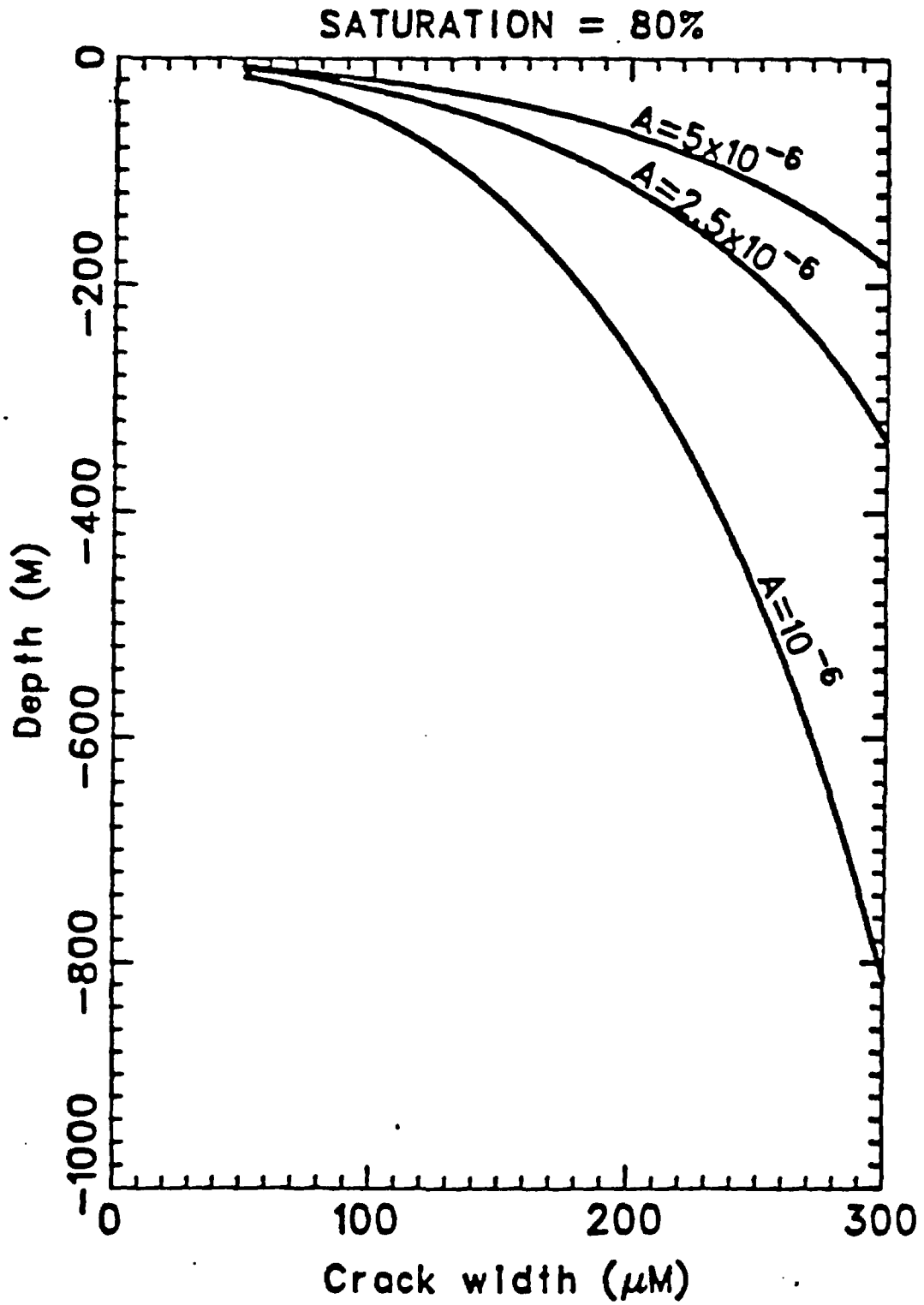


Fig. 5. Depth reached by water slug as a function of crack width and diffusion coefficient A for matrix saturation of 80%.

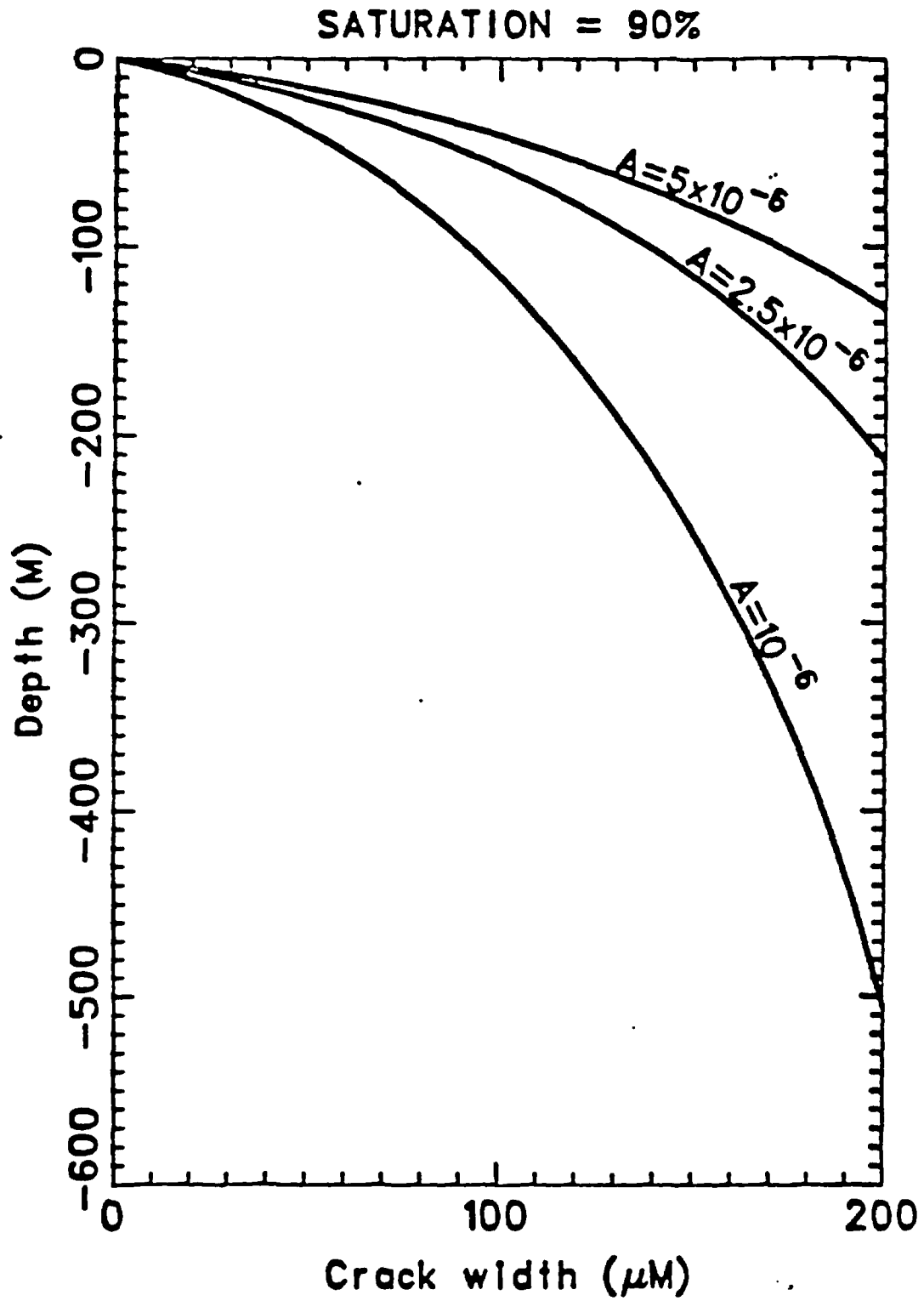


Fig. 6. Depth reached by water slug as a function of crack width and diffusion coefficient A for matrix saturation of 90%.

Another factor that cannot be evaluated at this time due to lack of data is connectivity of fractures. If fractures are present but not connected or intersecting, their impact on flow and transport will be greatly diminished. If they are a connected network, the path a water slug would travel would probably be tortuous and might involve branching into cracks in other directions. This three dimensionality would provide more surface area to a water slug, allowing more infiltration into the rock. Finally, evaporation may result in less effective fracture flow, especially in narrower cracks. Near the surface of Yucca Mountain, considerable evaporation may occur. Loss of water would increase capillary suction and reduce the depths which water flow in fractures can reach.

If recharge occurs in pulses or episodic events, and consequent water flux into a fracture occurs at too low a rate for water slug formation, we expect film flow in that fracture. Film flow should be much slower than slug flow resulting in longer residence time. This is equivalent in our analysis to using larger A values, which will correspond (Figs. 3-6) to shallower penetration.

The results of our fracture flow analysis should be consistent with the actual hydrologic condition of Yucca Mountain. The saturation profile vs. depth through the likely repository location shows¹³ regions of high saturation (80-90%) as well as several regions of low saturation (30-40%). Measurements¹⁴ of saturated matrix hydraulic conductivity in the Topopah Spring tuff range from 6 cm/year to 0.10 mm/year. In the Calico Hills tuff, values range from 45 cm/year to 1.2 mm/year. It is reasonable to expect the high saturation regions to correspond to low permeability values because these regions cannot drain very easily. In addition, the low-saturation regions correspond to high-permeability values because these regions can rapidly drain off the 8 mm or so of recharge per year. If we assume direct vertical flow to the water table, the simplest explanation for getting recharge through the low-permeability regions (whose matrix permeability is too low to allow 8 mm/year of recharge) is to allow fracture flow. This is consistent with our analysis. In the high-permeability, low-saturation regions, water will be drawn out of fractures. The flow primarily will be porous flow. In the low-permeability, high-saturation regions, flow primarily is through fractures (small A, high saturation). If this interpretation is correct, then

there are alternating layers of porous flow and fracture flow from the surface down to the water table. Experiments such as the $^{36}\text{Cl}^-$ detection would help test this interpretation.

There are other implications of this interpretation. Water in the high-saturation regions should be older than that in the low-saturation regions (unless the 8-mm recharge rate is high and the true recharge is almost 0). Also, water travel time from the repository to the water table would be approximately the travel time through the porous flow layers. This would be very roughly $50\text{-}100 \text{ m}/(8 \text{ mm/year}) \times \text{porosity} = 2,000$ to 4,000 years.

4. Data

What are the apertures of cracks in Yucca Mountain? Little data are available. An estimate of fracture width can be made for well J13, which extends into the Topopah Spring formation where it is saturated. The conductivity has been measured¹⁵ as about 1.0 m/day. This corresponds to about 0.8 darcy permeability and must come mainly from fractures. For this simple analysis, we ignore the distributed nature of apertures and look for an equivalent average aperture. If b is crack half-width and s is half the spacing between cracks, the overall permeability $k_s = k_c b/s$, where k_c is the crack permeability and is given¹¹ by $k_c = (2b)^2/12$. Then $k_s = 0.8 \times 10^{-8} \text{ cm}^2 = b^3/3s$. If $s = 3 \text{ cm}$, then $b = 41.6 \mu$, and the crack aperture is about 83 μ . An additional estimate of average fracture aperture in Topopah Spring tuff can be made. The saturated conductivity¹³ of Topopah Spring tuff is about 230 m/year. This corresponds to a permeability of 0.74 darcy. Using a fracture spacing of 6 cm, fracture aperture is about 81 μ . It appears that fractures do exist of sufficient width to allow significant water flow in the unsaturated region.

B. Radionuclide Transport

Although fractures are capable of transporting water to considerable depths, the situation with transport of radionuclides is quite different. The reason for this is molecular diffusion and chemical sorption. Consider again a water slug moving down a crack, now bearing a contaminant. The contaminant will diffuse into the pore spaces of the rock due to molecular diffusion, if a concentration difference exists. The time scale T on which

this will occur can be estimated from the effective diffusivity $D_e = \epsilon D_i / \tau$, where D_i is the ionic diffusivity, ϵ is porosity and τ is the constrictivity-tortuosity factor. The characteristic time for diffusion over a distance W is then

$$T = \frac{W^2}{D_e} .$$

For a 100- μ crack, $T = 25 \cdot 10^{-6} / (10^{-6} / 3) = 75$ s. In this time, the slug will have moved about 60 cm. For a 200- μ crack, $T = 300$ s, and a distance of 9.6 m will be traversed. The distance that a contaminant will be transported goes as W^4 . Wide cracks will carry contaminants a long way, assuming slug or saturated flow. Very wide fractures ($> 200 \mu$) may be rare, however, in situ because of the overburden stresses present. A large fracture may be more prone to fill in because it can accept more and larger particles. For reasonably sized fractures, radionuclide migration is much slower than water flow.

Almost all the radionuclides of interest (EPA 40 CFR 191)¹⁶ adsorb to the minerals in tuffs. The measured adsorption coefficients¹⁷ are large for most relevant radionuclides, ranging into the 100's and 1000's. The sorption coefficient (K_d) for technetium is small, however, and so are the values for uranium and neptunium (see Figs. 7 to 16, from Ref. 17). A quantity called the retardation factor R is defined as

$$R = 1 + \frac{\rho_m K_d}{\epsilon} ,$$

where ϵ is porosity and ρ_m is matrix density. Approximate R values are listed in Table I for the radionuclides in several stratigraphic units.

The transport pathway considered extends from the repository site to the water table (50 m of Topopah Spring tuff, about 15 m of bedded tuff, 135 m of Calico Hills tuff), and then laterally for 10 km in the saturated region. Flow rate in the saturated region is not known. Rough estimates of flow rate from H4 to J13 give about 24 m/year and from Pahute Mesa to Yucca Mountain an approximate flow rate¹⁸ is 5 to 6 m/year. We assume here that horizontal flow in the saturated region is similar to the larger scale recharge area-to-Yucca Mountain rate of 6 m/year. Fracture spacing in

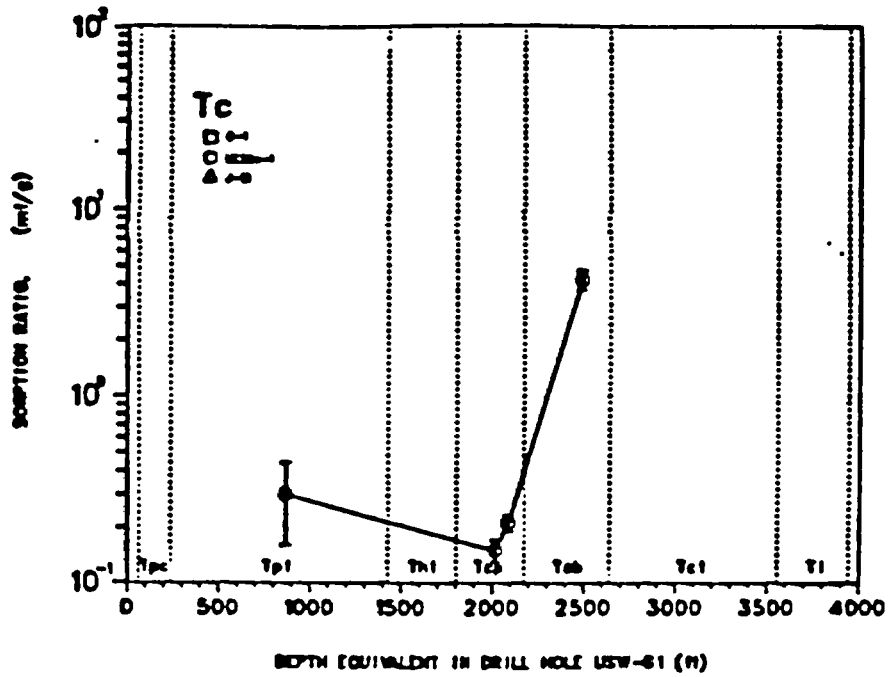


Fig. 7. Sorption ratio variation for technetium as a function of stratigraphic position. Samples are from drill hole UE25a-1.

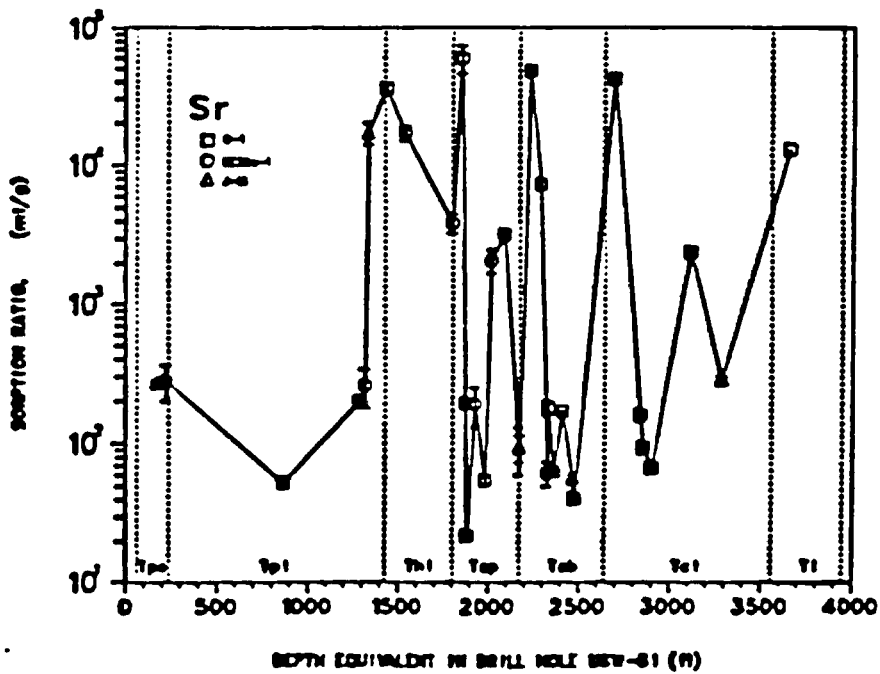


Fig. 8. Sorption ratio variation for strontium as a function of stratigraphic position. The drill holes from which each sample originated are indicated by symbols in this and subsequent figures.

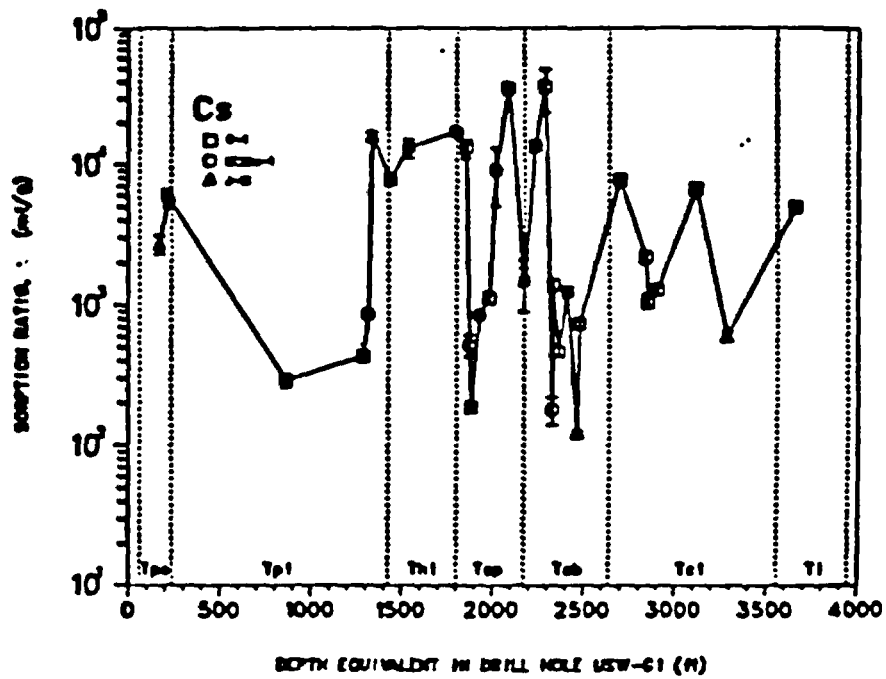


Fig. 9. Sorption ratio variation for cesium as a function of stratigraphic position.

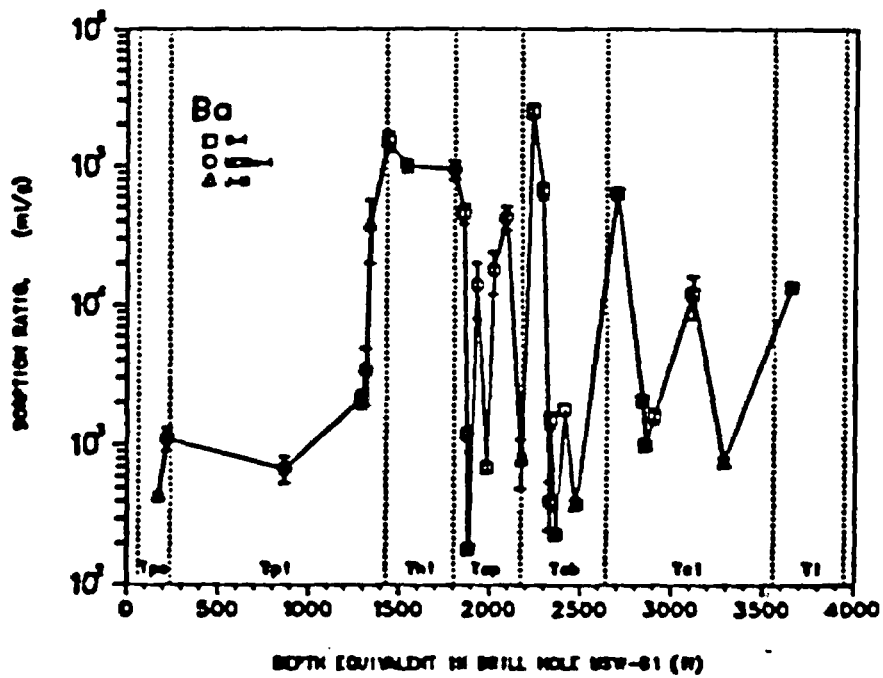


Fig. 10. Sorption ratio variation for barium as a function of stratigraphic position.

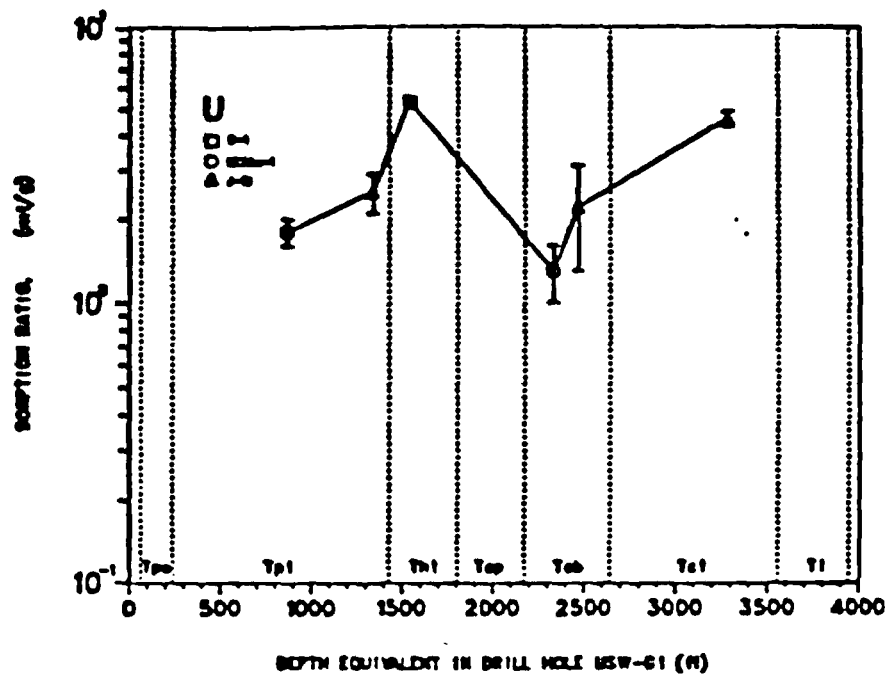


Fig. 11. Sorption ratio variation for uranium as a function of stratigraphic position.

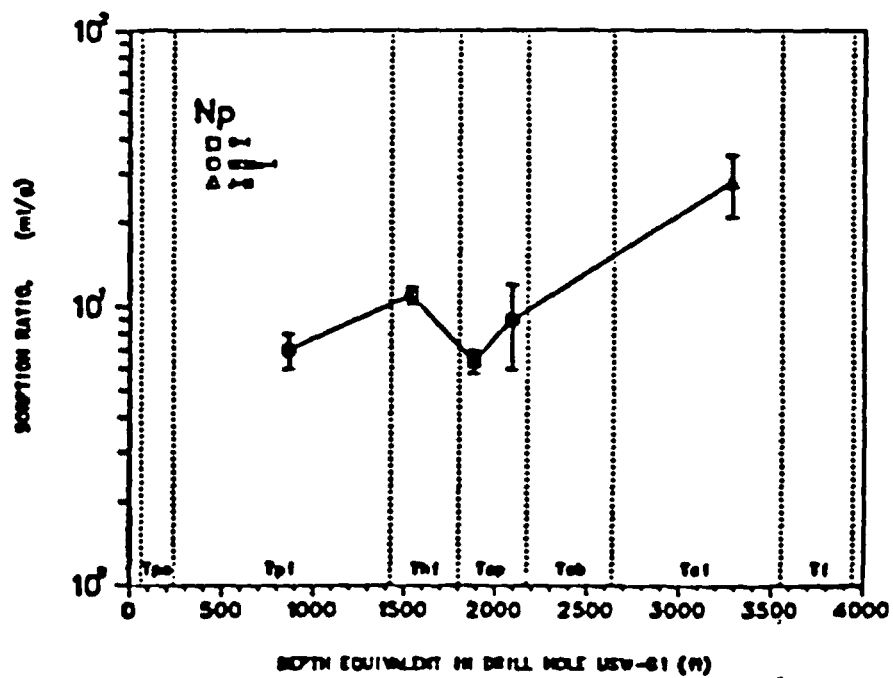


Fig. 12. Sorption ratio variation for neptunium as a function of stratigraphic position.

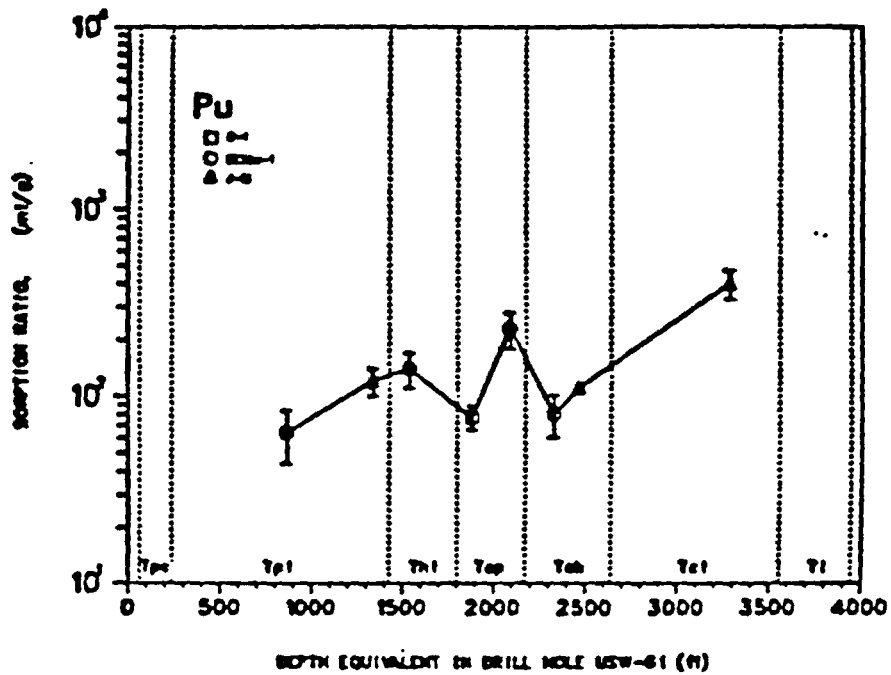


Fig. 13. Sorption ratio variation for plutonium as a function of stratigraphic position.

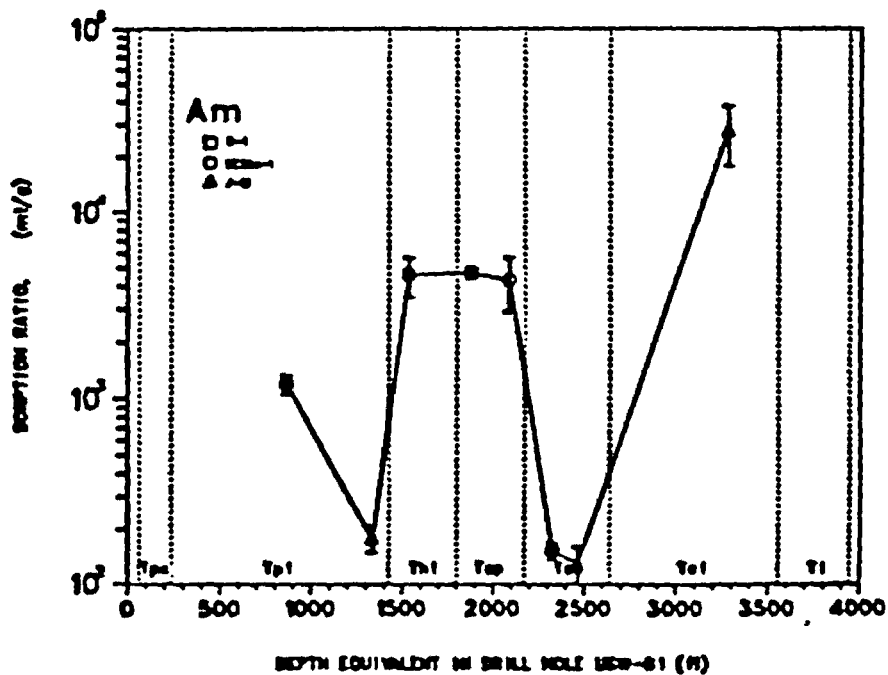


Fig. 14. Sorption ratio variation for americium as a function of stratigraphic position.

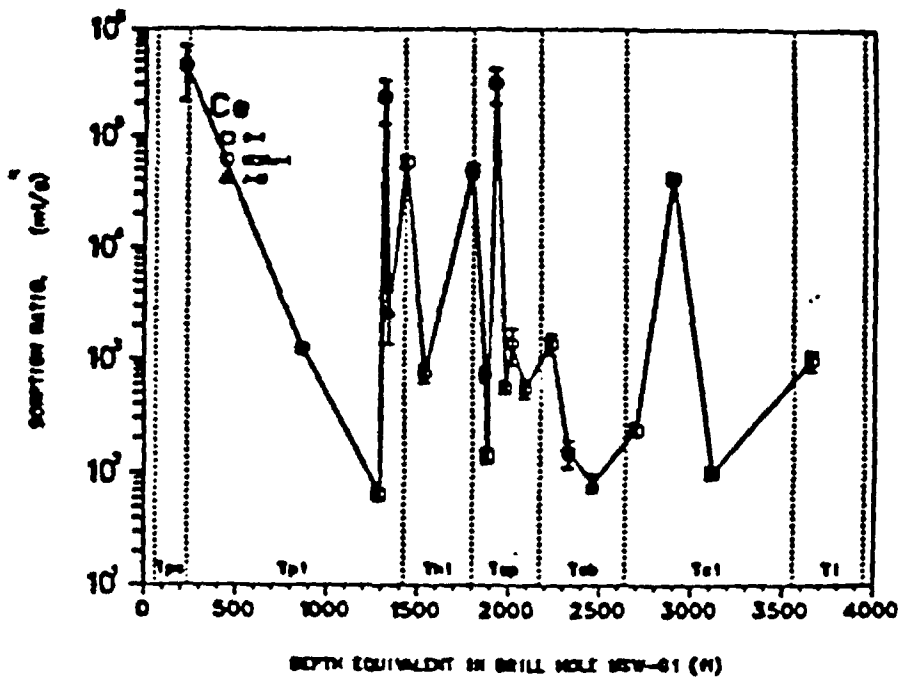


Fig. 15. Sorption ratio variation for cerium as a function of stratigraphic position.

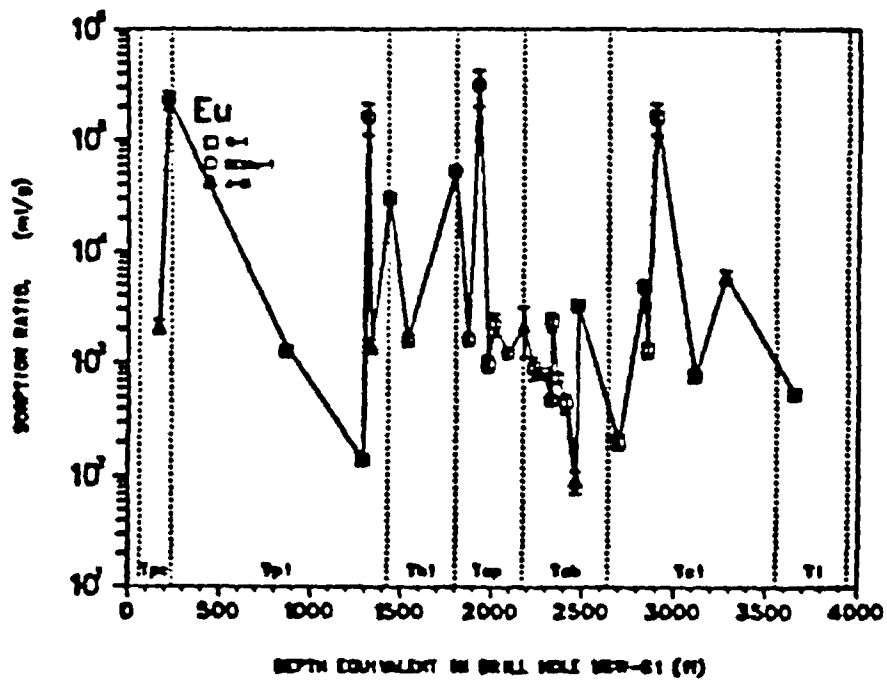


Fig. 16. Sorption ratio variation for europium as a function of stratigraphic position.

TABLE I

RETARDATION FACTORS FOR RADIONUCLIDES IN DIFFERENT STRATIGRAPHIC UNITS

<u>Element</u>	<u>Stratigraphic Unit</u>			
	<u>1</u>	<u>2</u>	<u>3</u>	<u>4</u>
^{141}Ce	2000	3×10^4	7000	5000
^{135}Cs	6000	7×10^4	4×10^4	1200
^{90}Sr	1100	8×10^4	2×10^4	140
^{99}Tc	7	12	2	2
^{238}U	40	40	33	16
^{237}Np	150	100	50	40
^{239}Pu	1300	540	630	480
^{243}Am	2.5×10^4	820	2×10^4	3000
^{152}Eu	10^4	3×10^4	2×10^4	10^4
^{133}Ba	2×10^4	2×10^5	7×10^5	4000

1 = Topopah Spring

} densely welded unit

2 = Bedded Tuff

3 = Calico Hills (lower clastic unit)

4 = Prow Pass (older volcanics)

Topopah Spring was taken as 5 cm; in the bedded tuff below the Topopah a fracture spacing of 6 cm was used; in the Calico Hills tuff, a fracture spacing of 1 m was assumed, and in the horizontal transport section a fracture spacing of 6 cm was used.¹ Porosities for these four layers are approximately 10%, 8%, 30%, and 30%, respectively. Saturations were estimated as 75%, 80%, 95%, and 100%, respectively.

We are assuming in this section that cracks will transmit water downward without loss of water to the matrix. This may overestimate the amount of contaminant transmitted a given distance. In the densely welded unit, matrix permeability is quite low. Flow should be primarily via fractures. In the lower clastic unit, water saturation is very high (95%) and so water loss from fractures into tuff should be small. Fracture flow in the lower clastic unit should be a small fraction of the total flow because of the very low fracture frequency and the high matrix permeability there.

For our first calculations, we have used an average fracture flow rate of 200 m/year for the unsaturated zone. This is also the estimated¹³ saturated flow rate through fractured Topopah Spring tuff. This is a very conservative assumption since (1) it assumes continuous flow and (2) it assumes saturated fracture flow. Flow rate in the saturated zone was set to 6 m/year. In the densely welded unit, no matrix flow is considered. In the lower clastic unit, flow is primarily matrix flow. We assume a flow rate of 3 cm/year (8 mm/year/porosity) in the rock of this unit. Subsequent calculations will treat episodic fracture flow and transport, which may considerably reduce the effective flow rate since water may actually enter during only a small fraction of a year.

Although the effect of matrix capillary suction was considered in the previous section, it is ignored here. We partially accounted here for the unsaturated nature of the tuffs by multiplying porosity and diffusivity by actual saturation values.

Migration times to the "accessible" environment can then be estimated. Analytic solutions exist^{4,5,6} for transport in a porous medium with steady flow and constant sources and also for transport in a porous medium containing a set of parallel equidistant fractures.

Table II lists additional properties of the radionuclides needed for the analytic solutions. The nuclides ^{141}Ce and ^{152}Eu are analogs for ^{151}Sm while ^{133}Ba is used for ^{226}Ra .

Results of these calculations are shown in Figs. 17 through 25, which show the migration history through the four regions for each of the ten radionuclides, assuming transport through 100- μ -wide cracks as well as porous-flow transport in the lower clastic unit. (We use 100- μ cracks based on the J13 transmissivity data.) Nuclides which do not appear in the plots decayed before reaching the bottom of the layer. In these calculations, a radionuclide is injected from a decaying source into a fracture at the top of a layer and the concentration history at the bottom of the same layer (in the fracture) is computed. Of the ten nuclides considered, the only one that can reach the water table in less than 10,000 years is ^{99}Tc . Diffusion into the matrix, chemical sorption, and radioactive decay prevent any of the radionuclides from reaching the accessible environment in less than 10,000 years, given the assumptions made in this study. Concentration breakthrough curves at the bottom of each layer (and at 10-km horizontal distance for the saturated zone) are shown in Figs. 17 through 25.

Figures 17 and 18 present concentration histories for the fractured Topopah Spring tuff in the densely welded unit. Even with the large fracture flow rate, only three nuclides (^{99}Tc , ^{238}U , and ^{237}Np) would get through this layer in less than 10,000 years. Figure 19 shows breakthrough times for a thin layer below the Topopah Spring tuff which has somewhat different retardation properties. Even though water is assumed to flow through fractures at 200 m/year, breakthrough takes at the very least (for ^{99}Tc) 400 times longer than the assumed water travel time for this layer. The next three figures (Figs. 20-22) indicate breakthrough curves for the Calico Hills tuff. Because of the large fracture spacing assumed here, even ^{99}Tc takes several thousand years to break through. These results may not be appropriate in general for the Calico Hills layer. This layer has a fairly large matrix permeability and it is believed flow will be primarily porous. However, the results of Figs. 20-22 might be appropriate for transport down a fault through this layer. Figure 23 shows breakthrough curves for the Calico Hills (lower clastic) if porous flow only is assumed. Only ^{99}Tc gets through in less than 10,000 years. The next radionuclide to break through is ^{238}U at over 100,000 years. Finally, Figs. 24 and 25 show the breakthrough for the horizontal pathway below the water table. Here, we

TABLE II

HALF-LIVES AND DIFFUSIVITIES OF RADIONUCLIDES

<u>Element</u>	<u>Halflife (years)</u>	<u>Diffusivity (m²/year)</u>
¹⁴¹ Ce	90	3.15x10 ⁻²
¹³⁵ Cs	3x10 ⁶	6.30x10 ⁻²
⁹⁰ Sr	28	2.44x10 ⁻²
⁹⁹ Tc	2x10 ⁵	3.15x10 ⁻²
²³⁸ U	4.5x10 ⁹	3.15x10 ⁻²
²³⁷ Np	2x10 ⁶	3.15x10 ⁻²
²³⁹ Pu	2.4x10 ⁴	3.15x10 ⁻²
²⁴³ Am	8x10 ³	3.15x10 ⁻²
¹⁵² Eu	90	3.15x10 ⁻²
¹³³ Ba	1.6x10 ³	3.15x10 ⁻²

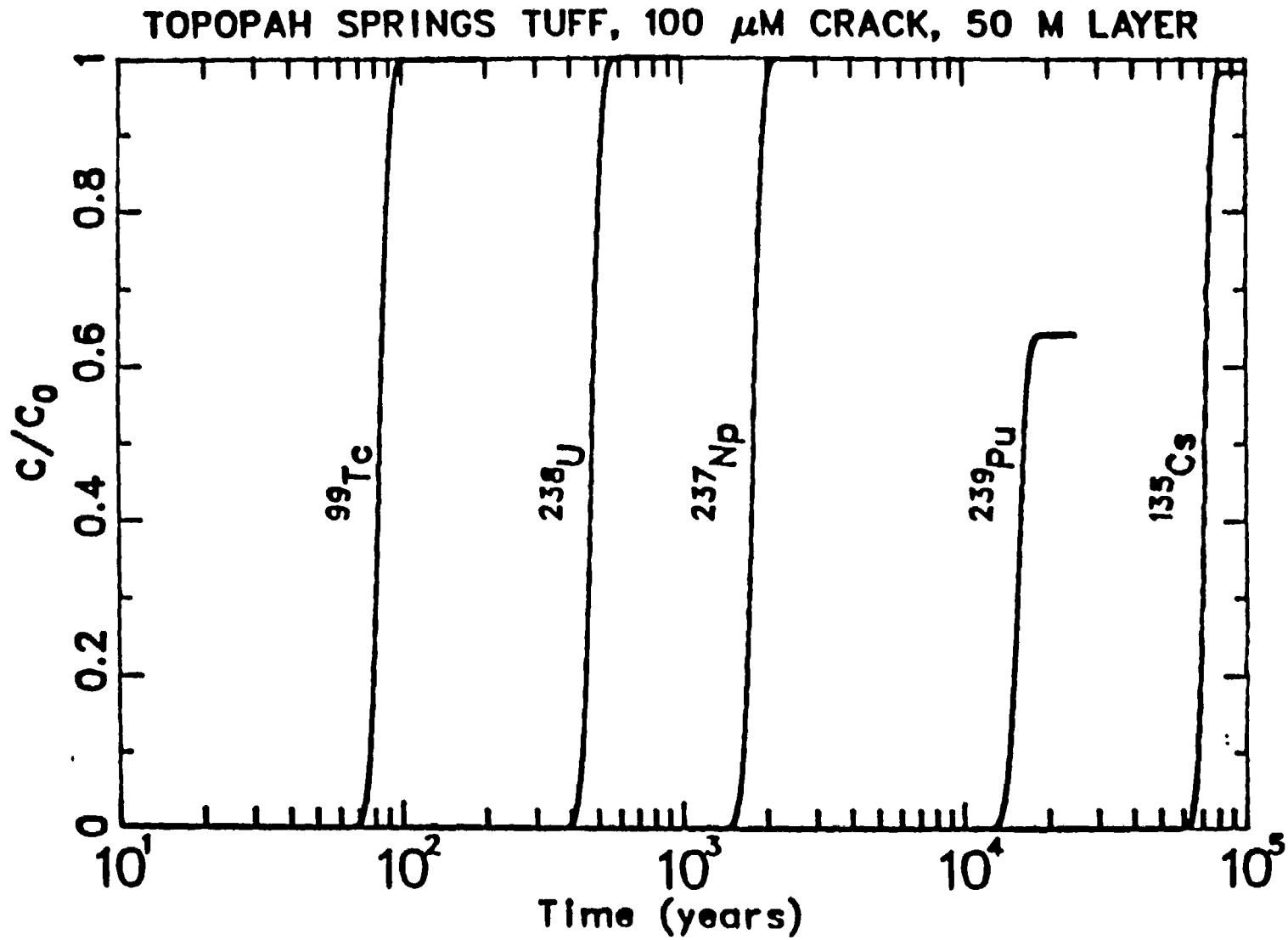


Fig. 17. Concentration histories at the bottom of a 50 m layer of Topopah Springs tuff for injection at the top of the layer in a 100 micron crack.

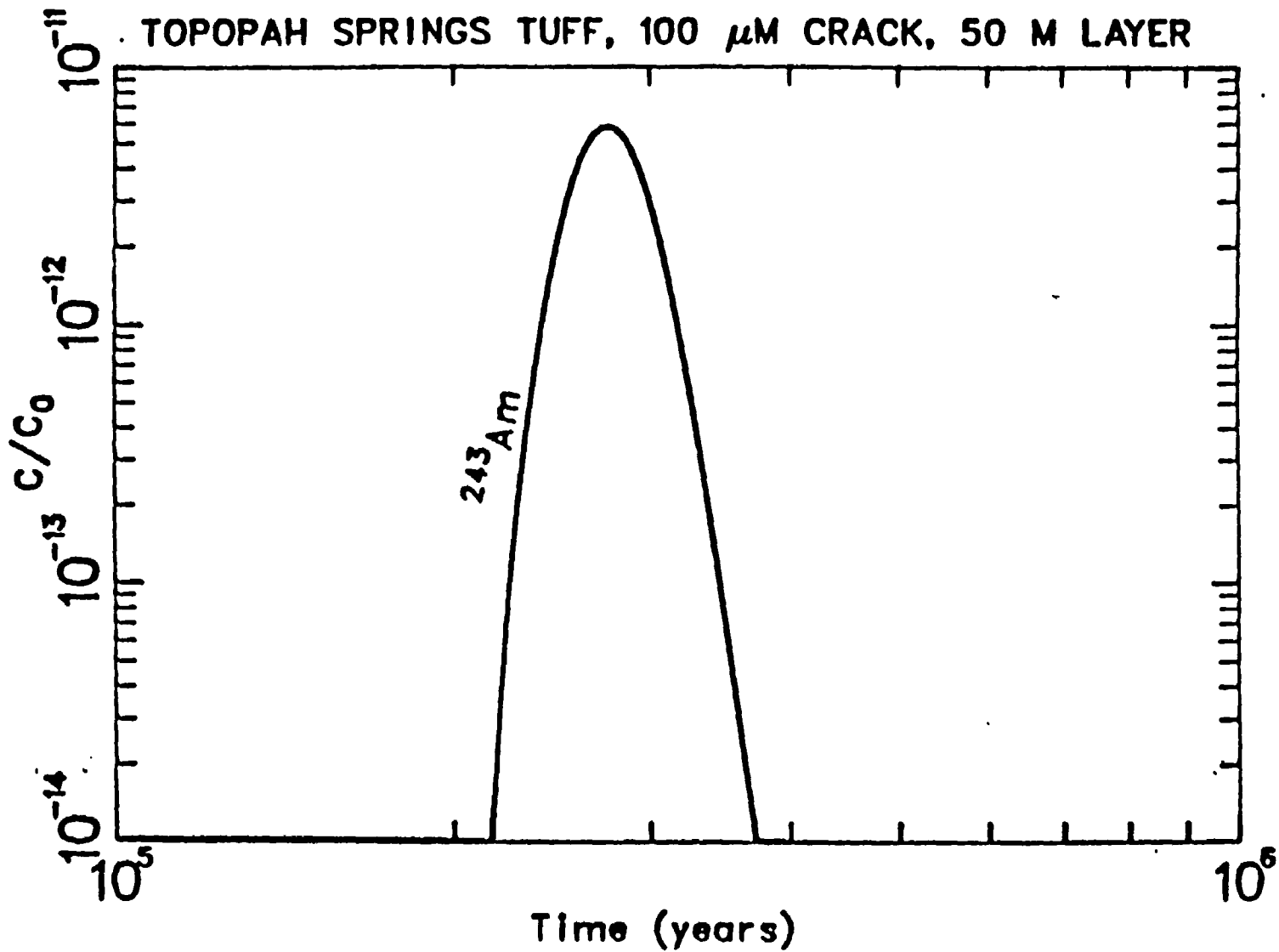


Fig. 18. Concentration history for ²⁴³Am at the bottom of the 50 m Topopah Springs tuff layer.

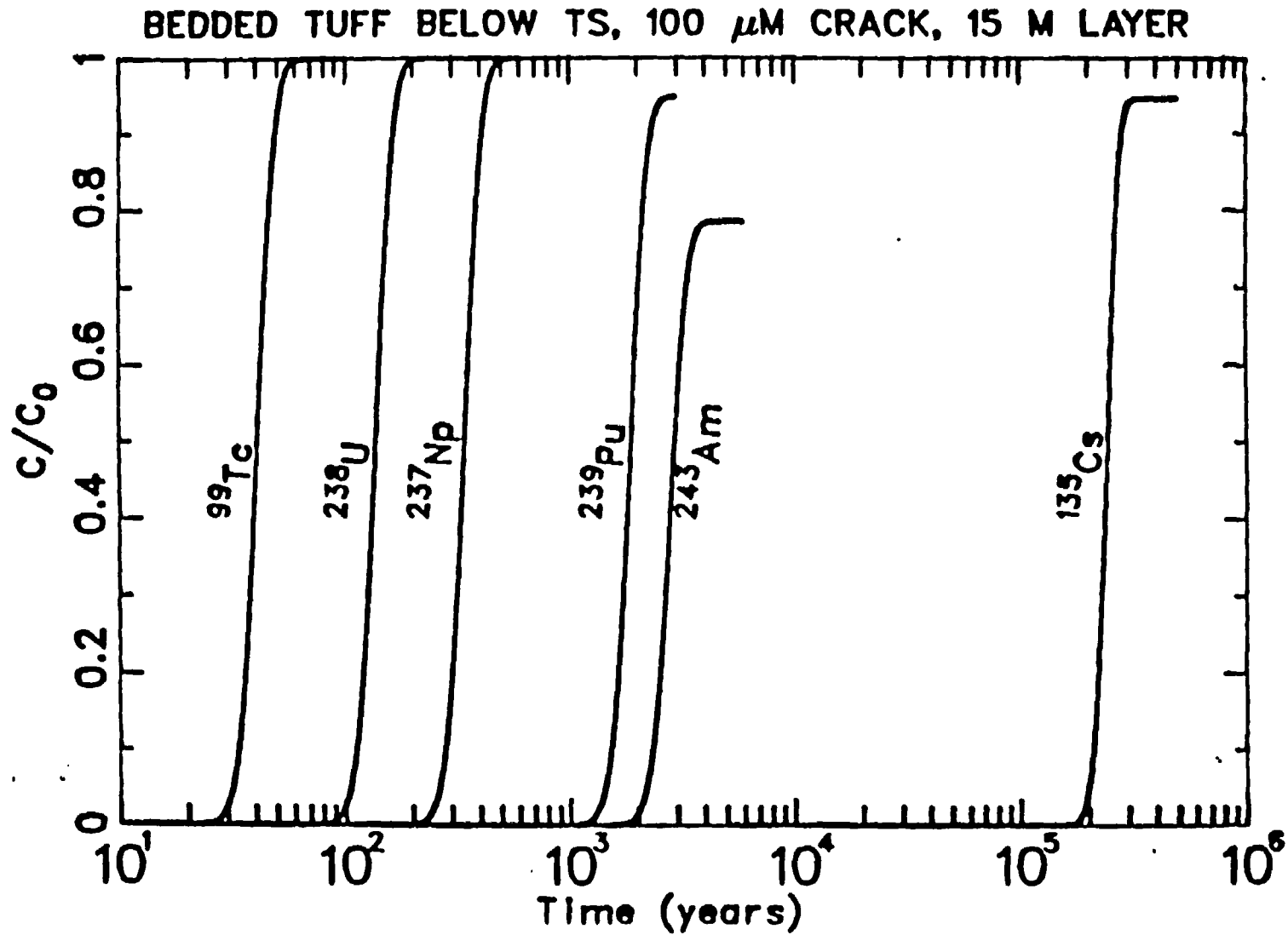


Fig. 19. Concentration histories at the bottom of the 15 m thick bedded tuff just below the Topopah Springs tuff for injection at the top of the layer in a 100 micron crack.

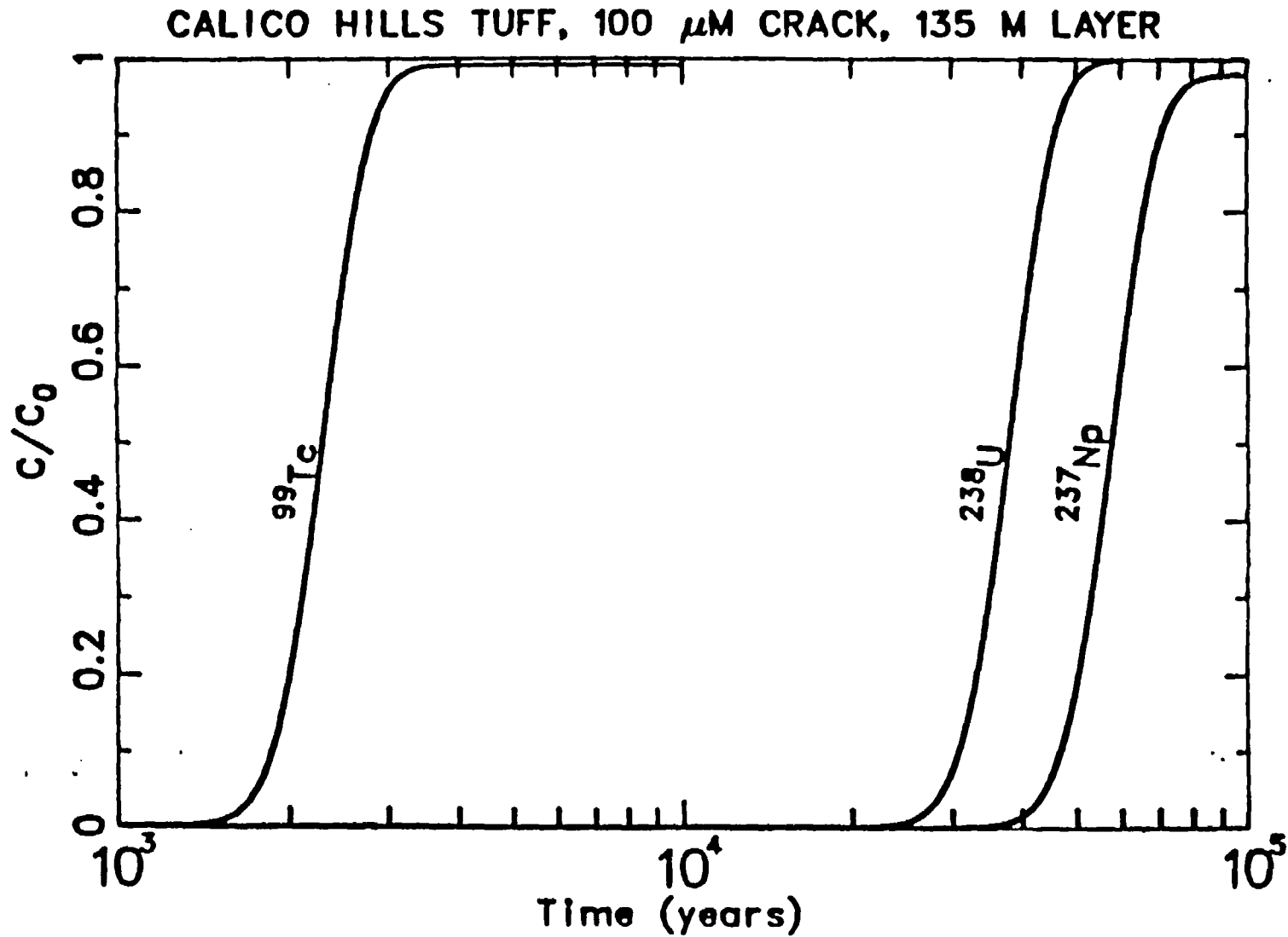


Fig. 20. Concentration histories at the bottom of the 135 m thick Calico Hills Tuff layer for injection at the top of the layer in a 100 micron crack.

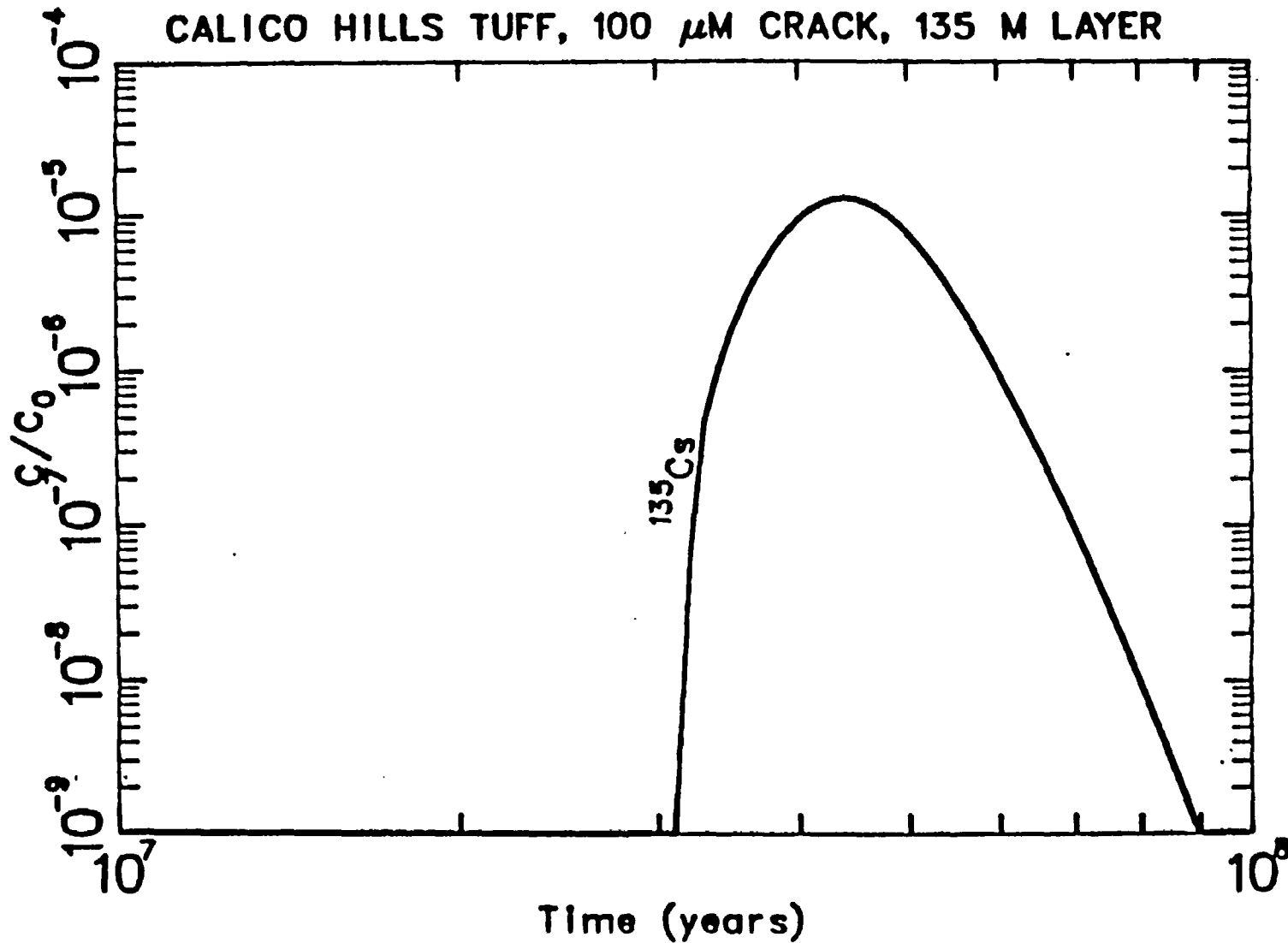


Fig. 21. Concentration history for ^{135}Cs at the bottom of the T1t layer for injection at the top of the layer in a 100 micron wide crack.

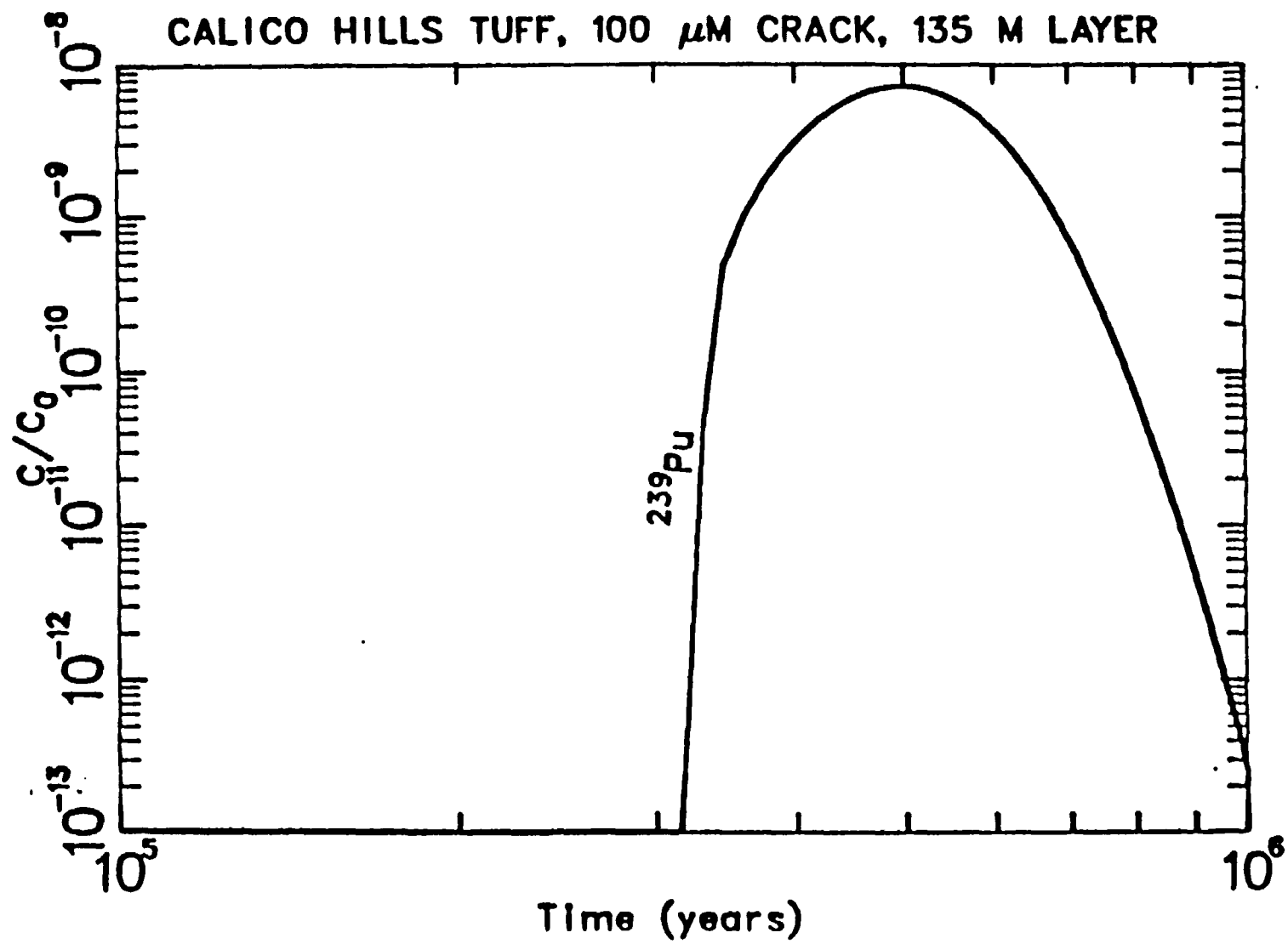


Fig. 22. Concentration history for ^{239}Pu at the bottom of the Calico Hills Tuff layer for injection at the top of the layer in a 100 micron crack.

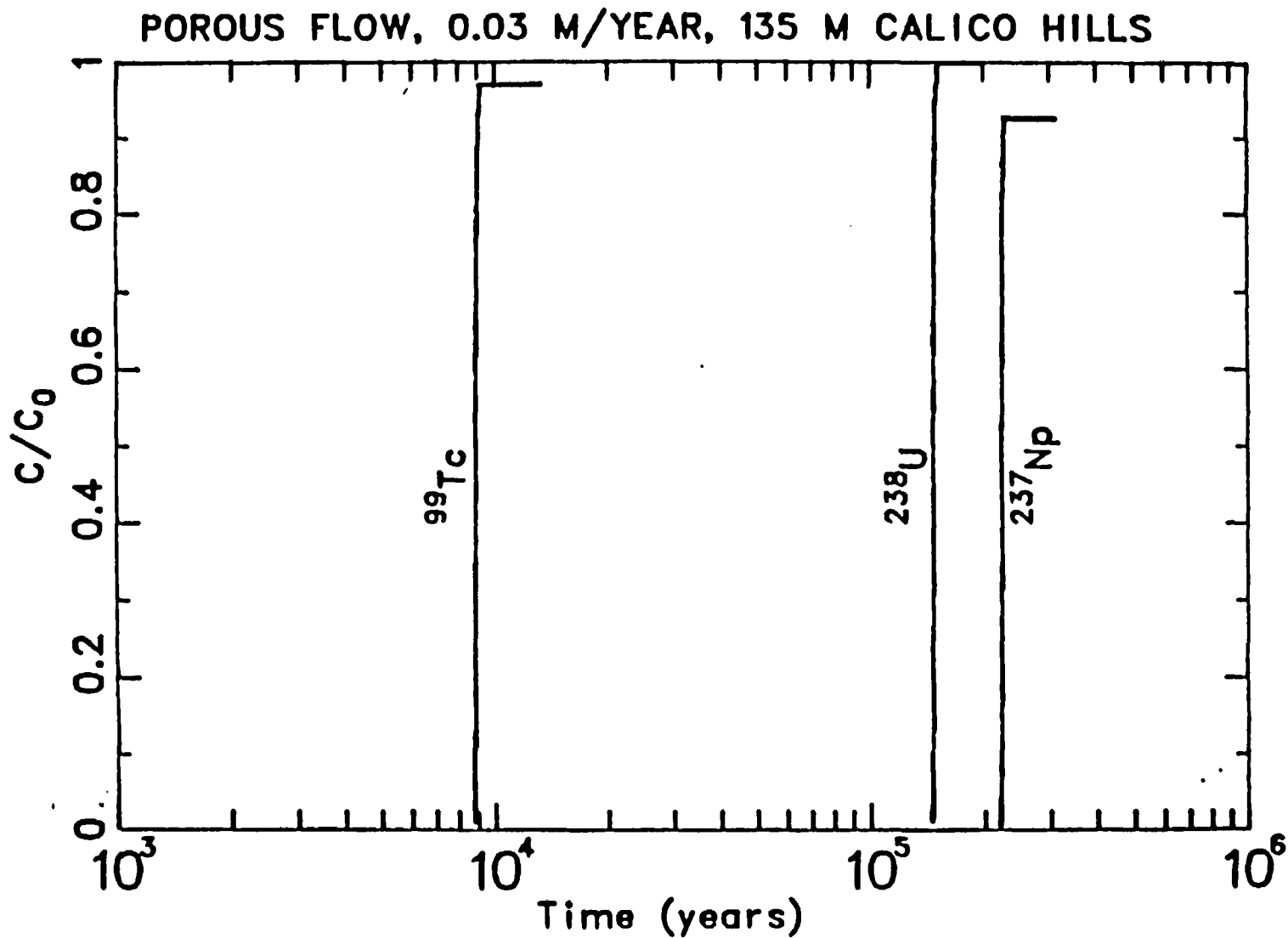


Fig. 23. Concentration histories for ⁹⁹Tc, ²³⁸U and ²³⁷Np at the bottom of the Calico Hills layer assuming porous flow only.

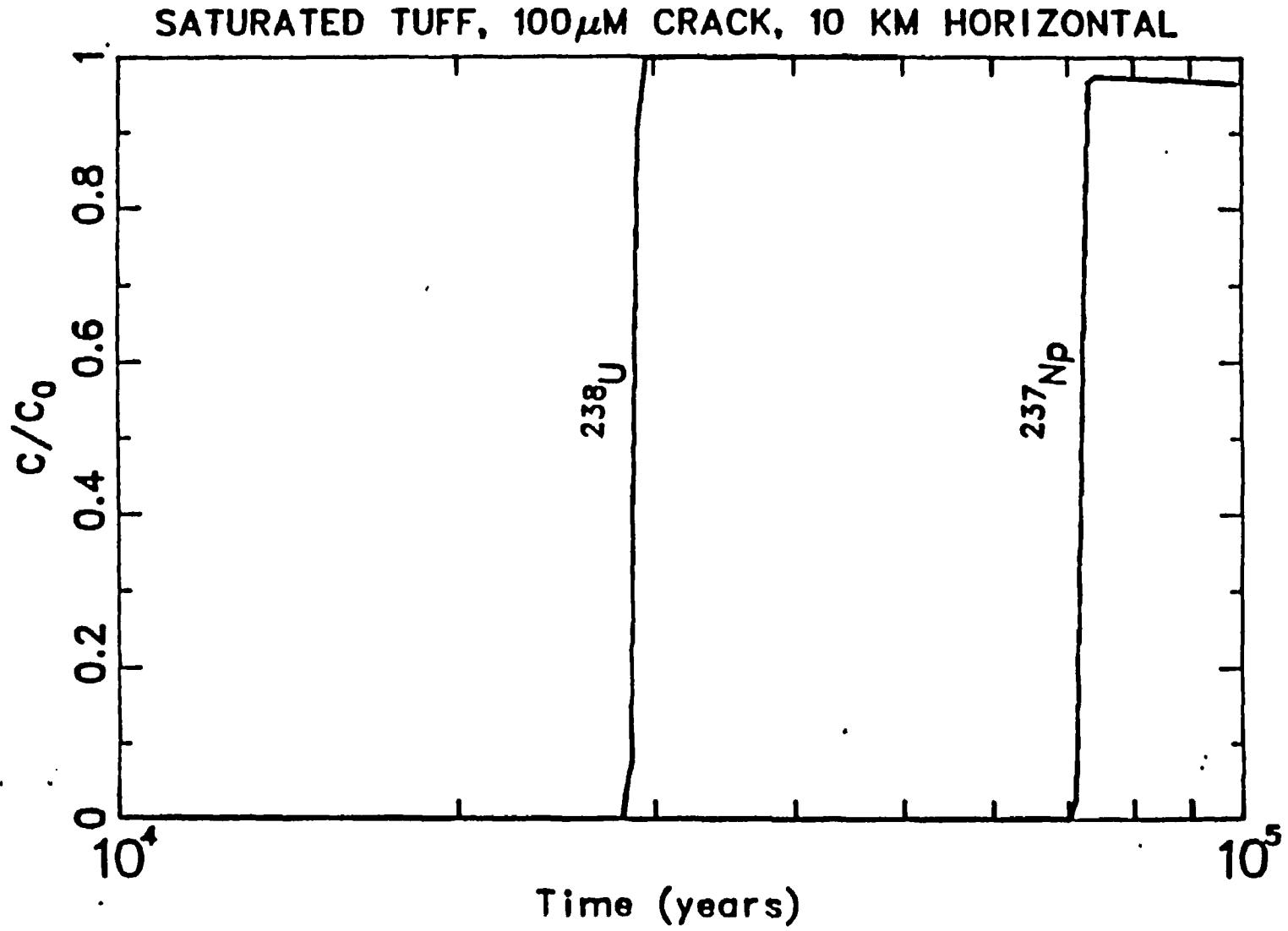


Fig. 24. Concentration breakthrough curves for ^{238}U and ^{237}Np at 10 km horizontal distance for injection into the water table below the repository location.

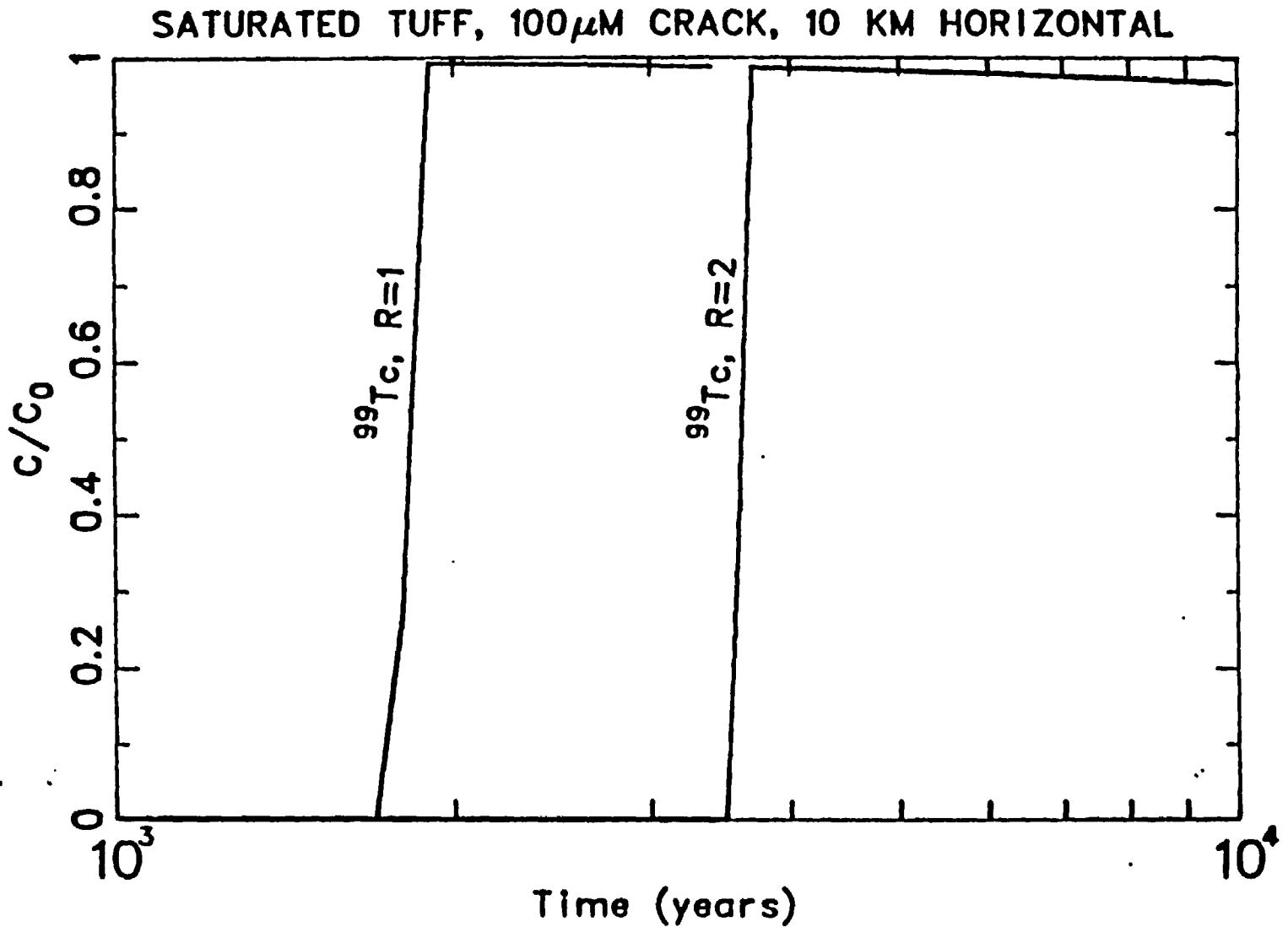


Fig. 25. Concentration breakthrough curves for ^{99}Tc at 10 km horizontal distance for injection into the water table below the repository location. Curve R=1 is for no retardation at all, while curve R=2 is with slight retardation.

are assuming fracture flow again. Total travel time for each nuclide is found by adding the transit times for each unit.

The fact that the radionuclides have varying affinities for adsorbing to tuffs has a beneficial effect. Their effective transport rates will be spread over a large range; thus, instead of having a single wave of high-curie-content water reaching the accessible environment, several pulses, each of considerably lower radioactivity, will break through over a very long time scale.

The concentration curves in Figs. 17-25 are shown for normalized or relative concentrations (C/C_0). Our results show how long it will take for various elements to traverse different geologic formations. Any decrease in amplitude is due to radioactive decay. To calculate the absolute concentration levels and cumulative curie release, we must know the solubilities of the radionuclides and the release rates. Solubilities have been estimated in Ref. 19. Many of the radionuclides have low solubilities; ^{99}Tc , however, has a large solubility¹⁹ in well J13 water and is, therefore, limited by the dissolution rate of the waste form, which is a somewhat speculative number at this time. We do not go through the exercise here of estimating cumulative curie release because (1) our analysis predicts no release to the accessible environment in less than 10,000 years if porous flow is the transport mechanism in the lower clastic unit and (2) the only element which may break through in 10,000 years or a little more is ^{99}Tc and the curie release for it depends on the waste form and its unknown dissolution rate.

Factors not considered here which may affect these results include: (1) fracture fill, (2) nonequilibrium adsorption, (3) colloid transport, and (4) geometric dispersion. Many fractures contain clay and other minerals which will affect the sorption and diffusion of radionuclides. We have allowed no sorption in fractures in this analysis, only in the rock matrix. Here equilibrium sorption has been assumed. However, nonequilibrium effects may occur in fractures for many of the radionuclides but only if rapid fracture flow occurs.

Transport via formation of colloids may be important. However, colloid formation is sensitive to the chemical composition of the water and much experimental work is needed yet to describe colloidal behavior for the radionuclides of concern. Finally, spatial spreading and consequent dilution have been ignored.

These effects will be treated in the next series of calculations. Decay chain effects have also been ignored. The calculations represent a parametric study because of the different R values and different layer thicknesses.

C. Heat Load Effect

Radioactive decay releases large amounts of thermal energy. This heat load can have a significant effect on the surrounding environment. The heat load estimated for a high-level waste repository in Yucca Mountain is around 50 kw/acre, and could be expected to last for perhaps a few hundred years. The local unsaturated hydrology could be strongly affected by this energy influx. Moreover, changes in the hydrologic state can in turn influence the rate of breakdown of a canister. For example, if heat loading were to cause boil off of pore water near each canister, the atmosphere surrounding a canister could change from wet air to a dry, steam-rich, oxygen-poor atmosphere, which would affect the canister's degradation. In addition, these temperature and hydrologic changes could alter the composition of the surrounding tuff.

In this section we present a few calculations which begin to address these matters. The results of our calculations suggest the following scenario.

Near the repository, water will boil off and move outward, to condense in cooler regions. The more or less uniform ambient saturation field will change to a dried-out region near the repository and a virtually fully saturated region at some distance. A convective or circulating flow pattern may develop if the effective Rayleigh number is large enough. This behavior will be reduced if the repository is kept well ventilated. At late times when the radionuclides have decayed and the region cools, the fully saturated regions above the repository will flow down fairly rapidly to and through the repository, providing a vehicle of relatively short duration for accelerated transport for any waste not contained.

The presence of fractures can alter the thermally induced flow patterns. Many small cracks will increase the overall permeability, making convection more likely. A few large, conducting cracks may prevent convective circulation, but would provide a path for fairly rapid movement of water and vapor and air. Other factors could also be important such as

thermomechanical behavior of cracks. Heat may close cracks or open them depending on the mechanical properties of the host rock.

A few calculations of heat loading in Topopah Spring tuff have been made to estimate the induced flow field. The material properties²⁰ used for tuff are those of Table III. A region 35 m in radius and 150 m high was considered. The horizontal cross-sectional area is about one acre. Lateral boundary conditions are zero gradient. Top and bottom conditions are kept at ambient. A heat load of 50 kw/acre was emplaced, centered at 250 m depth. The power rating is assumed to decay linearly to 0 in two centuries. Calculations were made with the WAFE code which computes one- or two-dimensional transient two-phase (air, vapor, and water) flow with heat transport. Saturations can range anywhere from 0 to 1 inclusive. Condensation and evaporation are treated. Details of this model along with examples of verification and validation are available in a separate report.³

Two calculations are considered. In the first, the tuff is uniform and the energy is deposited into a 2-m by 6-m room. In the second, the energy is spread uniformly across the cylinder, that is, in a region 2 m high by 35 m radius. No allowances for ventilation are made in these computations. Also, no thermomechanical effects are included.

Results of these simulations are presented in Figs. 26 through 39. Contour plots of temperature and water saturation and vector plots of water velocity and air and vapor velocity are shown in Figs. 26-33 at the times indicated. In Run 1, high temperatures are generated because of the small source volume and lack of ventilation. The dry region extends about 10 m around the repository. Some convective circulation occurs because the permeability used is large enough that convection is a more efficient energy transport mechanism than conduction. There also appears to be some interference from the ambient downward water flow. In Run 2, with lower energy density, the boiling is somewhat slower to develop, but the lack of divergence in this one-dimensional calculation allows eventually a region about 20 m above and about 30 m below the repository to dry out. Figures 34-39 show vertical profiles of normalized temperature and water saturation on axis at several times after introduction of the heat load. Above the repository, a fully saturated region has developed. The heat-induced flow is going against gravity and the natural downward matrix flow. Below the repository, saturation is elevated, but does not reach 100% because the

TABLE III
 PROPERTIES OF TOPOPAH SPRING TUFF

Material Property	Value
Saturated Permeability (darcys) (cases 1,2)	10^{-3}
Relative Permeabilities, (k_w, k_g)	$s^{3+2/\lambda}, (1-s)^{1+2/\lambda} (1-s)$
Porosity	0.12
Saturation (Z)	60
Thermal Conductivity (erg/ $^{\circ}$ C s)	1.6×10^5
Specific Heat (erg/gm $^{\circ}$ C)	10^7
Temperature ($^{\circ}$ C)	30
Grain Density (gm/cm ³)	2.6
Pore Size Index (λ)	3.0

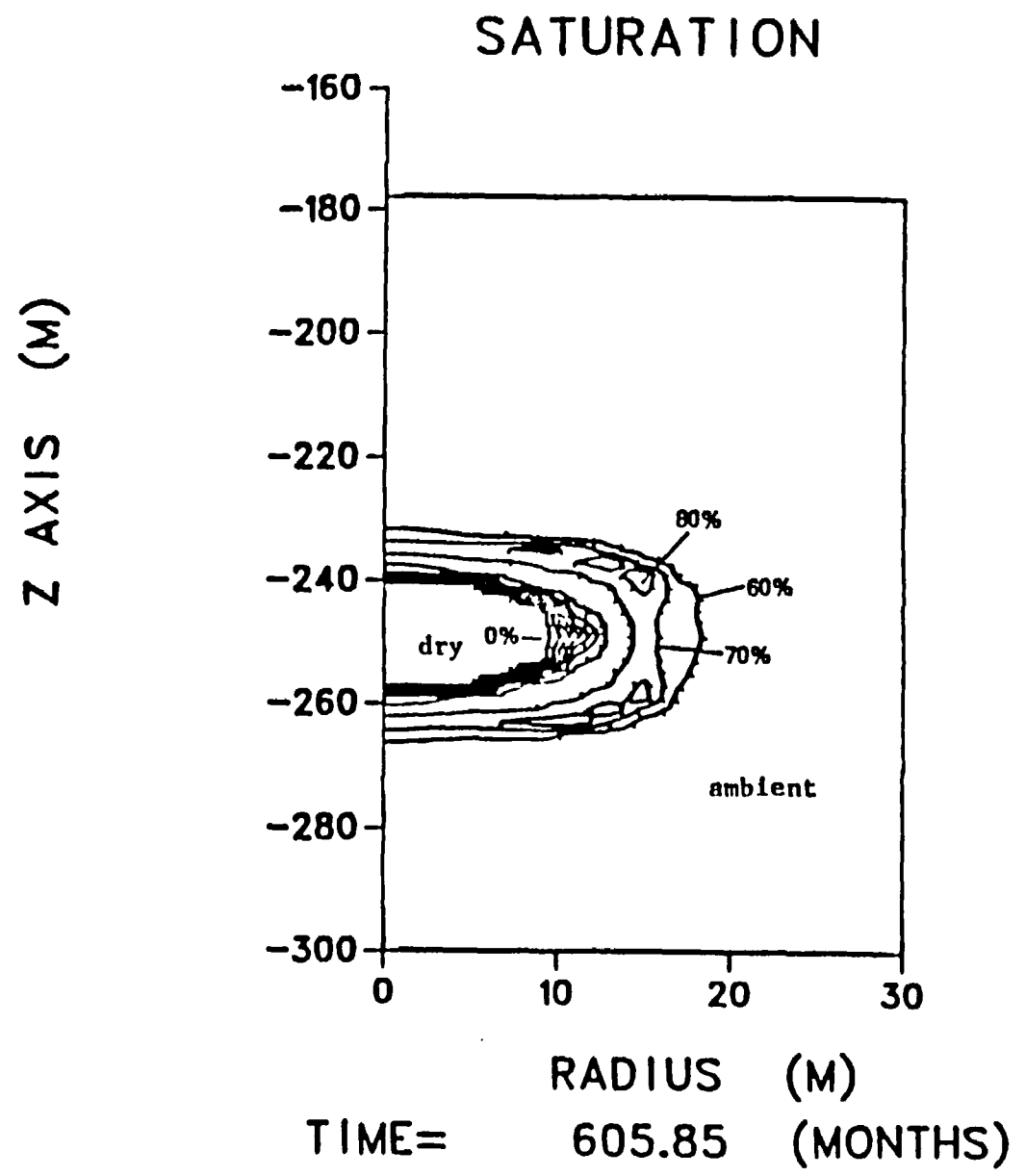
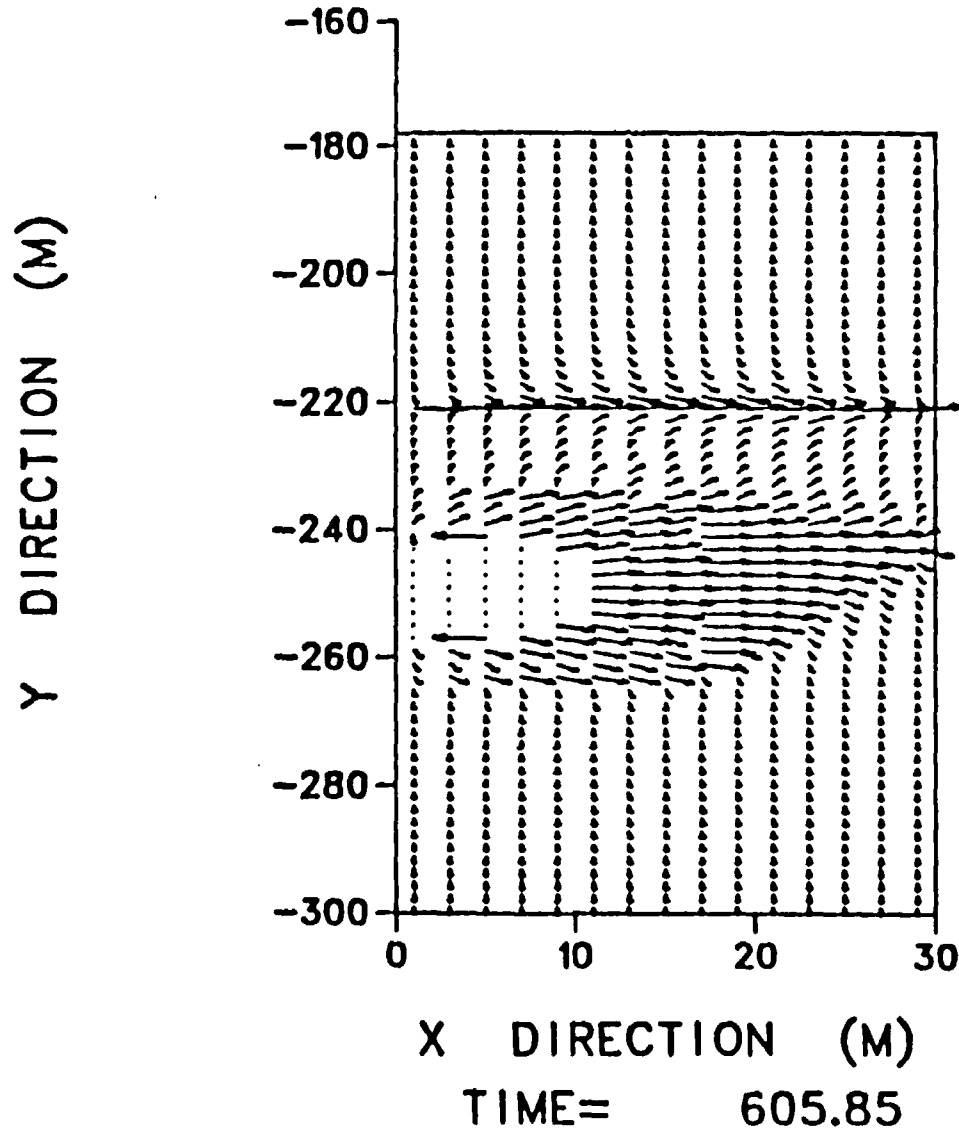


Fig. 26. Water saturation contours 50 years after emplacement of heat load.

LIQUID VELOCITY

Z LEVEL = 1



-41-

Fig. 27. Water velocity vectors 50 years after emplacement.

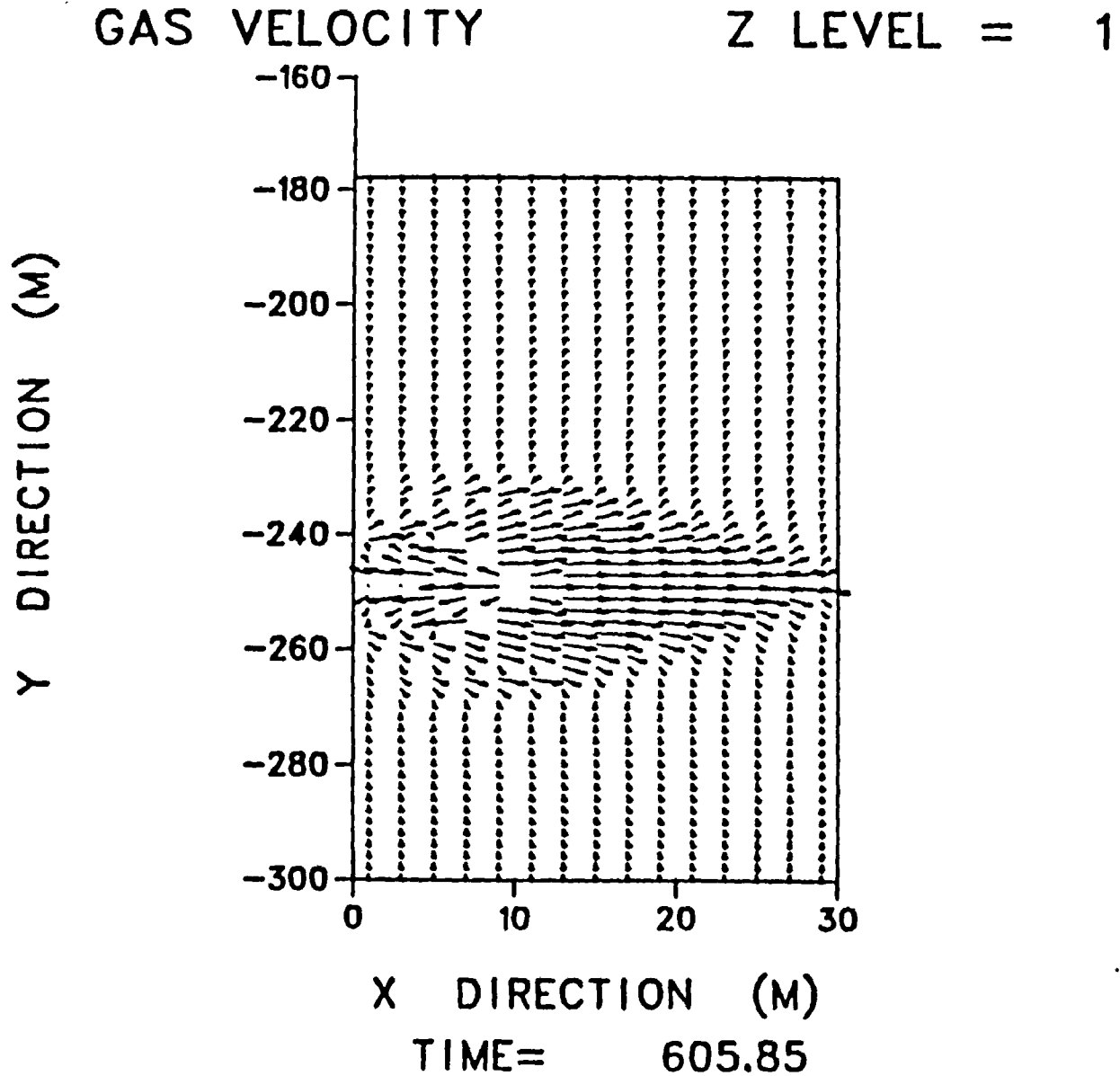


Fig. 28. Vapor + air velocity vector field at 50 years after emplacement. A convective pattern appears to be developing.

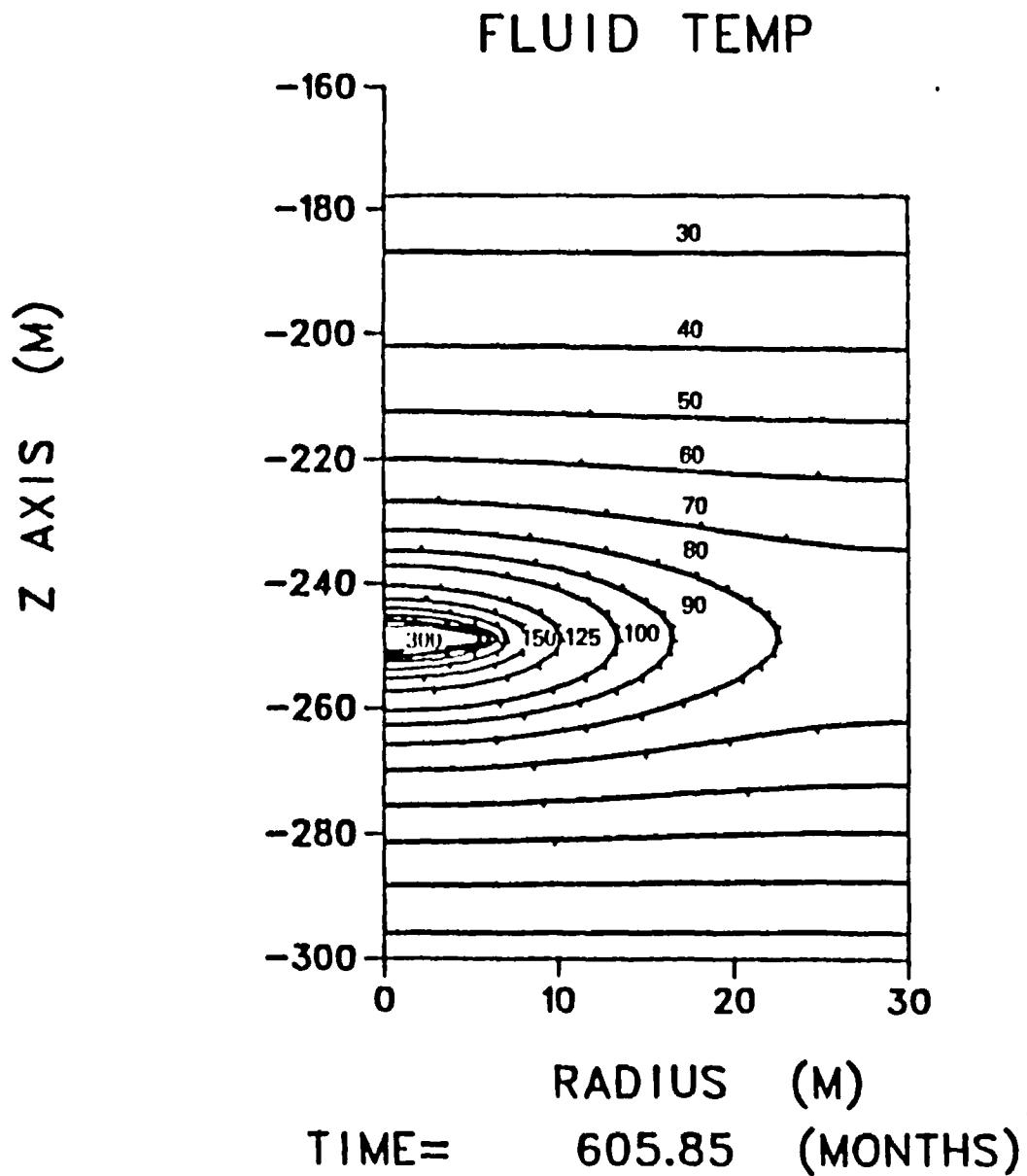


Fig. 29 Temperature contours 50 years after emplacement of the heat load.

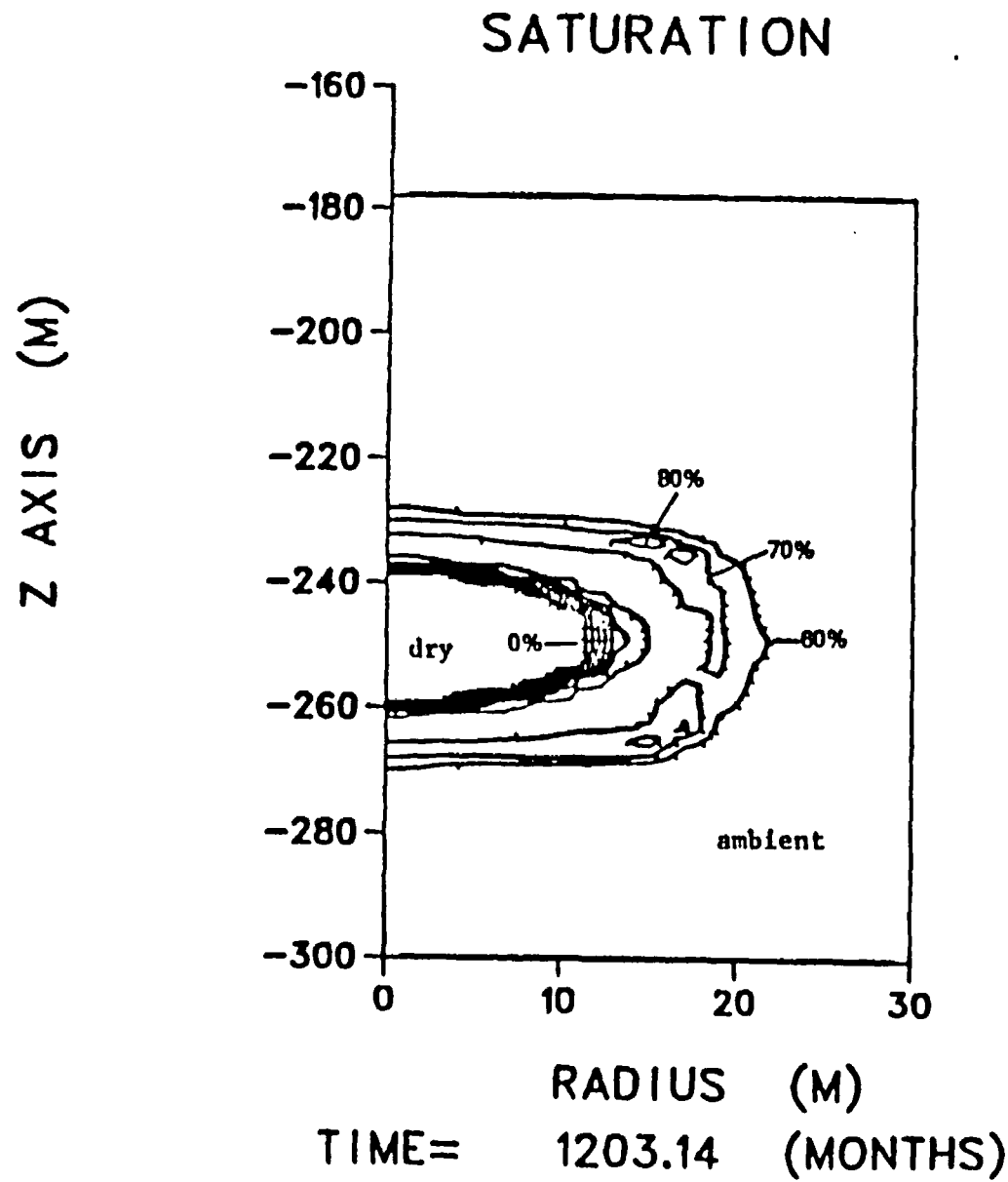
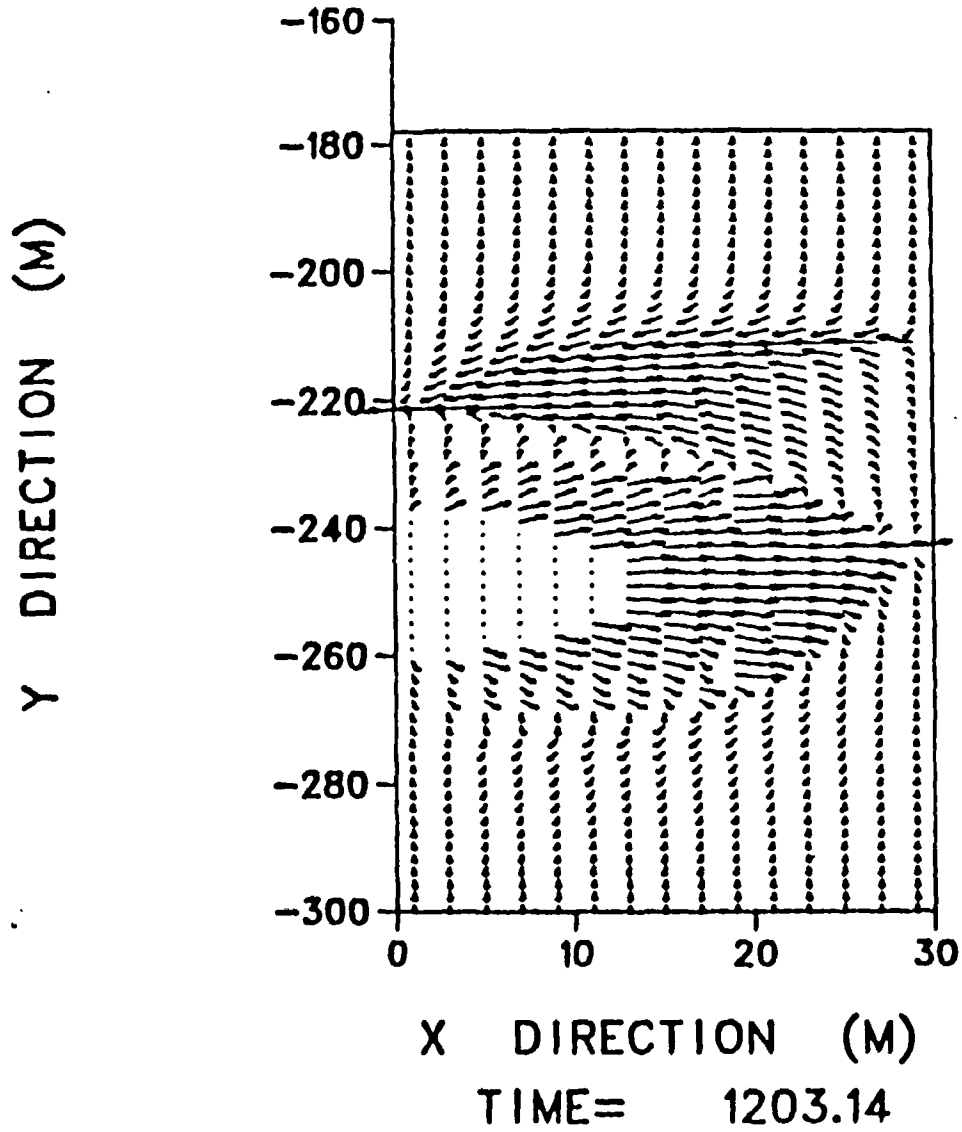


Fig. 30. Water saturation contours 100 years after emplacement of the heat load. Water is dripping around the side of the saturated region.

LIQUID VELOCITY

Z LEVEL = 1



-45-

Fig. 31. Water velocity field 100 years after emplacement of the heat load.

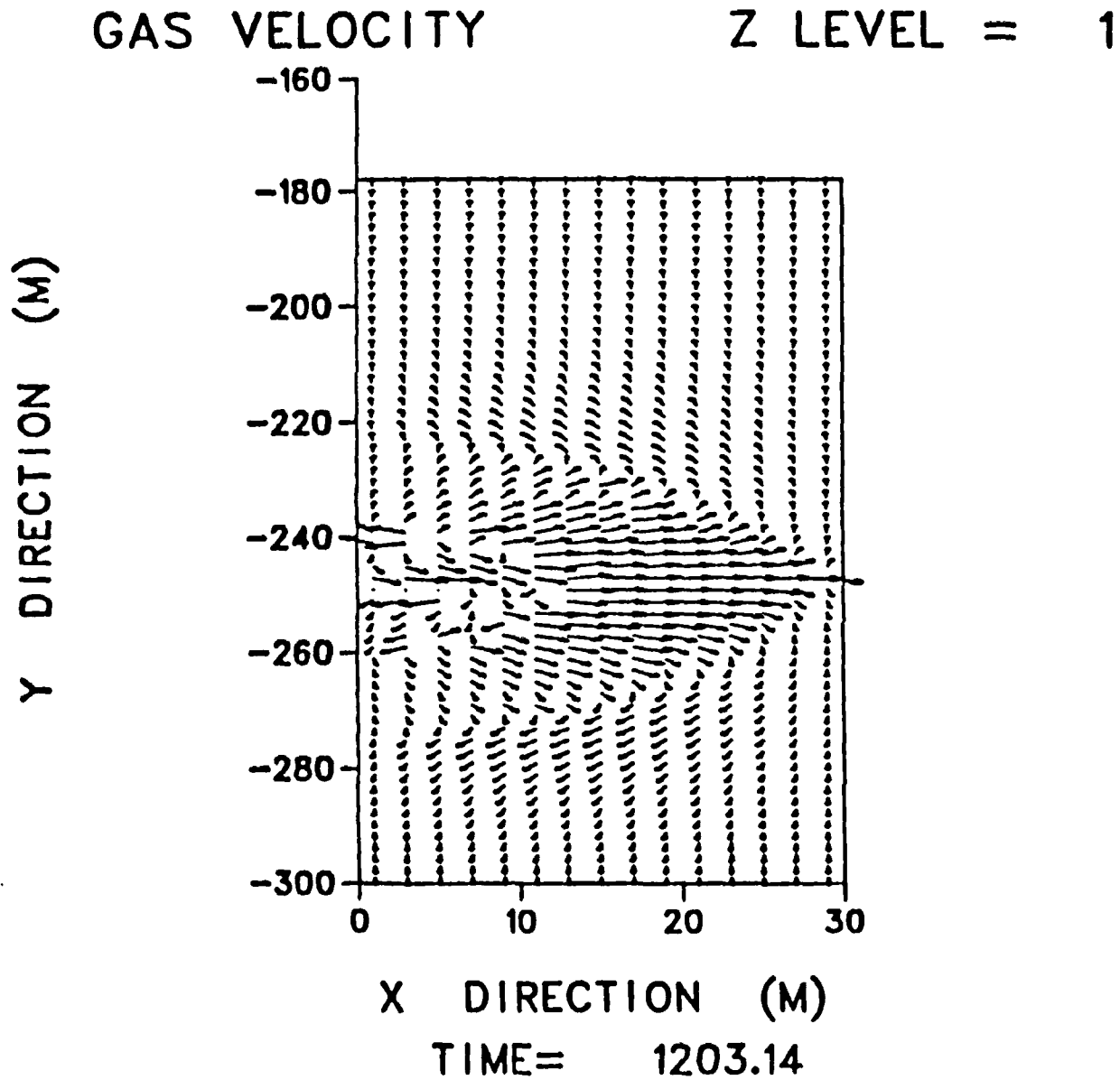


Fig. 32. Vapor + air velocity field 100 years after heat load emplacement. Note the complicated flow pattern in and inside the high saturation region.

-47-

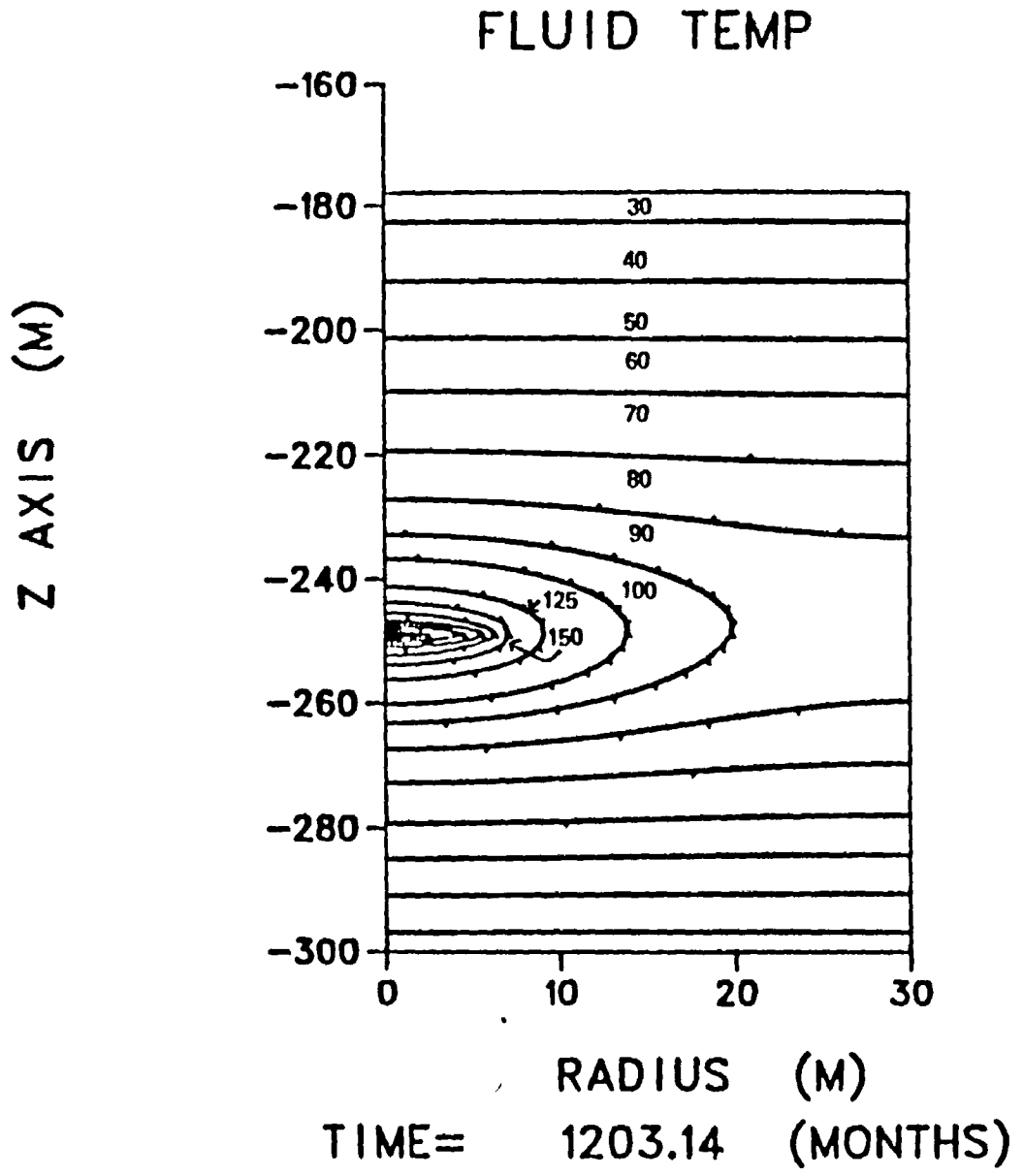
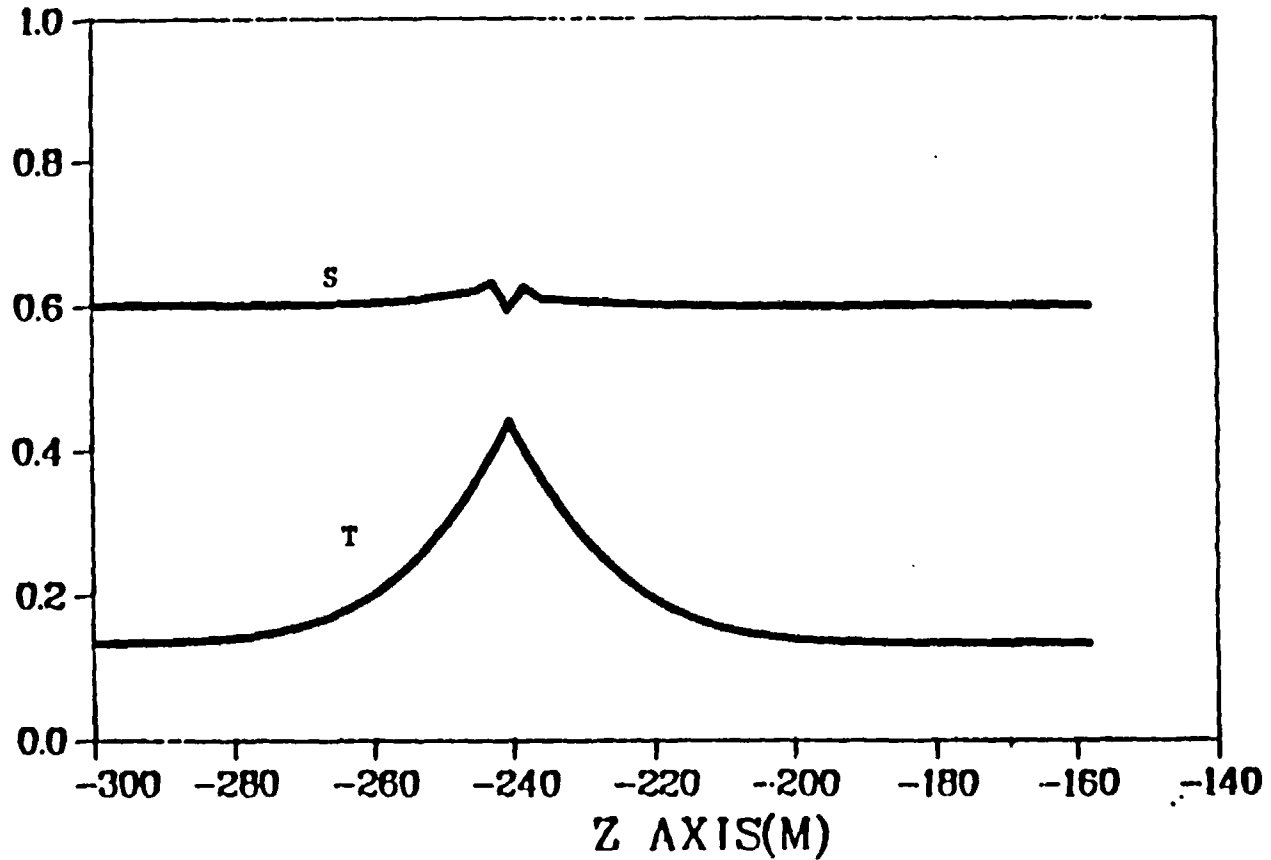


Fig. 33 Temperature contours 100 years after heat load emplacement.

NORMALIZED VARIABLE

CONVECTIVE FLOW IN TOPOPAH SPRINGS TUFF - 138 WATT/SQ.M HEAT LOAD
ALONG CONSTANT R(1)- 100 TIME= 9.99 (YEARS)

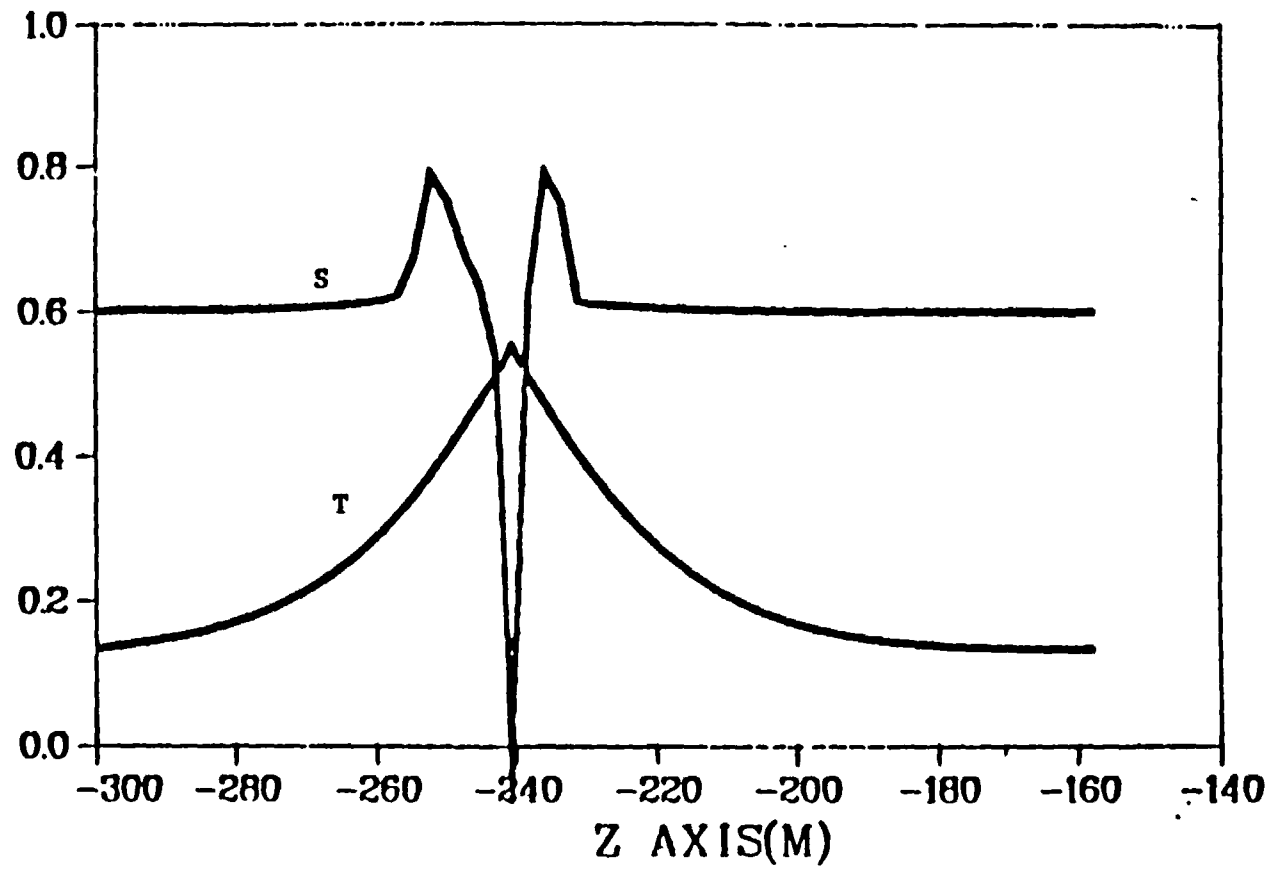


FLUID TEMP(CELSIUS)	MIN= 0.	RANGE= .225E+03
SATURATION	MIN= 0.	RANGE= .100E+01

Fig. 34. Profiles of temperature (T) and saturation (S) vs. depth on the centerline at 10 years.

CONVECTIVE FLOW IN TOPOPAH SPRINGS TUFF - 138 WATT/SQM HEAT LOAD
 ALONG CONSTANT R(I)= 1.00 TIME= 19.97 (YEARS)

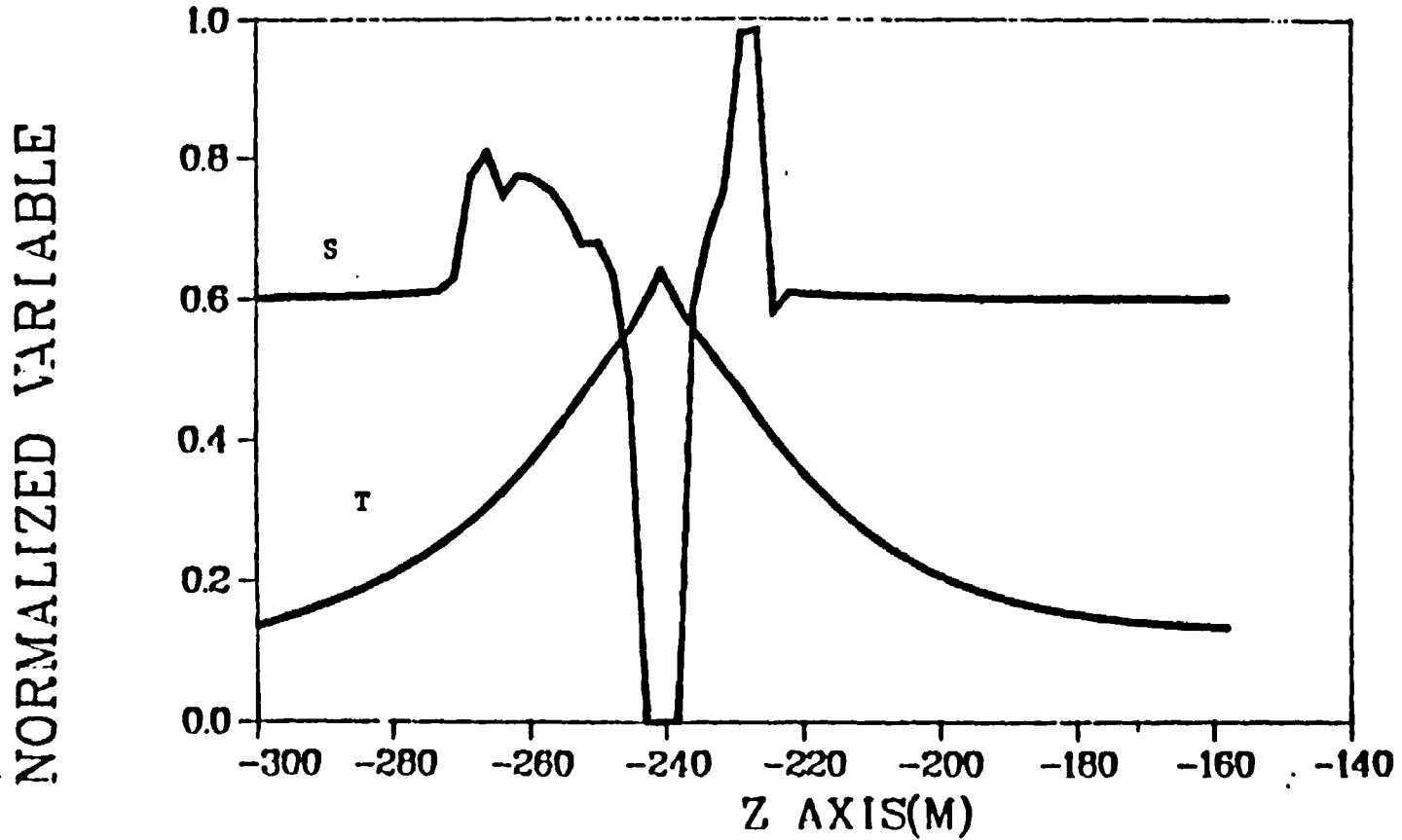
NORMALIZED VARIABLE



FLUID TEMP(CELSIUS) MIN= 0. RANGE= .225E+03
 SATURATION MIN= 0. RANGE= .100E+01

Fig. 35. Profiles of temperature (T) and saturation (S) vs. depth on the centerline at 20 years.

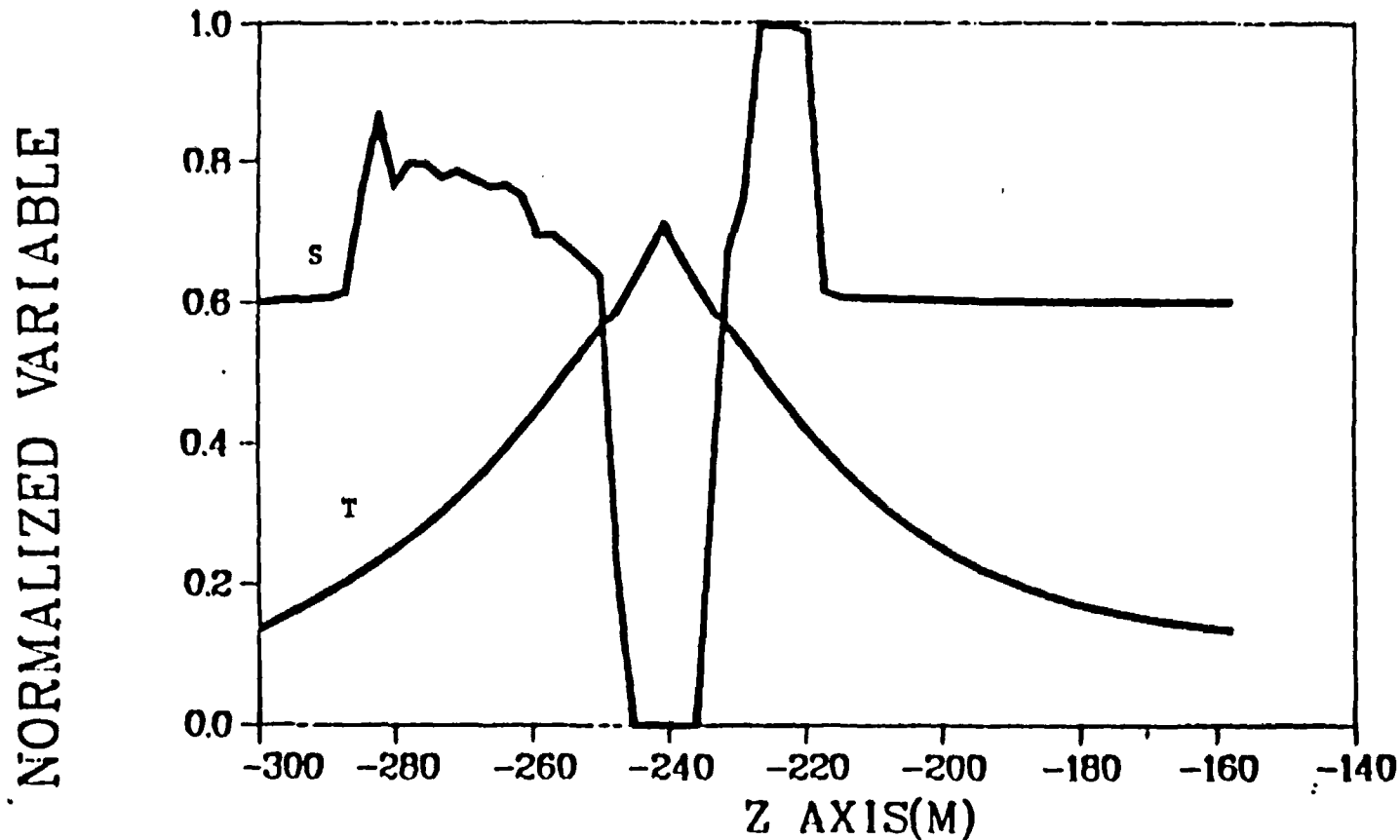
CONVECTIVE FLOW IN TOPOPAH SPRINGS TUFF - 136 WATT/SQ.M HEAT LOAD
ALONG CONSTANT R(I)= 100 TIME= 29.95 (YEARS)



FLUID TEMP(CELSIUS) MIN= 0. RANGE= .225E+03
SATURATION MIN= 0. RANGE= .100E+01

Fig. 36. Profiles of temperature (T) and saturation (S) vs. depth on the centerline at 30 years.

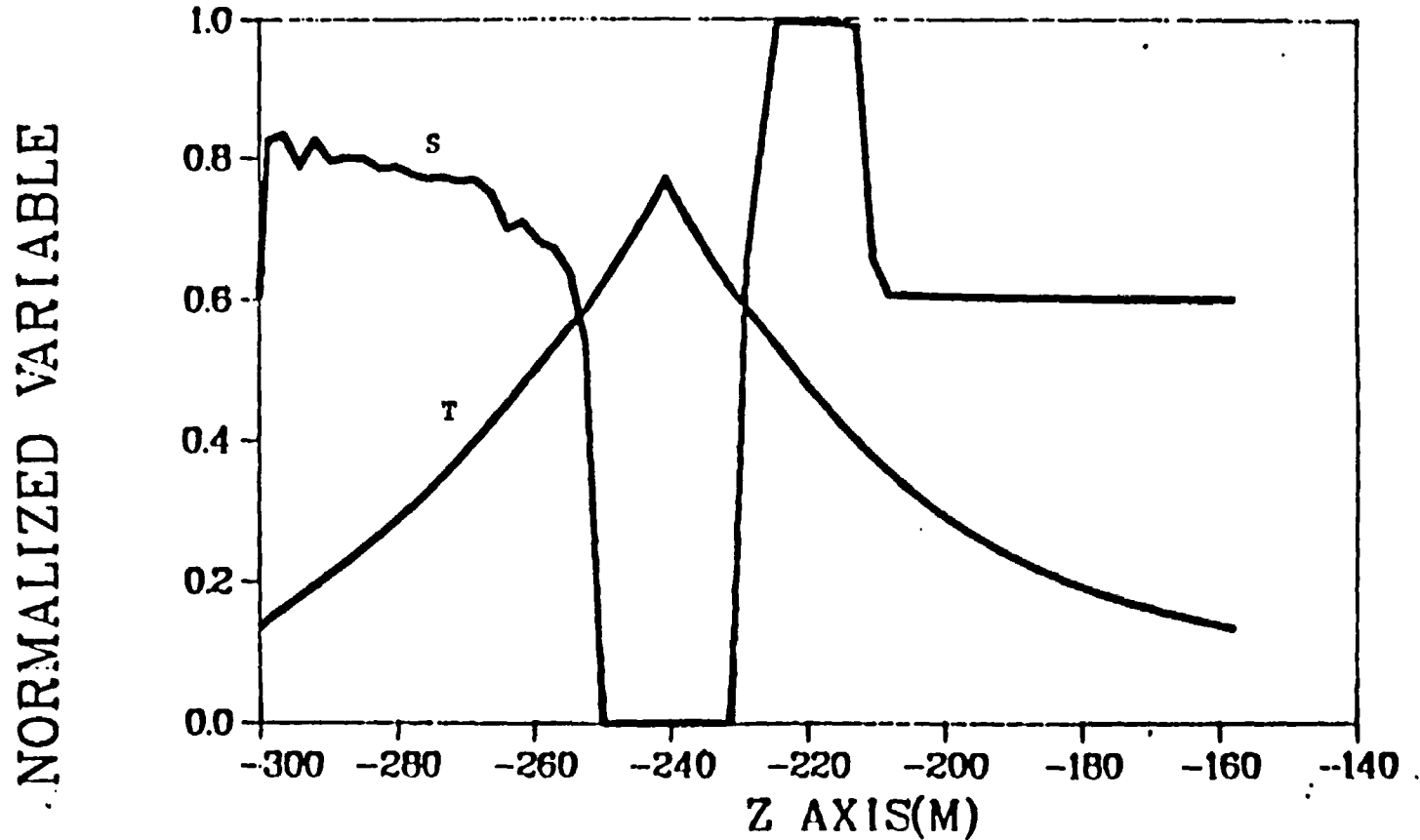
CONVECTIVE FLOW IN TOPOPAH SPRINGS TUFF - 138 WATT/SQM HEAT LOAD
ALONG CONSTANT R(1)= 1.00 TIME= 39.93 (YEARS)



FLUID TEMP(CELSIUS)	MIN= 0.	RANGE= .225E+03
SATURATION	MIN= 0.	RANGE= .100E+01

Fig. 37. Profiles of temperature (T) and saturation (S) vs. depth on the centerline at 40 years.

CONVECTIVE FLOW IN TOPOPALII SPRINGS TUFF - 138 WATT/SQ.M HEAT LOAD
ALONG CONSTANT R()= 1.00 TIME= 49.93 (YEARS)

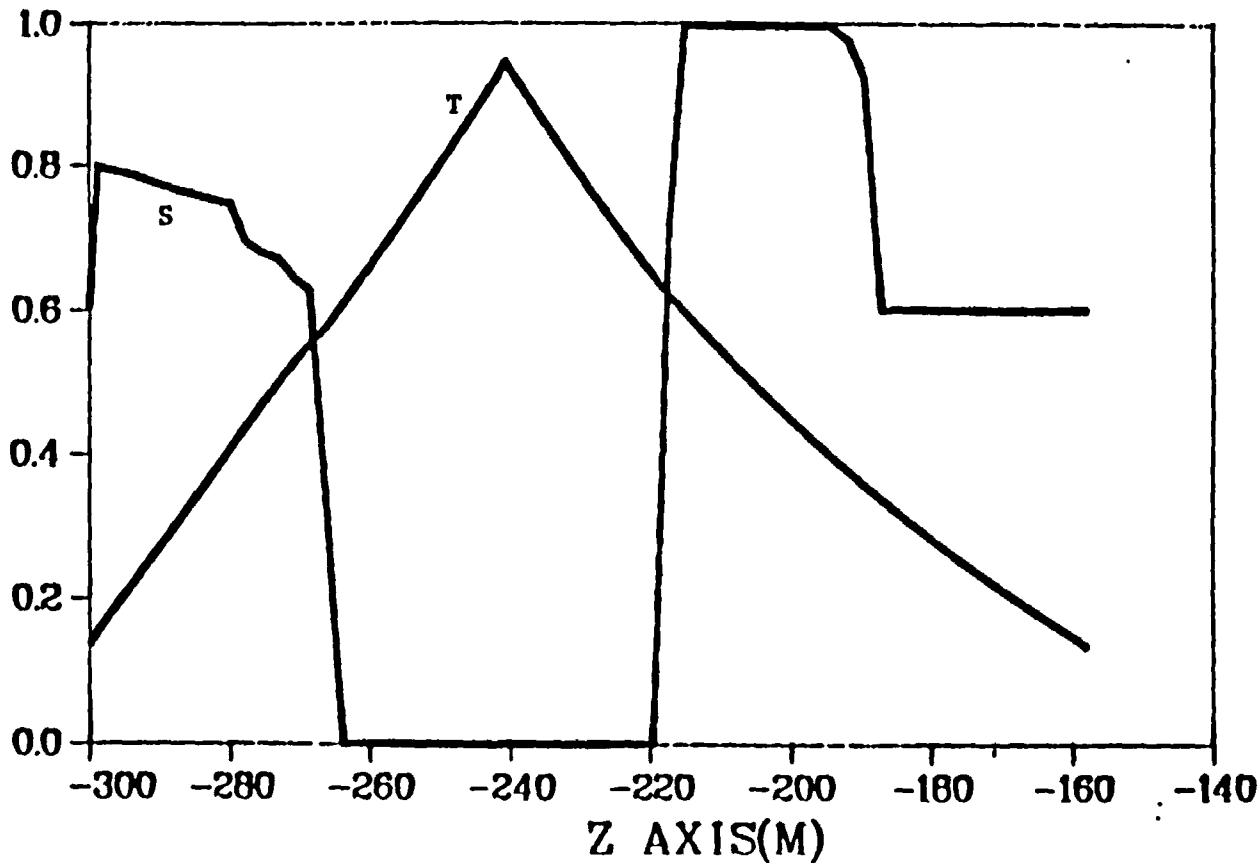


FLUID TEMP(CELSIUS) MIN= 0. RANGE= .225E+03
SATURATION MIN= 0. RANGE= .100E+01

Fig. 38. Profiles of temperature (T) and saturation (S) vs. depth on the centerline at 50 years.

NORMALIZED VARIABLE

CONVECTIVE FLOW IN TOIOPAH SPRINGS TUFF - 138 WATT/SQ.M HEAT LOAD
ALONG CONSTANT R(1)=- 1.00 TIME= 99.85 (YEARS)



FLUID TEMP(CELSIUS) MIN= 0. RANGE= .225E+03
SATURATION MIN= 0. RANGE= .100E+01

Fig. 39. Profiles of temperature (T) and saturation (S) vs. depth on the centerline at 100 years.

heat-induced flow is moving with the natural flow and gravity. The heating effects extend a very large distance, on the order of 100 m.

The dry-out region is larger in Run 2 than in Run 1 because of lack of divergence. In this one-dimensional case, pressure build up does not experience the cylindrical divergence of Run 1 and pressure remains higher, pushing water faster.

In both Runs 1 and 2, the effective tuff permeability is fairly large to simulate the effect of ubiquitous fractures. Also, the matrix water potential and relative permeability curves are very rough guesses and may be much too weak. The absolute numbers shown should be considered preliminary because of the large uncertainties in property values. However, the qualitative behavior is interesting and shows that at least under some conditions a substantial change in the local water conditions could occur.

In these calculations, as heat diffuses away from the source, water boils. The water vapor then is driven outward until it reaches cooler rock and condenses. Temperatures are buffered by the boiling process. Energy is going into boiling water rather than raising rock temperature. Peak temperatures at the wet edge of the boiling region are only about 140°C, considerably lower than peak waste temperature.

Factors which will reduce the size of the dry-out zone include strong matrix potential (which will act to draw water back into the dry region), rate of source heat decay (our assumed decay rate may be too slow), ventilation (we have assumed none), and low rock permeability.

Since Run 1 and Run 2 were computed, additional information has become available, and more computer calculations have been performed, two of which are briefly described below.

Two additional calculations (Runs 3 and 4) consider heat flow from a single waste canister. We consider only one-dimensional flow perpendicular to the canister axis. Heat load history was obtained from M. Revelli of the Lawrence Livermore National Laboratory. One calculation allows no venting while the other does.

For both calculations, material properties used are shown in Tables IV, V, and VI. The energy source is given in Table VII. For these preliminary one-dimensional runs, a uniform computational mesh was used, starting at the hole radius. Energy was deposited into the first zone of the computational mesh. For the no-venting case, no mass or energy was allowed to flow back

TABLE IV

MATERIAL PROPERTIES USED IN RUNS 3 AND 4

Saturated Permeability (darcys)	1.0×10^{-5}
Grain Density (gm/cm^3)	2.5
Porosity	0.12
Saturation	0.60
Specific Heat ($\text{ergs/gm} \cdot ^\circ\text{C}$)	0.689×10^7
Thermal Conductivity ($\text{ergs/cm} \cdot ^\circ\text{C} \cdot \text{s}$)	1.8×10^5

TABLE V
MATRIX POTENTIAL vs. SATURATION

<u>Saturation</u>	<u>Matrix Potential (bars)</u>
0.05	500.0
0.10	100.0
0.20	60.0
0.60	10.0
0.80	1.0
0.90	0.1
0.999	0.05
1.0	0.

TABLE VI

RELATIVE PERMEABILITY vs. SATURATION

<u>Saturation</u>	<u>Air Rel. Perm.</u>	<u>Water Rel. Perm.</u>
0.	1.00	0.
0.018	0.96	1.8×10^{-16}
0.036	0.93	8.2×10^{-12}
0.104	0.80	8.9×10^{-9}
0.171	0.69	1.0×10^{-7}
0.233	0.58	4.7×10^{-7}
0.370	0.40	7.3×10^{-6}
0.479	0.27	5.6×10^{-5}
0.562	0.19	2.45×10^{-4}
0.617	0.15	6.6×10^{-4}
0.754	0.06	7.0×10^{-3}
0.862	0.02	0.04
0.931	0.005	0.19
0.965	0.001	0.43
1.0	0.	1.00

TABLE VII

ENERGY SOURCE

<u>Time (years)</u>	<u>Energy (ergs/s/cm)</u>
0	3.63×10^4
5	3.017×10^4
10	2.63×10^4
15	2.4×10^4
20	2.18×10^4
30	1.727×10^4
50	9.816×10^3
70	6.178×10^3
100	4.546×10^3
300	2.0×10^3
500	1.092×10^3
800	5.46×10^2
1000	3.618×10^2

out of the matrix into the canister hole. For the venting case, the canister hole was kept at 100 kPa pressure. Mass and energy flow from the matrix was allowed back into the canister hole if such is the tendency.

The results of these calculations are summarized in Figs. 40-52, which are plots of normalized temperature, pressure, and saturation vs. radius at selected times.

Qualitatively the results are the same as found in Runs 1 and 2. However, the extent of the dry-out zone is much less because of lower matrix permeability, faster heat decay rate, and stronger matrix potential and relative permeability curves.

Venting certainly had a noticeable affect on the saturation and temperature and pressure fields. With venting, the boiling region is smaller and the saturation perturbation does not extend as far out as in the no-venting case. There is some pressure build up in the matrix due to vapor pressure in the boiling region and the low matrix permeability. More complete analyses of the heat load effects will be included in the next report.

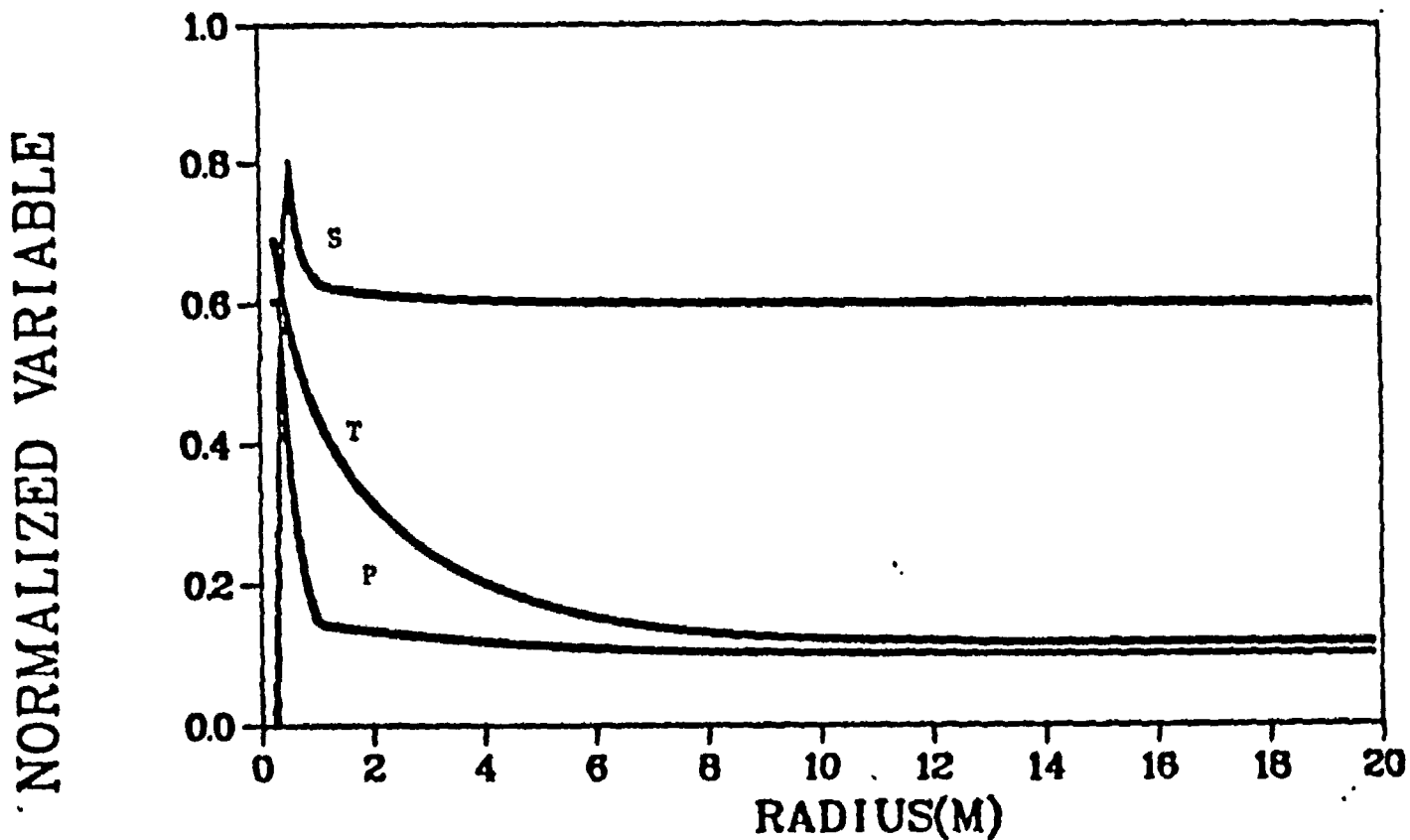
D. Three Dimensionality

A number of assumptions and simplifications have been made in the analyses in this report. The three dimensionality of flow and transport has been simplified to two dimensions or to quasi-one dimension. Also, water and contaminant sources have been treated as infinite in spatial extent. In other words, the lateral spreading of water and contaminant fronts has been ignored. Lateral spreading could significantly retard transport by increasing the surface area available for diffusion into the rock.

IV. Conclusions

Several conclusions can be made. (1) Significant fracture flow can occur above the water table, but only through high-saturation, low-permeability tuff. (2) Diffusion into the matrix and adsorption have a profound effect on transport. Migration times just to the water table for all but one of the important radionuclides are considerably longer than 10,000 years, and none of the radionuclides considered reaches the accessible environment in less than 10,000 years. (3) Heat load in partially saturated tuff can result in a dry, steam-filled region extending several meters above and below a repository with recharge during cooldown phase.

WAFE RUN FOR LLNL/WP, 1-D, LOW PERMEABILITY, NO VENTING, CYL
ALONG CONSTANT Z(1)= .01 TIME= .50 (YEARS)

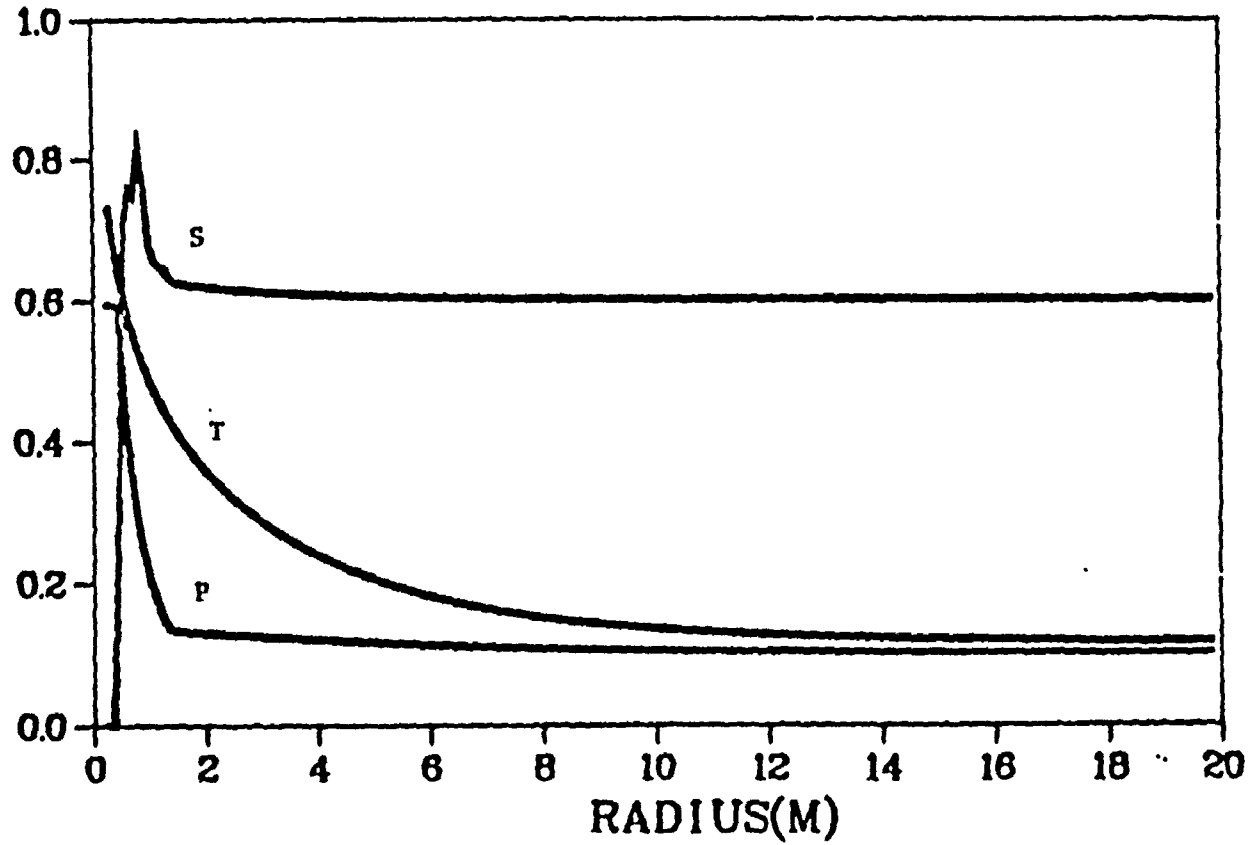


PRESSURE (KPA)	MIN= 0.	RANGE= .100E+04
FLUID TEMP(CELSIUS)	MIN= 0.	RANGE= .250E+03
SATURATION	MIN= 0.	RANGE= .100E+01

Fig. 40. Saturation, temperature, and pressure profiles at 0.5 years for no-venting case.

WAVE RUN FOR LLNL/WP, 1-D, LOW PERMEABILITY, NO VENTING, CYL
ALONG CONSTANT Z(1)= .01 TIME= .99 (YEARS)

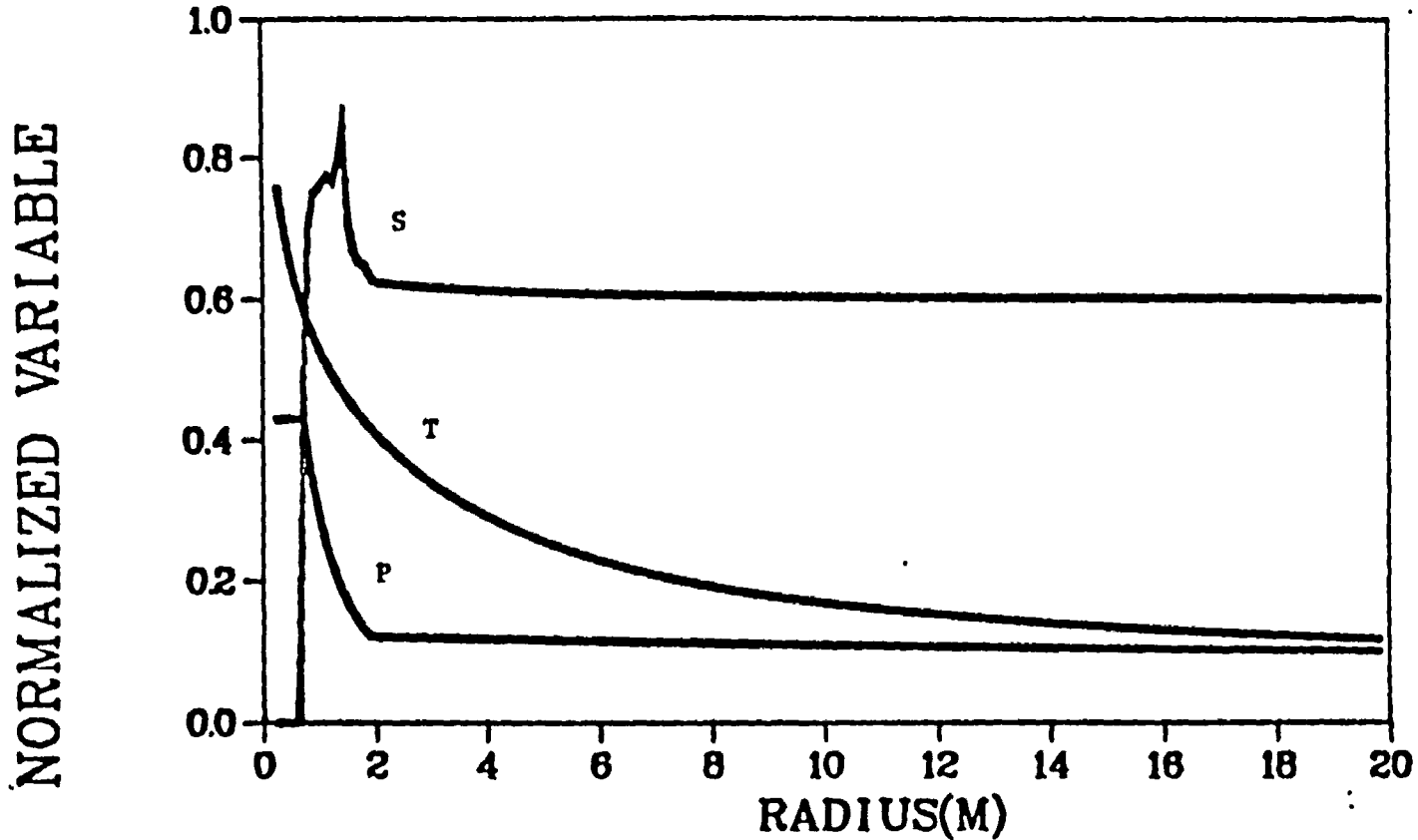
NORMALIZED VARIABLE



PRESSURE (KPA)	MIN= 0.	RANGE= .100E+04
FLUID TEMP(CELSIUS)	MIN= 0.	RANGE= .250E+03
SATURATION	MIN= 0.	RANGE= .100E+01

Fig. 41. Saturation, temperature, and pressure profiles at one year for no-venting case.

WAVE RUN FOR LLNL/WP, 1-D, LOW PERMEABILITY, NO VENTING, CYL
ALONG CONSTANT Z(1)= .01 TIME= 3.00 (YEARS)

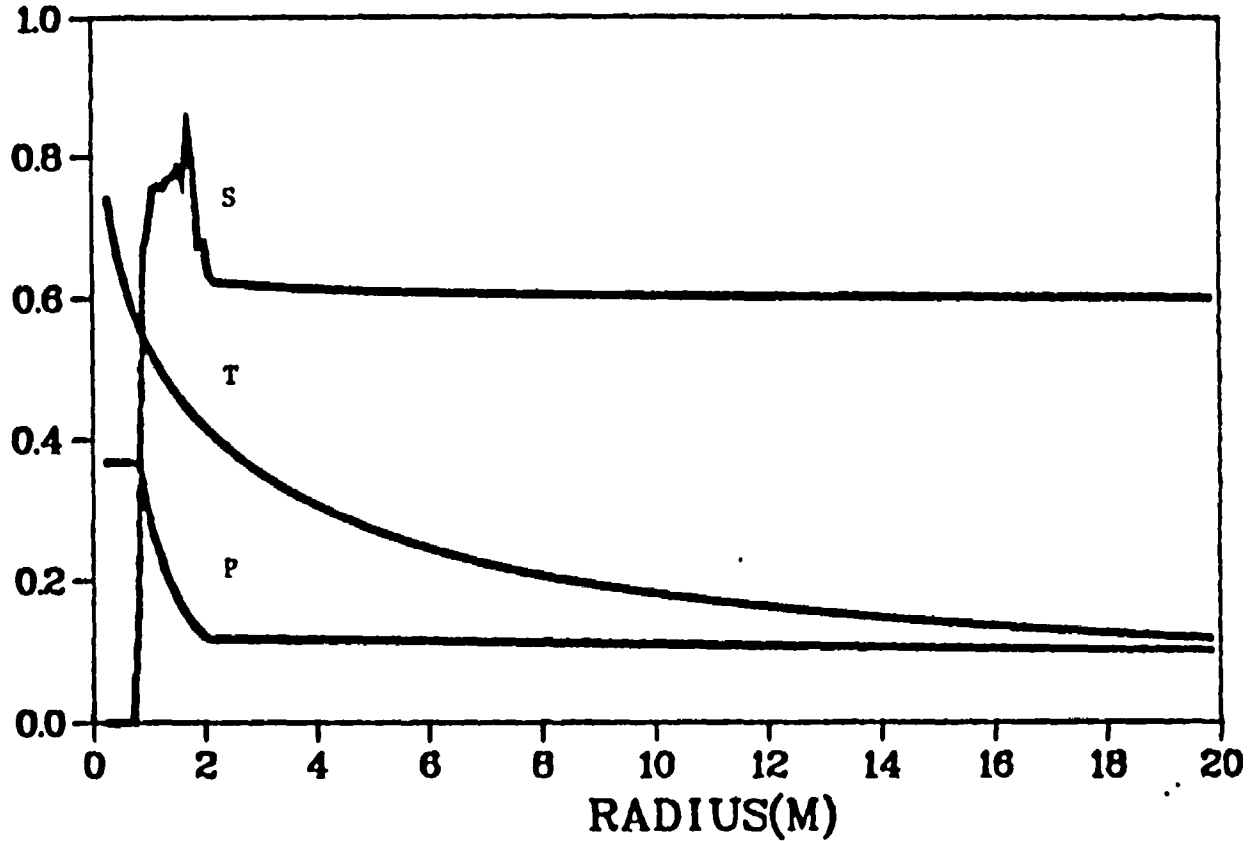


PRESSURE (KPA)	MIN= 0.	RANGE= .100E+04
FLUID TEMP(CELSIUS)	MIN= 0.	RANGE= .250E+03
SATURATION	MIN= 0.	RANGE= .100E+01

Fig. 42. Saturation, temperature, and pressure profiles at 3 years for no-venting case.

WAVE RUN FOR LLNL/WP. 1-D, LOW PERMEABILITY, NO VENTING, CYL
ALONG CONSTANT Z(1)= .01 TIME= 5.00 (YEARS)

NORMALIZED VARIABLE

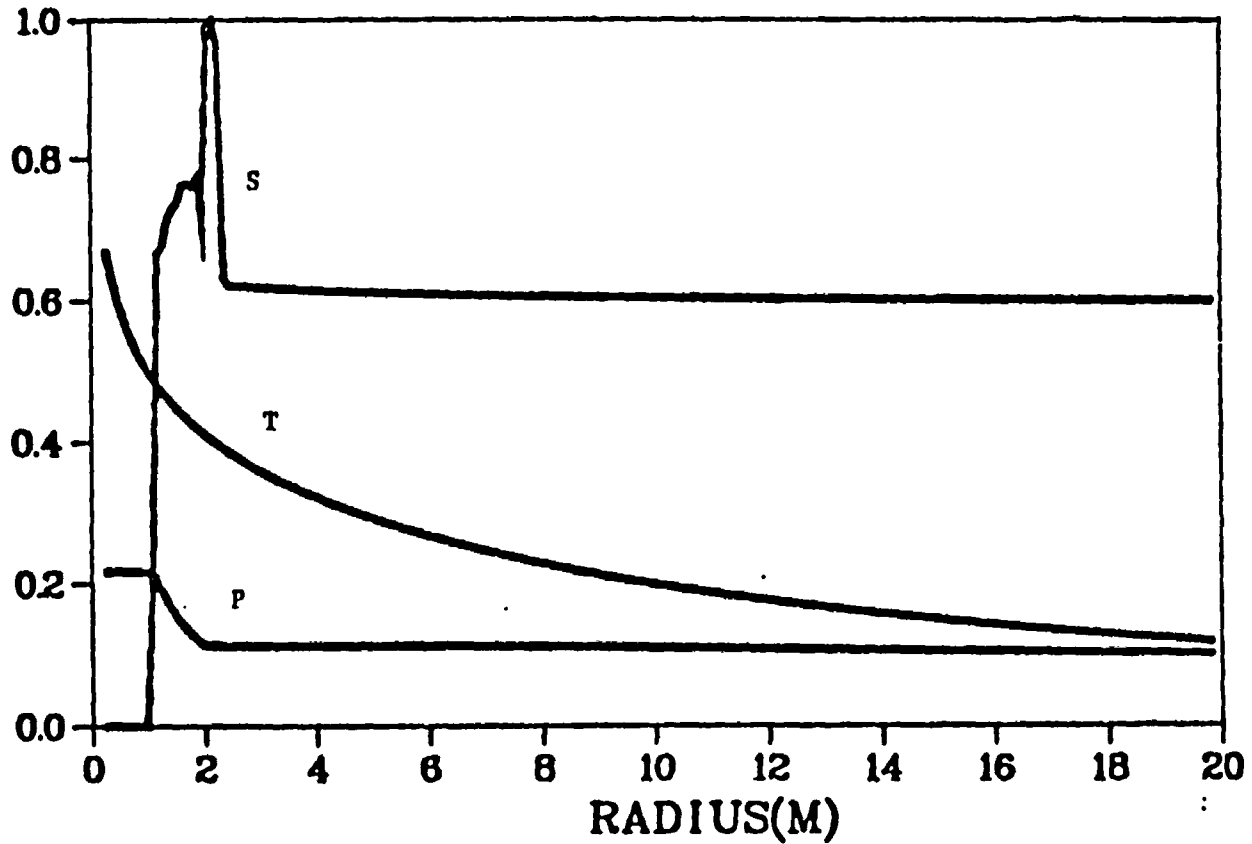


PRESSURE (KPA)	MIN= 0.	RANGE= .100E+04
FLUID TEMP(CELSIUS)	MIN= 0.	RANGE= .250E+03
SATURATION	MIN= 0.	RANGE= .100E+01

Fig. 43. Saturation, temperature, and pressure profiles at 5 years for no-venting case.

WAVE RUN FOR LLNL/WP. 1-D, LOW PERMEABILITY, NO VENTING, CYL.
 ALONG CONSTANT Z(1)= .01 TIME= 14.98 (YEARS)

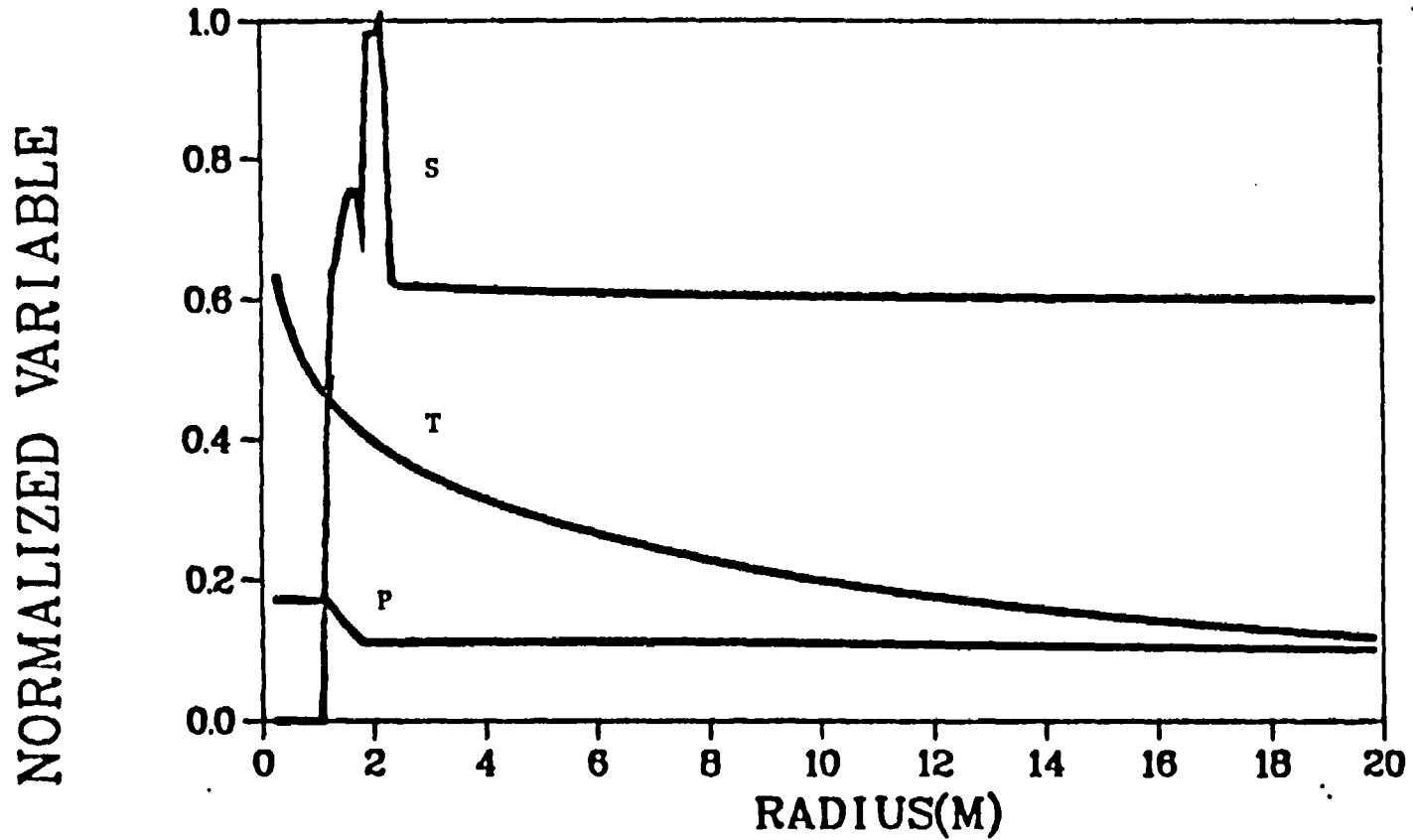
NORMALIZED VARIABLE



PRESSURE (KPA)	MIN= 0.	RANGE= .100E+04
FLUID TEMP(CELSIUS)	MIN= 0.	RANGE= .250E+03
SATURATION	MIN= 0.	RANGE= .100E+01

Fig. 44. Saturation, temperature, and pressure profiles at 15 years for no-venting case.

WAVE RUN FOR LLNL/WP, 1-D, LOW PERMEABILITY, NO VENTING, CYL
ALONG CONSTANT Z(1)= .01 TIME= 19.97 (YEARS)

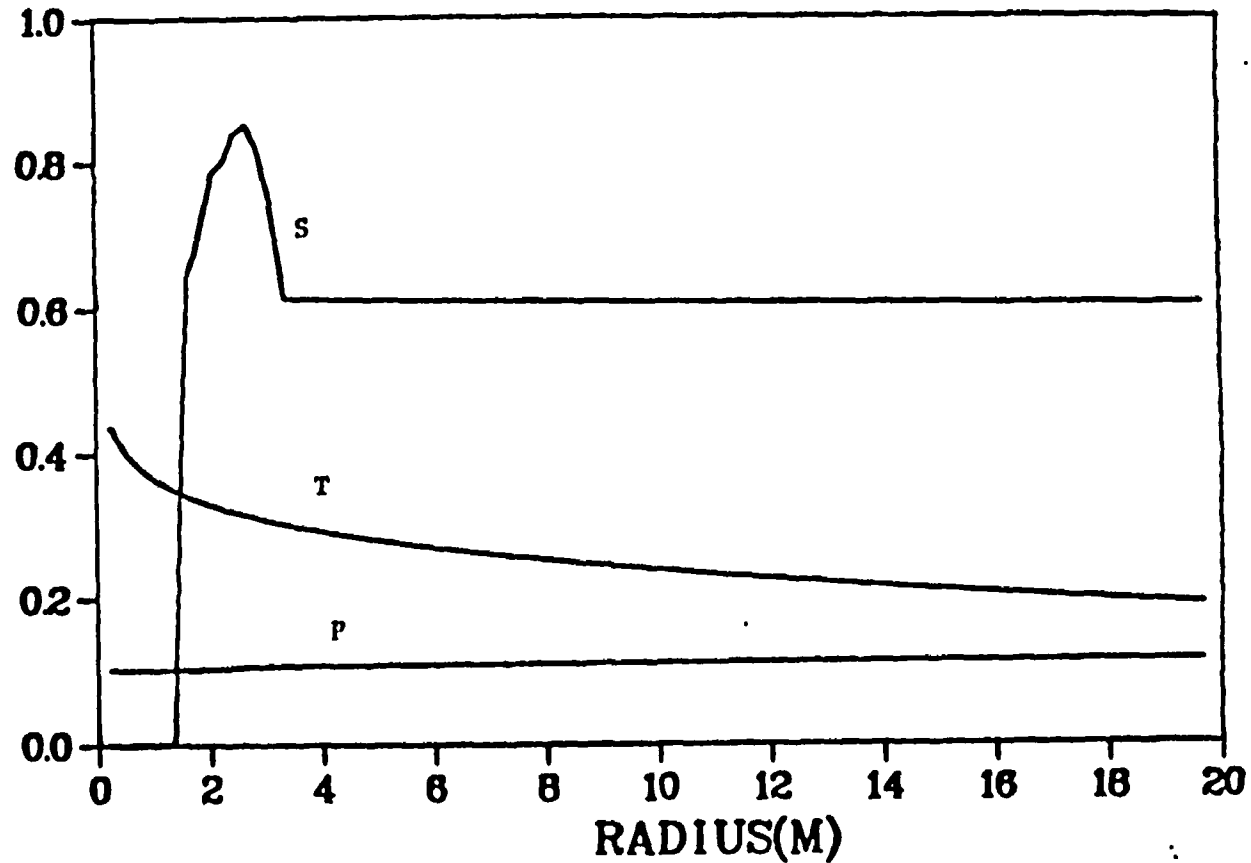


PRESSURE (KPA)	MIN= 0.	RANGE= .100E+04
FLUID TEMP(CELSIUS)	MIN= 0.	RANGE= .250E+03
SATURATION	MIN= 0.	RANGE= .100E+01

Fig. 45. Saturation, temperature, and pressure profiles at 20 years for no venting case.

NORMALIZED VARIABLE

WAFE RUN FOR LLNL/WP, 1-D, LOW PERMEABILITY, NO VENTING, CYL.
ALONG CONSTANT Z(1)= .01 TIME= 49.91 (YEARS)

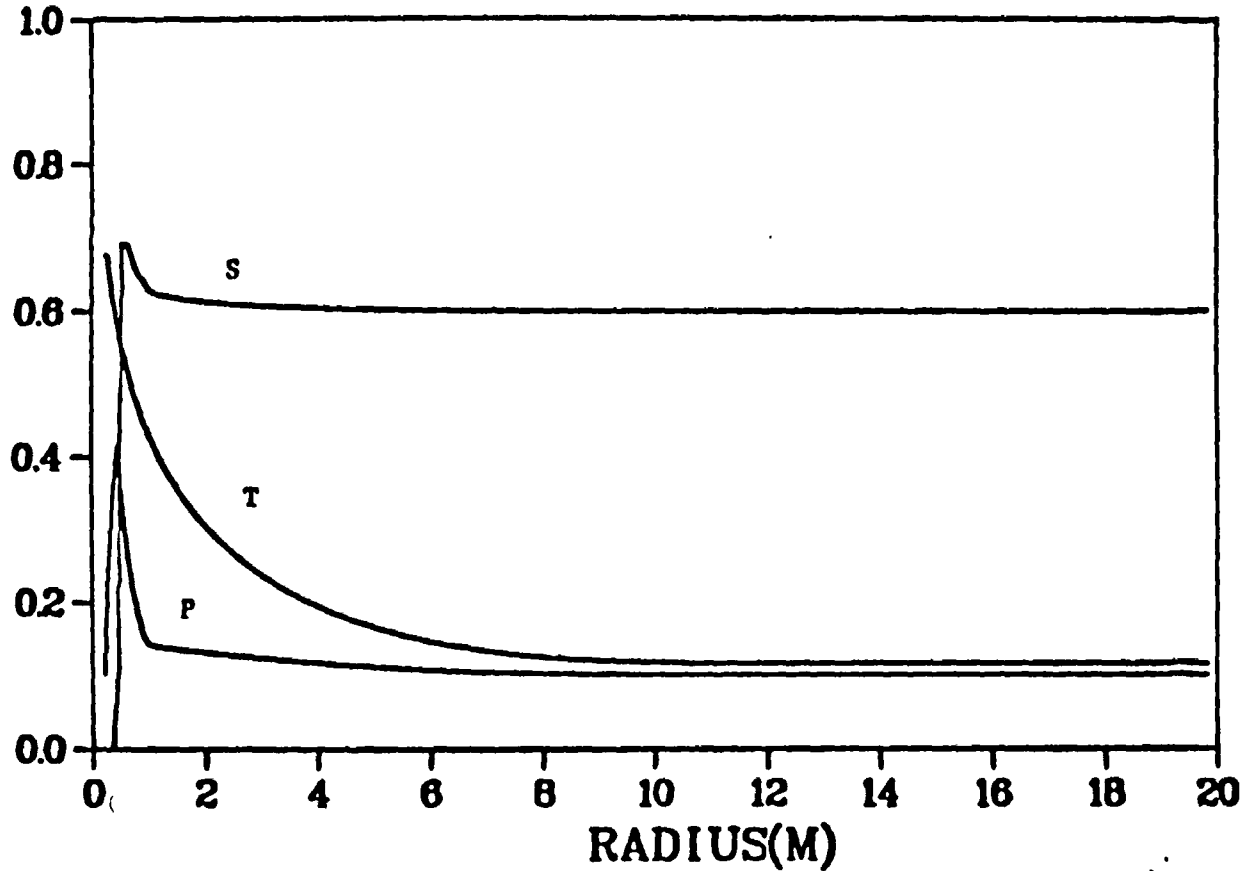


PRESSURE (KPA)	MIN= 0.	RANGE= .100E+04
FLUID TEMP(CELSIUS)	MIN= 0.	RANGE= 250E+03
SATURATION	MIN= 0.	RANGE= .100E+01

Fig. 46. Saturation, temperature, and pressure profiles at 50 years for no-venting case.

WAVE RUN FOR LLNL/WP, 1-D, LOW PERMEABILITY, VENTING, CYL.
 ALONG CONSTANT Z(1)= .01 TIME= .49 (YEARS)

NORMALIZED VARIABLE

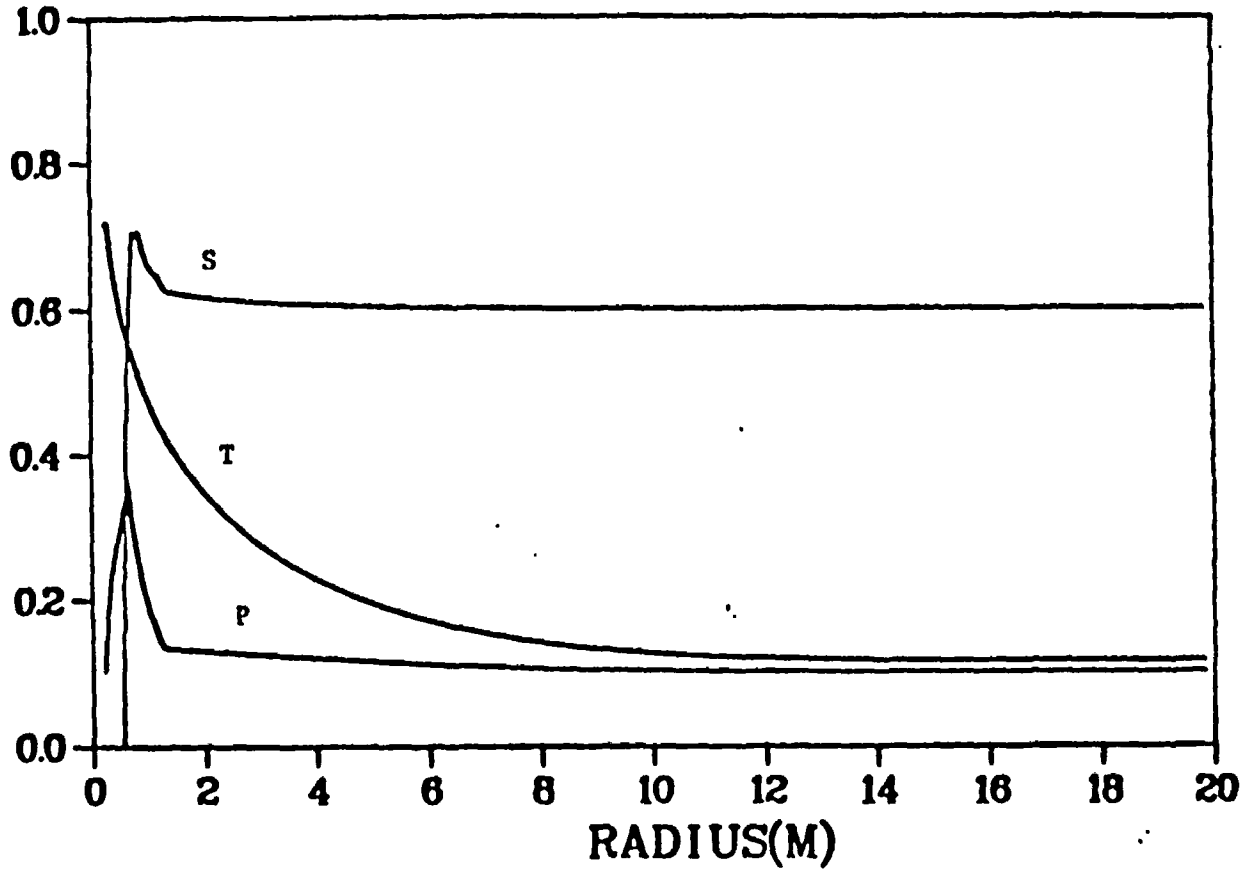


PRESSURE (KPA)	MIN= 0.	RANGE= .100E+04
FLUID TEMP(CELSIUS)	MIN= 0.	RANGE= .250E+03
SATURATION	MIN= 0.	RANGE= .100E+01

Fig. 47. Saturation, temperature, and pressure profiles at 0.5 years with venting.

NORMALIZED VARIABLE

WAFE RUN FOR LLNL/WP, 1-D,LOW PERMEABILITY, VENTING, CYL.
ALONG CONSTANT Z(1)= .01 TIME= .99 (YEARS)

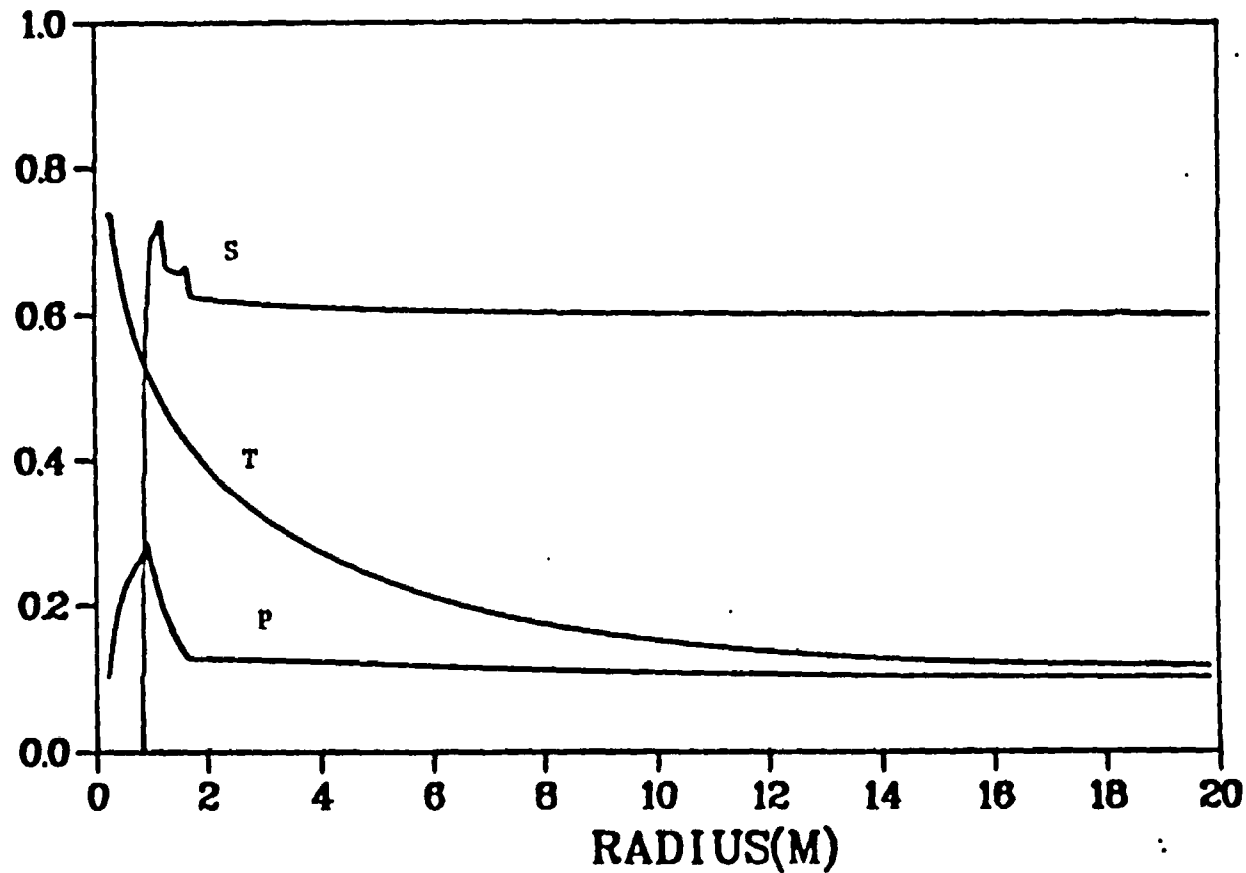


PRESSURE (KPA)	MIN= 0.	RANGE= .100E+04
FLUID TEMP(CELSIUS)	MIN= 0.	RANGE= .250E+03
SATURATION	MIN= 0.	RANGE= .100E+01

Fig. 48. Saturation, temperature, and pressure profiles at one year with venting.

WAVE RUN FOR LLNL/WP, 1-D, LOW PERMEABILITY, VENTING, CYL.
 ALONG CONSTANT Z(1)= .01 TIME= 2.99 (YEARS)

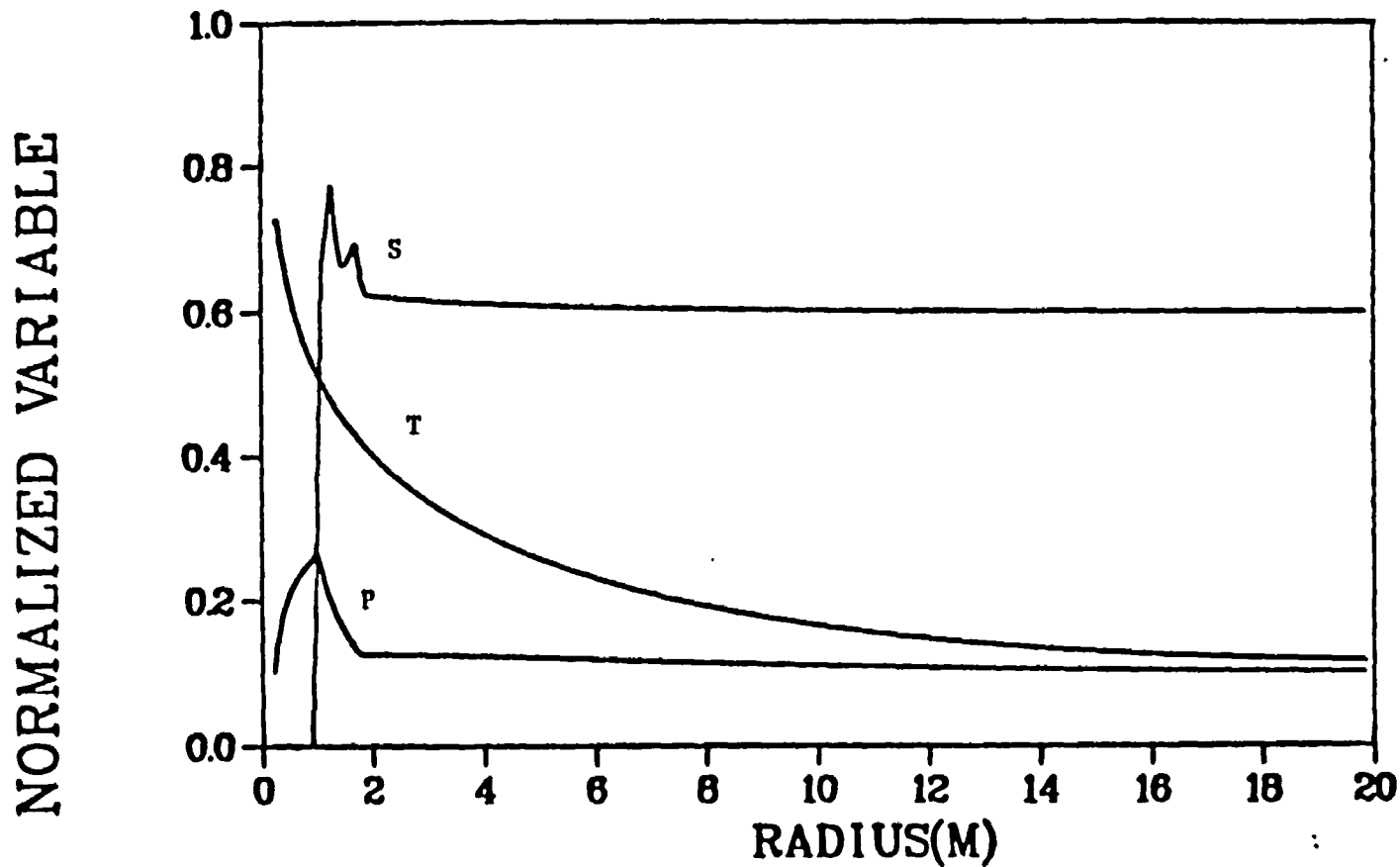
NORMALIZED VARIABLE



PRESSURE (KPA)	MIN= 0.	RANGE= .100E+04
FLUID TEMP(CELSIUS)	MIN= 0.	RANGE= .250E+03
SATURATION	MIN= 0.	RANGE= .100E+01

Fig. 49. Saturation, temperature, and pressure profiles at 3 years with venting.

WAFE RUN FOR LLNL/WP, 1-D, LOW PERMEABILITY, VENTING, CYL.
 ALONG CONSTANT Z(1)= .01 TIME= 4.99 (YEARS)

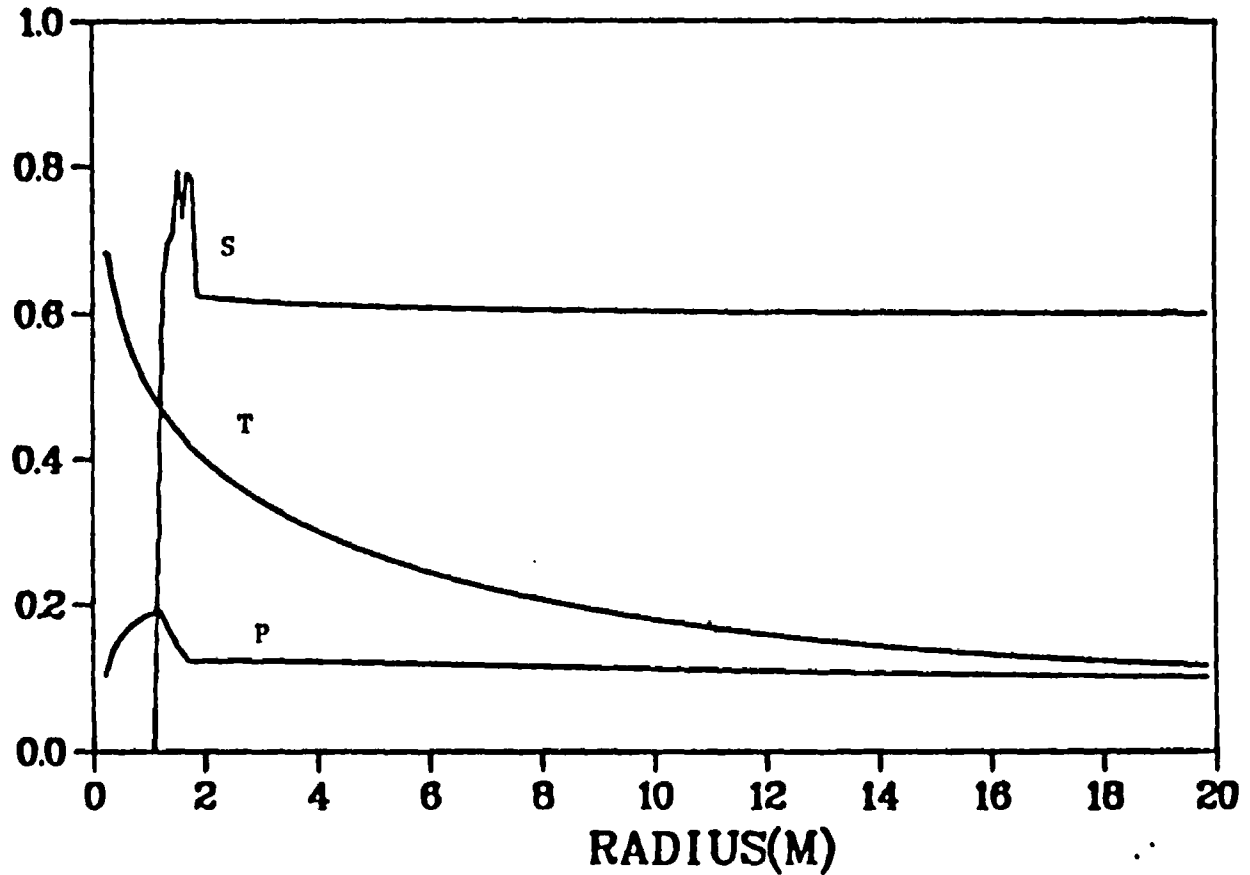


PRESSURE (KPA)	MIN= 0.	RANGE= .100E+04
FLUID TEMP(CELSIUS)	MIN= 0.	RANGE= .250E+03
SATURATION	MIN= 0.	RANGE= .100E+01

Fig. 50. Saturation, temperature, and pressure profiles at 5 years with venting.

WAFE RUN FOR LLNL/WP, 1-D, LOW PERMEABILITY, VENTING, CYL.
 ALONG CONSTANT Z(1)= .01 TIME= 9.98 (YEARS)

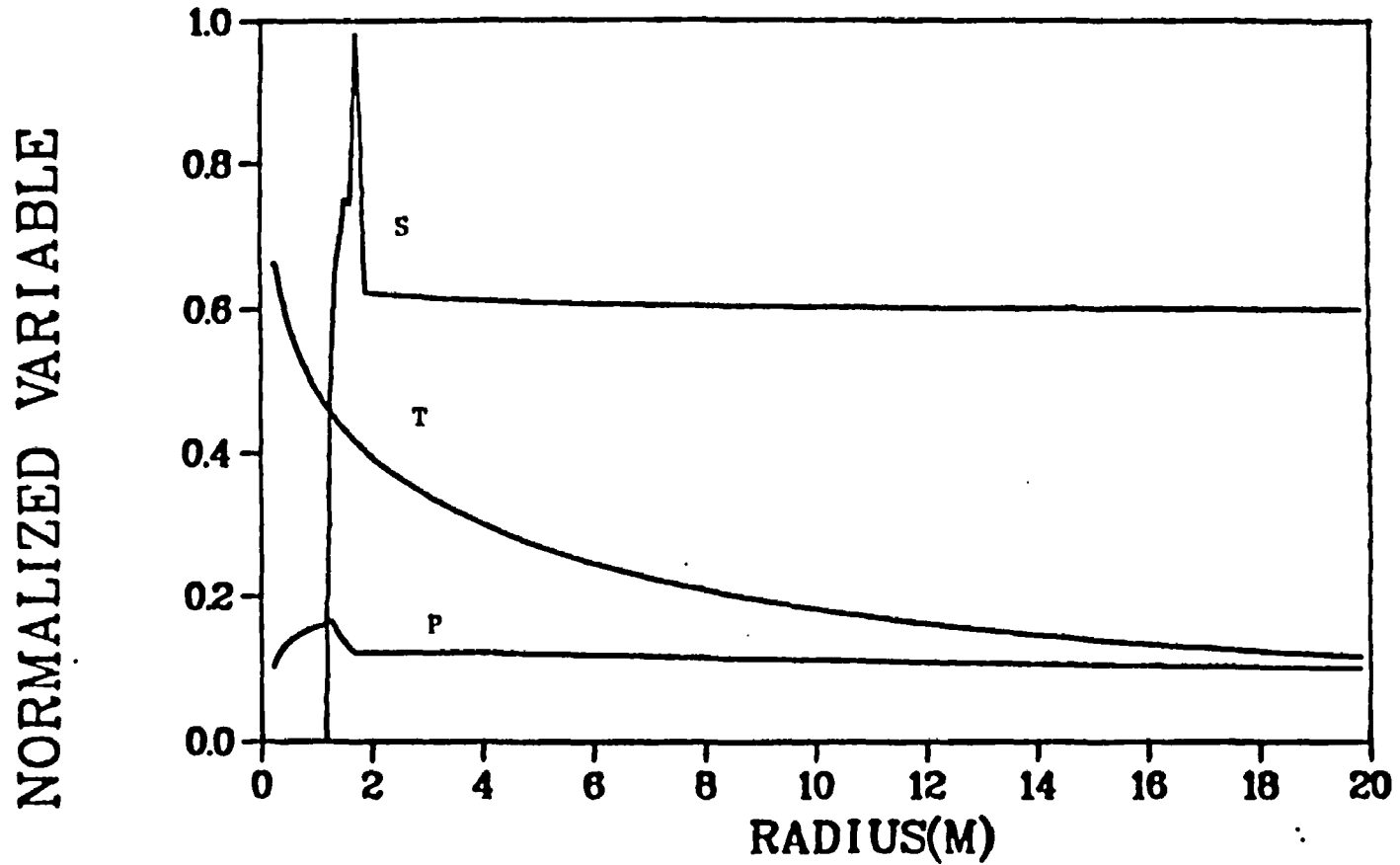
NORMALIZED VARIABLE



PRESSURE (KPA)	MIN= 0.	RANGE= .100E+04
FLUID TEMP(CELSIUS)	MIN= 0.	RANGE= .250E+03
SATURATION	MIN= 0.	RANGE= .100E+01

Fig. 51. Saturation, temperature, and pressure profiles at 10 years with venting.

WAFE RUN FOR LLNL/WP, 1-D,LOW PERMEABILITY, VENTING, CYL.
 ALONG CONSTANT Z(1)= .01 TIME= 12.92 (YEARS)



PRESSURE (KPA)	MIN= 0.	RANGE= .100E+04
FLUID TEMP(CELSIUS)	MIN= 0.	RANGE= .250E+03
SATURATION	MIN= 0.	RANGE= .100E+01

Fig. 52. Saturation, temperature, and pressure profiles at 13 years with venting.

It is very important that the reader bear in mind the various assumptions and simplifications made in this preliminary analysis. Future analyses which include more detail may indicate considerably longer migration times and considerably different heat effects. ..

References

1. R. B. Scott, R. W. Spengler, S. Diehl, A. R. Lappin, and M. P. Chornack, "Geologic Character of the Unsaturated Zone in Ash-Flow Tuff at Yucca Mountain, Southwestern Nevada," in Role of the Unsaturated Zone in Radioactive and Hazardous Waste Disposal, Ann Arbor Science, p. 289-335.
2. B. J. Travis, "TRACR3D: A Model of Flow and Transport in Porous/Fractured Media," Los Alamos National Laboratory report LA-9667-MS (January, 1984).
3. B. J. Travis, "WAFE: A Model for Two-Phase Multicomponent Mass and Heat Transport in Porous, Sorptive Media," Los Alamos National Laboratory report (in preparation).
4. H. E. Nuttall and A. K. Ray, "A Combined Fracture-Porous Media Model for Contaminant Transport," Journal of Energy, Vol. 5, pp. 376-380 (October, 1981).
5. D. H. Tang, E. O. Frind, and E. A. Sudicky, "Contaminant Transport in Fractured Porous Media: Analytical Solution for a Single Fracture," Water Resources Research, Vol. 17, No. 3, pp. 555-564 (June, 1981).
6. E. A. Sudicky and E. O. Frind, "Contaminant Transport in Fractured Porous Media: Analytical Solutions for a System of Parallel Fractures," Water Resource Research, Vol. 18, No. 6, pp. 1634-1642 (December, 1982).
7. J. H. Sass and A. H. Lachenbruch, "Preliminary Interpretation of Thermal Data From the Nevada Test Site," U.S. Geological Survey Open-File report 82-973 (1982).
8. T. E. Eakin, G. B. Maxey, T. W. Robinson, J. C. Fredericks, and O. J. Loeltz, "Estimated Annual Increment to Ground Water," in Contributions to the Hydrology of Eastern Nevada, Nevada State Engr., Water Resources Bulletin 12, p. 26-27 (1951).
9. I. J. Winograd and W. Thordarson, "Hydrogeologic and Hydrochemical Framework, South-Central Great Basin, Nevada-California, with a special Reference to the Nevada Test Site," U.S. Geological Survey Professional paper 712-C, p. 126 (1975).

10. F. E. Rush, "Regional Ground-Water Systems in the Nevada Test Site Area Nye, Lincoln and Clark Counties, Nevada," Nevada Department of Conservation and Natural Resources, Division of Water Resources, Water Resources Reconnaissance Series report 54, p. 25 (1970).
11. D. D. Evans, "Unsaturated Flow and Transport Through Fractured Rock-Related to High-Level Waste Repositories," Final Report-Phase 1, Department of Hydrology and Water Resources, University of Arizona, prepared for U.S. Nuclear Regulatory Commission, NUREG/CR-3206 (March, 1983).
12. P. A. Witherspoon, J. S. Y. Wang, K. Iwai, and J. E. Gale, "Validity of Cubic Law For Fluid Flow in a Deformable Rock Fracture," Technical Information report 23, Lawrence Berkeley Laboratory report LBL-9557 (October, 1979).
13. R. Waddel, from minutes of NNWSI Performance Assessment Working Group Meeting, Sandia National Laboratories, Albuquerque, New Mexico, April 21-22, 1983.
14. C. Duffy, written communication, 1983.
15. W. Thordarson, "Geohydrologic Data and Test Results From Well J13, Nevada Test site, Nye County, Nevada," U.S. Geological Survey Water Resources Investigation report 83-4171 (in preparation).
16. "Environmental Standards for Management and Disposal of Spent Nuclear Fuel, High-Level and Transuranic Radioactive Wastes," U.S. Environmental Protection Agency, Office of Radiation Programs, EPA 520/1-82-025 (December, 1982).
17. W. R. Daniels, et al., "Summary Report on the Geochemistry of Yucca Mountain and Environs," Los Alamos National Laboratory report LA-9328-MS (December, 1982).
18. R. K. Blankennagel and J. E. Weir, Jr., "Geohydrology of the Eastern Part of Pahute Mesa, Nevada Test Site, Nye County, Nevada," U.S. Geological Survey Professional paper 712-B, p. 35 (1973).
19. J. F. Kerrisk, "Solubility Limits on Radionuclide Dissolution at a Yucca Mountain Repository," Los Alamos National Laboratory report (in preparation).
20. J. K. Johnstone, R. R. Peters, and P. F. Gnirk, "Unit Evaluation at Yucca Mountain: Summary Report and Recommendation," SAND 83-0372 (in preparation).